Small Cell-Cell Fusogens Activate a PI3K-mTORC2-Akt Signalling Axis and Macropinocytosis for Efficient Cell Fusion

by

Duncan MacKenzie

Submitted in partial fulfilment of the requirements
for the degree of Doctor of Philosophy

at

Dalhousie University
Halifax, Nova Scotia
April 2023

Dalhousie University is located in Mi'kma'ki, the ancestral and unceded territory of the Mi'kmaq. We are all Treaty people.

Table of Contents

List of figures

Abstract

Cell-cell fusion is mediated by distinct types of protein fusogens. Class I, II and III enveloped virus fusogens facilitate fusion through interaction with receptors on an apposing membrane that trigger conformational transitions in the fusogen that provide the energy necessary to fuse the two apposed membranes. Small fusogens, such as the reovirus fusion-associated small transmembrane (FAST) proteins and the vertebrate muscle fusogen myomerger, have small extracellular domains that do not span the intermembrane aqueous layer and have not been observed to undergo large conformational changes to drive the fusion process. These small fusogens may co-opt cell machinery and processes to drive cell fusion. To investigate this possibility, I conducted genetic and drug kinase screens that identified the PI3K(p110α)-Akt kinase pathway as essential for syncytiogenesis mediated by the reovirus p15 and p14 FAST proteins and myomerger, but dispensable for SARS CoV2 spike syncytium formation. I demonstrate that small fusogen-mediated fusion increases PIP(3,4,5) production through PI3K(p110α), that PIP(3,4,5) is necessary for fusion, and that PIP(3,4,5) and p14 colocalize to membrane ruffles at the fusion synapse. Using genetic and small molecule kinase inhibitors, I also show that Akt phosphorylation by PDK1 and mTORC2 but not mTORC1 is essential for small fusogen-mediated cell fusion. Furthermore, I demonstrate that p14 upregulates membrane ruffling and macropinocytosis through the PI3K-Akt pathway, which colocalizes spatiotemporally with the cell fusion synapse. In combination with the inhibitory effect of mechanistically diverse macropinocytosis inhibitors on p14 and myomerger fusion, these findings indicate that macropinocytosis is essential for efficient small fusogen-mediated cell-cell fusion and may promote fusion by increasing membrane tension via macropinosome formation.

List of abbreviations and symbols used

AKT: Protein kinase B (a serine/threonine-specific protein kinase)
AP1: Activator protein 1 (a transcription factor)
ARV: Avian Reovirus (a virus that infects birds)
AqRV: Aquareovirus (a genus of viruses within the family Reoviridae)
AtRV: Atriplex lentiformis Reovirus (a type of virus)
AX: Annexin (a family of proteins that bind to phospholipids in a calcium-dependent manner)
BAI3: Brain-specific Angiogenesis Inhibitor 3 (a protein involved in inhibiting angiogenesis)
BRV: Bovine Rotavirus (a virus that causes diarrhea in calves)
CD: Cluster of Differentiation (a protocol used for the identification and investigation of cell surface molecules present on leukocytes)
CSC: Cancer Stem Cell (a cell within a tumor that possesses the capacity to self-renew and to cause the heterogeneous lineages of cancer cells that comprise the tumor)
CtBP1/BARS: C-terminal Binding Protein 1/Brefeldin A-ADP Ribosylated Substrate (a protein involved in transcriptional co-repression)
DMEM: Dulbecco's Modified Eagle Medium (a type of nutrient solution used to sustain the growth of cells in culture)
DOX: Doxorubicin (a chemotherapy drug)
DMSO: Dimethyl Sulfoxide (a chemical often used as a solvent in biological experiments)
EFF-1: Epithelial Fusion Failure 1 (a protein involved in cell fusion)
EGF: Epidermal Growth Factor (a protein that stimulates cell growth)
EGFR: Epidermal Growth Factor Receptor (a protein on the cell surface that binds to epidermal growth factor)
ER: Endoplasmic Reticulum (a part of the cell involved in protein and lipid synthesis)
FAST: Fluorescent Amplification for Signal Transduction (a technique for studying cellular signaling)
FBGC: Foreign Body Giant Cell (a type of immune cell that forms in response to foreign bodies)
FBS: Fetal Bovine Serum (a supplement used in cell culture)
FLiPS: Fluorescence localization with photobleaching of single molecules (a technique for studying molecular movement)
FOXO: Forkhead Box O (a family of transcription factors)
GAB: GRB2-Associated Binding Protein (a protein involved in signal transduction)
GEF: Guanine Nucleotide Exchange Factor (proteins that stimulate the exchange of GDP for GTP)
GFP: Green Fluorescent Protein (a protein used as a reporter in molecular biology)
GPCR: G-Protein Coupled Receptor (a type of cell surface receptor involved in signal transduction)
GRB2: Growth Factor Receptor-Bound Protein 2 (an adapter protein involved in signal transduction)
GSK-3β: Glycogen Synthase Kinase 3 beta (an enzyme involved in energy metabolism and cellular signaling)
Hap2: Hapless 2 (a protein essential for fertilization in many organisms)
HBSS: Hank's Balanced Salt Solution (a balanced salt solution used in biological research)
HERV-W: Human Endogenous Retrovirus-W (a human endogenous retrovirus)
HPV16: Human Papillomavirus 16 (a strain of HPV associated with cancer)

HS: Horse Serum (a supplement used in cell culture)
HVJ: Hemagglutinating Virus of Japan (also known as Sendai virus)
IFN: Interferon (a type of cytokine that modulates immune responses)
IGF-1: Insulin-like Growth Factor 1 (a hormone that plays an important role in childhood growth and continues to have anabolic effects in adults)
IL: Interleukin (a type of cytokine that modulates immune responses)
IL-6: Interleukin 6 (a cytokine that influences inflammation and immune response)
INPP 4A and 4B: Inositol Polyphosphate-4-Phosphatase Type I and II (enzymes involved in inositol phosphate metabolism)
JAK/STAT: Janus Kinase/Signal Transducers and Activators of Transcription (a pathway involved in cell signaling)
kDa: Kilodalton (a unit of molecular mass)
LGC: Leukocyte Giant Cell (a type of immune cell)
MaPi: MacroPinocytosis (a process by which cells intake extracellular molecules)
MCSF: Macrophage Colony-Stimulating Factor (a cytokine that stimulates the production of macrophages)
MHC: Major Histocompatibility Complex (a set of genes that code for proteins on the surfaces of cells that help the immune system recognize foreign substances)
MPER: Membrane-Proximal External Region (a region of the HIV envelope glycoprotein gp41)
MRF: Myogenic Regulatory Factor (a family of transcription factors that regulate muscle cell differentiation)
mTORC1: Mammalian Target Of Rapamycin Complex 1 (a protein complex involved in regulating growth and metabolism)
mTORC2: Mammalian Target Of Rapamycin Complex 2 (a protein complex involved in regulating growth and metabolism)
Myf5: Myogenic factor 5 (a protein that is part of the myogenic regulatory factor family)
MyoD: Myoblast Determination Protein (a protein that plays a key role in regulating muscle differentiation)
NBV: Nelson Bay virus (a type of virus in the paramyxovirus family)
NF1: Neurofibromatosis type 1 (a genetic disorder)
Nsp: Non-structural protein (a protein coded by a virus that is not part of the virus particle structure)
ORV: Orthoreovirus (a genus of viruses within the family Reoviridae)
PAK1: p21 Activated Kinase 1 (an enzyme involved in signal transduction)
PDGF: Platelet-derived Growth Factor (a protein that regulates cell growth and division)
PGCC: Polyploid Giant Cancer Cell (an atypical cancer cell with more than two copies of each chromosome)
PH: Pleckstrin Homology (a protein domain involved in cell signaling)
PIP(3,4): Phosphatidylinositol (3,4)-bisphosphate (a second messenger molecule)
PIP(3,4,5): Phosphatidylinositol (3,4,5)-trisphosphate (a second messenger molecule)
PIP2: Phosphatidylinositol 4,5-bisphosphate (a type of phospholipid important in cell signaling)
PIP3: Phosphatidylinositol (3,4,5)-trisphosphate (a second messenger molecule)
PKC: Protein Kinase C (a family of protein kinases)
PLC: Phospholipase C (an enzyme involved in signal transduction)

PDK1: Phosphoinositide-dependent kinase-1 (an enzyme involved in cell signaling)
PTEN: Phosphatase and Tensin Homolog (a protein that acts as a tumor suppressor)
PTP-PEST: Protein Tyrosine Phosphatase PEST (an enzyme involved in cell adhesion and migration)
QM5: Quail myoblast cell line 5 (a cell line used in scientific research)
Rab: A member of the Rab family, small GTPases involved in intracellular membrane trafficking
RANKL: Receptor Activator of Nuclear factor Kappa-B Ligand (a protein involved in immune regulation and bone remodeling)
Raptor: Regulatory Associated Protein of mTOR (a component of mTORC1)
Rictor: Rapamycin-insensitive companion of mTOR (a component of mTORC2)
ROI: Region of Interest (a term used in image analysis)
RTK: Receptor Tyrosine Kinase (a type of protein kinase involved in signal transduction)
SDS-PAGE: Sodium Dodecyl Sulfate-Polyacrylamide Gel Electrophoresis (a technique for separating proteins based on their size)
SEM: Scanning Electron Microscope (a type of electron microscope)
SHIP: SH2-containing Inositol 5'-Phosphatase (an enzyme that dephosphorylates certain phosphatidylinositols)
shRNA: Short Hairpin RNA (a sequence of RNA that makes a tight hairpin turn that can be used to silence gene expression)
siRNA: Small Interfering RNA (a type of RNA molecule used in RNA interference)
Sin: Sin1 (a component of mTORC2 complex)
SGK: Serum and Glucocorticoid-regulated Kinase (a family of protein kinases)
SNARE: Soluble NSF Attachment Protein Receptor (a large protein complex responsible for fusion of vesicles and target membranes)
SOS: Son of Sevenless (a protein involved in signal transduction)
Tmem8c: Transmembrane Protein 8C (a protein that is expressed in several tissues)
TM: Transmembrane (refers to a protein domain that spans the membrane of a cell)
WASP: Wiskott-Aldrich Syndrome Protein (a protein involved in cytoskeletal organization)
WAVE: WASP Family Verprolin-homologous protein (a protein involved in cytoskeletal organization)
WGA: Wheat Germ Agglutinin (a lectin that binds to N-acetyl-D-glucosamine)

Symbols:

°C: degrees Celsius
uM: micromolar (a unit of concentration)
mM: millimolar (a unit of concentration)
p: Pico (a metric prefix indicating one trillionth)
α: Alpha
β: Beta
γ: Gamma

Acknowledgements

First and foremost, my heartfelt appreciation goes to my thesis supervisor, Dr. Roy Duncan. His patience, guidance, and unwavering support have been the cornerstone of my academic journey. Dr. Duncan not only shaped my approach to scientific inquiries but also cultivated in me the virtues of a rigorous scientist and an effective communicator. I am indebted to him for his faith in my abilities and for challenging me to strive for excellence.

I would like to extend a special thanks to Nichole McMullen, whose unending support and encouragement have been instrumental in my progress. Her belief in me and our many "therapy sessions" were often the spark I needed to move forward. Her vigilance in ensuring that I didn't "burn the lab down" was both literal and metaphorical, and I cannot express enough how grateful I am for her friendship and mentorship.

To my incredible wife, Brianna, words cannot capture the gratitude I feel for your unwavering love and support. You saw potential in a master's student with thinning hair and cheered me on to become the bald Doctor I am today. Your constant source of encouragement and your confidence in my pursuit of a Ph.D.. I thank you for your love, understanding, and for taking that chance on me.

Last but not least, I would like to express my deepest gratitude to my parents for their enduring love and support throughout this journey. My father, in particular, has been a beacon of scientific, emotional, and most importantly financial support. His wisdom, insight, and relentless optimism have guided me through the toughest of times, and I owe a large part of my success to his unwavering belief in me.

Chapter 1: Introduction

1.1. Cell-cell fusion overview

Cell-cell fusion is a crucial biological process that plays a significant role in various physiological processes such as fertilization, development, and immune responses. These programmed cell-cell fusion events occur in response to specific signals and activate actin- and membrane-remodeling pathways required to construct a fusion synapse and recruit protein fusogens to mediate cell-cell membrane fusion (Brukman et al., 2019; Hernández & Podbilewicz, 2017). Much of our understanding of these cellular pathways derives from studies of muscle cell fusion in *Drosophila melanogaster*, where formation of an actin-driven membrane protrusion projects into the adjoining cell inducing membrane tension and fusion (Bothe et al., 2014; E. H. Chen, 2011; Chuang et al., 2019; Randrianarison-Huetz et al., 2017; Segal et al., 2016; Vasyutina et al., 2009). In addition, the process of cell-cell fusion can also be induced by viruses for the purposes of infection and spread (R. Duncan, 2019; Harrison, 2015; Podbilewicz, 2014). These virally induced cell fusion events usually reflect the activity of an enveloped virus membrane fusion protein. These large, complex, multimeric, membrane fusion proteins evolved primarily to mediate virus-cell fusion, but when present in the plasma membrane can function as cell-cell fusogens to promote the fusion of host cells and lateral dissemination of the infection. Over the past few years, several homologues of enveloped virus membrane fusion proteins were identified as the fusogens mediating programmed cell-cell fusion processes such as syncytiotrophoblast fusion (syncytin), epidermal fusion in *Caenorhabditis elegans* (Epithelial fusion failure 1 (EFF-1)), and gamete fusion in Chlamydomonas (Hapless 2 (Hap2)) (Krey et al., 2017; Mi et al., 2000; Mohler et al., 2002). In the case of EFF-1, similar invadosomes as observed in Drosophila muscle cell fusion were envisioned to drive the cell-cell fusion process (Shilagardi et al., 2013a).

There are two exceptions to the above generalizations and specific examples of cell-cell fusogens; the fusion-associated small transmembrane (FAST) proteins encoded by fusogenic dsRNA viruses, and the small component of a bi-partite muscle cell fusion

protein complex discovered independently by three labs in 2017, variously referred to as myomerger, myomixer, or minion (Bi et al., 2017; Quinn et al., 2017; Q. Zhang et al., 2017). The FAST proteins and myomerger share similar biophysical and biochemical properties, with some notable exceptions (e.g., their inverse membrane topologies) (R. Duncan, 2019; Segev et al., 2018; Vance & Lee, 2020), and both are clearly structurally and evolutionarily distinct from the enveloped virus fusogens and their cellular paralogues (Fig. 1A).

At the time I started my graduate research, the only detailed understanding of the architecture of a fusion synapse and the processes involved in its construction was the aforementioned *Drosophila* developmental myogenesis model. It was unclear how these cellular processes might apply to other physiological cell-cell fusion events, and whether FAST proteins rely on similar processes to construct a FAST protein fusion synapse. My objective was to use high-content screens to identify tentative cellular pathways and mediators needed for FAST protein-induced syncytium formation, and to then characterize how these events contribute to cell-cell fusion and syncytiogenesis. As the field advanced, I included an analysis of the newly discovered myomerger fusogen.

To establish the context for my research, the subsequent sections of this Introduction will address several key topics vital to comprehending membrane fusion and its impact on cell biology and virology. We'll begin by exploring the common attributes observed in cell-cell fusion across numerous biological systems. The aim here is to unravel the regulatory mechanisms that govern this process across different cellular contexts. The next section will detail with the hemifusion stalk-pore model of membrane fusion, a theoretical model that characterizes the step-by-step process of membrane fusion. This section will focus on the energy dynamics associated with fusion, the function of fusogens and lipids, and the transition states such as hemifusion and stalk formation. We will then transition into various cell fusion paradigms, demonstrating the breadth of biological scenarios where fusion is indispensable, from myogenesis to fertilization, and more. Subsequently, we will investigate how enveloped viruses instigate cell fusion. This portion will center on the strategies utilized by these viruses to

induce membrane fusion, facilitating successful infection, while concurrently offering insights into the overarching principles of membrane fusion. After examining viruses, we will proceed to metazoan cell fusion. We'll review its roles in different biological processes and organisms, focusing on the underlying molecular mechanisms and signaling pathways. Finally, we'll turn our focus to the specific pathways implicated in FAST protein-mediated fusion. Here, the primary emphasis will be on the PI3K-Akt pathway and macropinocytosis, both of which have been found to play crucial roles in this process. Collectively, these sections aim to provide a thorough understanding of membrane fusion, its biological implications, and the intricate mechanisms that viruses utilize, thus setting the stage for an in-depth analysis of the research conducted in this domain.

1.2. Cell fusion paradigms

In the evolution of life on earth, the transition of reproducing entities from what were likely phase condensates to membrane bound entities, both cells and eventually cellular organelles, were critical steps in the emergence of complex multicellular life forms. Equally, the merging or fusion of membrane bound units, both organelles and cells, underpins many elements of metazoan development. Within the cell, membrane fusion is critical to both the import and export of biomolecules, intracellular trafficking of proteins, and the homeostatic maintenance of membrane delimited organelles such as the endoplasmic reticulum and mitochondrial network. Cellular fusion itself is seen in a diversity of roles including fertilization, syncytiotrophoblast formation, myogenesis, osteogenesis, elements of the immune system, platelet formation, stem cell–mediated tissue regeneration and eye lens formation (Hernández & Podbilewicz, 2017; Ogle et al., 2005). Pathologic cell-cell fusion can also be seen in cancer progression and many viral infections (Bastida-Ruiz et al., 2016). Interest in virally mediated cell-cell fusion was catalyzed 60 years ago by Yoshio Okada's observation of giant polynuclear cell formation caused by incubating Sendai virus (then referred to as Hemagglutinating virus of Japan or HVJ virus) with Ehrlich tumor cells (Okada, 1962). Virally, and then chemically induced

cell-cell fusion was used in the intervening decades for analysis of gene expression, chromosomal mapping, monoclonal antibody production, and even cancer immunotherapy (E. H. Chen & Olson, 2005).

1.2.1. Enveloped virus class I, II and III fusogens

The entry of enveloped viruses into host cells involves the fusion of the viral envelope and host cell membrane, an energetically unfavorable action which is wholly dependent on viral transmembrane fusion proteins or "fusogens". In addition to driving the fusion of virus with cells, many viral fusogens can also trigger cell-cell fusion as well (Brukman et al., 2019; R. Duncan, 2019; Hernández & Podbilewicz, 2017; Podbilewicz, 2014; Vance & Lee, 2020).

There exist three known enveloped viral fusogen classes defined by the distinct topologies of the fusogens themselves (Harrison, 2015; Segev et al., 2018) (Fig. 2B):

- Class I fusogens found in viruses such as influenza, coronavirus, human immunodeficiency virus (HIV), and Ebola form coiled-coil trimers
- Class II fusogens normally exist as dimers but, during fusion, produce an elongated β sheet rich ectodomain and transition to a hairpin trimer. Class 2 fusogens are encoded by Dengue, West Nile, Zika and tick-borne encephalitis viruses.
- Class III proteins, found in vesicular stomatitis virus, herpes simplex virus 1, and rabies virus, combine elements from class 1 and 2, taking on a post-fusion coiled-coil trimerization region similar to class I, and an elongated trimer of hairpins as in class 2 following cell fusion.

Gene analogues of viral class I-III fusogens can be found in metazoans including humans. This includes the syncytins, the endogenous retroviral envelope proteins required for multinucleated syncytiotrophoblast generation during placental development (Mi et al., 2000; Renaud & Jeyarajah, 2022). The N- and C-terminal heptad repeats domains of syncytin-1 share significant structural homology with the corresponding N-peptide and C-peptide of class I viral fusogen HIV gp160 (Y. Yang & Margam, 2021). Two other fusogens, EFF-1 with wide ranging cell fusion activity in C.

elegans and HAP2 that mediates gamete fusion in invertebrates resemble class II viral fusogens, containing three beta-sheet-rich domains (Krey et al., 2017; Pérez-Vargas et al., 2014). The structural similarities between these three cell–cell fusogens and viral fusogens and the obvious viral origin of the syncytins have led some to suggest that all eukaryotic cell fusion proteins may have descended from a viral ancestor (Krey et al., 2017; Vance & Lee, 2020).

1.2.2. The FAST proteins

There is a fourth distinct class of viral fusogens encoded by the double-stranded RNA reoviruses. Unlike the viruses encoding class I-III fusogens, reoviruses lack a lipid envelope and package their segmented genome within multi-layered capsids, obviating the need for the viral envelope-cell membrane fusion driven by the enveloped virus fusogens (Duncan, 2019; Eledge et al., 2019). Nonetheless, these nonenveloped virus fusion proteins, known as FAST proteins, are potent fusogens. The FAST proteins are not part of the mature virion and although not involved in initial viral entry, are expressed inside virus-infected cells and can fuse multiple cells into multinucleate cells or syncytia at later stages of infection. This helps both with the local spread of virus between cells while inducing cell death to promote eventual lysis and release of viral progeny.

FAST proteins including avian orthoreovirus p10, reptilian orthoreovirus p14, and baboon orthoreovirus p15 are nonstructural viral proteins which, ranging in size from 100–200 amino acids, are much smaller than are the other viral fusogens (Fig. 2A) (R. Duncan, 2019). All FAST proteins identified to date are type I transmembrane proteins of a similar small size (10 to 22 kDa), with a characteristic modular architecture: an N terminal 20–40 amino acid structurally diverse ectodomain, including polyproline helices and cysteine loops, a single transmembrane domain, and a larger (~40–140 residues) cytoplasmic C terminus (Fig. 2B). All domains save the polyproline patch in the p14 cytosolic domain are essential for FAST protein fusion activity (Barry & Duncan, 2009; Corcoran & Duncan, 2004; R. Duncan, 2019).

In general, the ectodomains of the FAST proteins consist of small, amphiphilic peptides. Most of these peptides undergo a post-translational modification known as myristoylation at the penultimate N-terminal glycine, a critical step to ensure fusion competency. The cytoplasmic endodomains of FAST proteins are marked by three key features. Firstly, they exhibit intrinsic disorder, which potentially allows for interactions with a diverse array of cellular partners. Secondly, they possess a juxtamembranous polybasic motif with at least three basic residues (Shmulevitz et al., 2004). In the case of the p14 protein, this motif facilitates, in a sequence-independent manner, the protein's interaction with Ras associated binding protein (Rab) 11 (Rab11) and its subsequent sorting into adaptor protein 1 (AP1) -coated vesicles (Parmar & Duncan, 2016). This allows for the anterograde transport of p14 to the plasma membrane. Thirdly, these endodomains contain at least one amphipathic α-helix region, frequently referred to as a hydrophobic patch. This structural feature is thought to promote the formation of the essential fusion pores (Read et al., 2015). These shared characteristics hint at a common mechanistic underpinning for the fusogenic activity of these proteins, notwithstanding the viral species from which they originate (Fig. 1B).

Following expression in virus-infected cells, FAST proteins are channeled through the endoplasmic reticulum (ER)-Golgi secretory pathway to the plasma membrane. This trafficking mechanism is mediated by the membrane-proximal polybasic motif inherent to these proteins. Notably, the p14 FAST protein exhibits multimeric functionality, which is established during transit through the Golgi apparatus (Corcoran et al., 2011). This propensity for multimerization isn't confined to p14; the Nelson Bay Virus (NBV) and Avian Reovirus (ARV) p10 proteins also form octameric assemblies on the plasma membrane. Intriguingly, this octameric organization of p10 is contingent on the presence of cholesterol within lipid rafts, underscoring the complex interplay between viral proteins and host cellular membrane components (Key & Duncan, 2014).

Evolutionarily, FAST proteins appear to diverge into two distinct clades, broadly categorized as p16 and p22 Aquareovirus (AqRV) FAST proteins and p10, p13, p14, and p15 Orthoreovirus (ORV) FAST proteins (Nibert & Duncan, 2013; Y. Yang et al., 2020). A

recent discovery includes a new FAST protein, nonstructural protein 1-1 (NSP1-1), identified in the genomes of multiple species of rotaviruses. Phylogenetic analysis places NSP1-1 within a clade closely related to Baboon Reovirus (BRV) p15 (Diller et al., 2019). The emergence of NSP1-1 may have resulted from a gene transfer event, further complicating the evolutionary narrative of these proteins. The term 'viroporins' has been proposed to represent a common ancestor of the FAST proteins found in both clades. These small, non-fusogenic membrane-associated proteins are encoded by most viruses and possess the ability to form oligomeric pores or to modulate membrane ion flow in other ways (Nieva et al., 2012). However, the lack of sequence similarity and the divergence in both structure and membrane topologies between viroporins and FAST proteins suggest that these groups may have arisen by convergent evolution. Nevertheless, viroporins carry motifs, such as transmembrane domains and amphipathic helices, analogous to those found in FAST proteins, which are capable of altering membrane curvature and remodeling intracellular membranes.

1.2.3. The hemifusion stalk-pore model of membrane fusion

Membrane fusion is a fundamentally important physiological process, and understanding its energy dynamics is crucial to comprehend how the process is regulated. According to the classical model proposed by Koslov and Markin in 1983, and refined over time by many researchers, the process of membrane fusion involves overcoming several energy barriers (Chakraborty et al., 2013; Chernomordik et al., 1987; Giraudo et al., 2005; Kawamoto & Shinoda, 2014; Kozlov & Markin, 1983; Lu et al., 2005). The model describes the fusion process as a progression through several energy-demanding stages (Chernomordik & Kozlov, 2008). The first barrier is bringing two negatively charged membranes close together, which involves overcoming electrostatic repulsion forces (Fig. 2A&B). This proximity facilitates the induction of small hydrophobic defects in the opposing bilayers, leading to the formation of a stalk-like intermediate. This stage is characterized by high energy due to the exposure of hydrophobic lipid tails to the aqueous environment. Next, the expansion of the stalk structure into a

hemifusion diaphragm is energetically favorable (Chakraborty et al., 2013; Dong Woog Lee et al., 2015; Lu et al., 2005). However, the subsequent barrier is the opening of a fusion pore within the hemifusion diaphragm, once again exposing hydrophobic lipid tails to water. Finally, the fusion pore expands, which is typically energetically favorable due to the increase in the radius of curvature at the fusion pore edge (Chernomordik & Kozlov, 2008; Lai et al., 2013; Martens & McMahon, 2008).

Importantly, fusion proteins, or fusogens, are key players in navigating these energy barriers (Shuhei Kawamoto et al., 2015). They undergo conformational changes that lower the energy barriers, facilitating the progression through the fusion pathway. For instance, in the case of soluble N-ethylmaleimide-sensitive factor attachment protein receptor (SNARE) proteins involved in vesicle fusion, the formation of the trans-SNARE complex pulls the membranes together through binding then zippering of vesicle-SNAREs to target-SNAREs, providing the energy required to overcome the initial energy barriers to membrane fusion (J. Han et al., 2017). Moreover, lipid composition can also modulate these energy barriers. For example, the presence of cholesterol or certain types of phospholipids can reduce the energy required for the transition between various fusion intermediates (Haque et al., 2001; Key & Duncan, 2014; Meher & Chakraborty, 2019). However, these lipid characteristics supplement the primary driving force - the fusogen applying force to membrane through conformational changes and membrane associated domains which alter membrane curvature, that predominantly determine the energy dynamics of the pore formation and expansion process.

1.2.4. FAST protein-mediated cell-cell fusion

In the pre-fusion state, FAST proteins are enriched in cholesterol-dependent membrane microdomains or lipid rafts, somewhat thicker than adjacent normal lipid bilayers (Corcoran et al., 2011). The membrane fusion reaction is contingent upon the presence of strong membrane apposition driven by cellular cadherins in so-called adherens junctions, regions to which FAST proteins nonspecifically localize (Salsman et al., 2008; Y. Yang & Margam, 2021). At this stage, actin-mediated membrane protrusions presumed

to decrease the distance helping trigger the fusion reaction are observed (K. M. C. Chan et al., 2020, 2021; R. Duncan, 2019). As outlined in this thesis, we have reason to believe these actin-driven membrane protrusions are macropinocytosis-related membrane ruffles which are induced by FAST proteins. The fusion peptide and membrane-proximal external region (MPER) motifs found in the ectodomain and motifs present in the transmembrane (TM) domain are envisioned to cooperate in altering lipid hydration and lipid packing inducing positive curvature in the outer plasma membrane leaflet which mitigates tension in the membrane (R. Duncan, 2019; Read et al., 2015)

In the period prior to fusion, the FAST protein ectodomains are structurally dynamic, possibly permitting their reversible interaction with both the donor membrane as well as the closely apposed target membrane. In most fusion models the site of fusion is proposed to involve a highly curved membrane under tension (Akimov et al., 2020; Kozlov & Chernomordik, 2015; Martens & McMahon, 2008). The compression of the phospholipid heads of the outer leaflet occurring with donor membrane curvature results in negative curvature of the inner membrane. The juxta-membranous amphipathic helix (AH) motif residing in FAST protein endodomain functions as a lipid packing sensor resulting in FAST protein partitioning into and thus importantly stabilizing the tightly packed phospholipids in the inner membrane present in highly curved membranes. This characteristic, which is proposed to lower the energy barrier to pre-fusion donor-target membrane leaflet mixing, is seen in studies of liposomes of varying dimensions with the FAST protein p15 AH showing a predilection to bind to smaller (and thus more curved) vesicles (Read et al., 2015). Significantly, within the realm of FAST-mediated fusion, the AH domains are postulated to function as fusion-inducing lipid packing sensors (FLiPS) (Read et al., 2015). These domains, housed in the cytosolic endodomain of the FAST proteins, exhibit a hydrophobic helix-loop-helix structure, which demonstrates a predilection for insertion into high positive curvature membranes, akin to those found at the rim of nascent fusion pores. Further, these AH domains display substantial structural plasticity, manifesting as a spectrum of conformations from linear amphipathic helix-kink-helix structures to amphipathic helical hairpins (Giménez-

Andrés et al., 2018). This dynamic structural adaptability may be a critical aspect of their functional role in membrane fusion.

Once the FAST proteins are embedded in the outer leaflet of the curved donor membrane and closely apposed to an adjacent target cell membrane under actin-driven stresses, their structurally dynamic, myristoylated ectodomains can embed readily not only in a "cis" fashion to donor membranes but also into the outer leaflet of the target membrane thus serving as a critical fusion promoting tether (Corcoran & Duncan, 2004). At this stage of initial lipid intermingling between the outer contacting leaflets of the two bilayers an unstable transient hemifusion intermediate is generated (depicted as a stalk-like structure in Fig. 2A). It should be acknowledged that the discussion of stages as discrete entities is likely an oversimplification; and at the very least, one hypothetical stage likely overlaps significantly with the next. The labile hemifused stalk then either returns to a two planar bilayer configuration or progresses to a nascent fusion pore, a critical entity in cell fusion and frequently a point of no return for the process of cell fusion (Kawamoto & Shinoda, 2014; Lu et al., 2005; Risselada et al., 2014; Schwenen et al., 2015).

A successful membrane fusion reaction results in a fusion pore that, being only a few nanometers in diameter, initially has an energetically unfavorable high degree of rim curvature and thus, if it is not to be quickly resorbed, requires a rapid expansion to micrometer-sized macropore. Such pore enlargement is contingent upon the recruitment of the calcium-dependent membrane-binding protein annexin A1 (AX1) by the disordered endodomains of the membrane resident FAST protein. This results in the calcium-dependent activation of AX1 impacting membrane curvature and promoting membrane aggregation. In one study, both AXI knockdown and calcium chelation inhibited syncytium formation but not the inter-cellular transfer of small aqueous fluors, in keeping with a role for AX1 in pore expansion following pore formation (Ciechonska et al., 2014).

Exactly how annexins modulate membrane curvature is unclear although the annexin core domain which contains membrane attachment sites is shaped as a convex

disc (Huber et al., 1990); attachment at these sites may naturally lead to increased membrane curvature. In a recent study, AX1 along with AX2, of the nine annexins studied, were the only ones found to rapidly induce blebbing and vesiculation in planar membrane patches. This activity was ascribed to an asymmetric binding of annexin to the outer leaflet of the membrane and subsequent generation of a spontaneous curvature (Boye et al., 2018). Interestingly, the AX1 involvement observed in FAST protein associated pore expansion and syncytium formation, contrasting to its role in enveloped virus fusogens and both macrophage and myoblast fusion where Annexin A1 is a protein that can facilitate cell-cell fusion by binding to phosphatidylserine and inducing membrane cross-linking prior to hemifusion. Annexin A1 may also play a role in subsequent steps of the fusion process as the alteration of membrane curvature by annexins as well as dynamins during post-fusion pore expansion has been observed (Leikina et al., 2013, 2015; Richard et al., 2011; Verma et al., 2014).

It is unclear what the source of intracellular calcium that is also needed for pore expansion is, whether it is an influx through the cell membrane mediated by FAST protein porin activity or it is derived intracellularly by the formation of membrane-proximal AHs into calcium-conducting ion channels as has been documented for rotaviral nsp4 and picornaviral 2B viroporins (R. Duncan, 2019; Pham et al., 2017; van Kuppeveld et al., 1997). Another plausible source of increased intracellular calcium could be attributable to "leaky fusion," a process where disordered lipids in the plasma membrane during fusion render the membrane somewhat permeable. Regardless of the source, the modulation of calcium influx could be a significant contributor to the cytotoxicity induced by the FAST protein. Interestingly, recent studies have shown that amphiphilic nanoparticles can precondition two bilipid membranes to fuse when exposed to high concentrations of calcium, which is hypothesized to influence the outer leaflet. In this scenario, calcium effectively condenses the area-per-lipid of the inner leaflet, generating positive curvature in the outer leaflet. This asymmetry eventually drives trans leaflet contact and swiftly expands the stalk into a fusion pore (Tahir et al., 2020).

1.2.5. Myogenic cell fusion

Myogenic cell fusion, an essential process in myogenesis, is characterized by the intricate interaction of myoblasts, myotubes, and fusion-related proteins. This process begins with the activation of quiescent muscle stem cells, or satellite cells, residing beneath the basal lamina of mature muscle fibers. In response to muscular injury or physiological signals, these satellite cells proliferate and differentiate into myoblasts, which are primed for fusion (Lehka & Rędowicz, 2020). The myoblasts' commitment to a muscle-specific lineage is guided by the expression of myogenic regulatory factors (MRFs) like myogenic differentiation 1 (MyoD) and myogenic factor 5 (Myf5). This leads to the initiation of the fusion process, comprising two primary stages: the formation of multinucleated myotubes through myoblast-myoblast fusion, and the subsequent accretion of myoblasts to these newly formed myotubes, referred to as myoblast-myotube fusion (Zammit, 2017).

Key proteins play a crucial role in the fusion process. Cell adhesion molecules, including N-cadherin and integrins, enable the initial recognition and adhesion of myoblasts, leading to their alignment along the same axis (Y. Liu et al., 2021). Fusogenic proteins then mediate the merging of the plasma membranes, with proteins like Myomaker (Tmem8c) and Myomerger (Myomixer or Minion) in mice playing a pivotal role in the formation of nascent myotubes (Bi et al., 2017; Millay et al., 2013; Quinn et al., 2017; Q. Zhang et al., 2017). Additionally, Dysferlin protein contributes to the repair of the sarcolemma after fusion (Defour et al., 2014). Recently, Brain-specific angiogenesis inhibitor 3 (BAI3) has been identified as playing a significant role in myoblast fusion and muscle development. BAI3 interfaces between extracellular signals and the intracellular signaling machinery by binding with engulfment and cell motility (ELMO) proteins, facilitating the activation of the small GTPase Rac, thereby promoting myoblast fusion (Hamoud et al., 2014). Furthermore, signaling pathways like the Janus kinase/signal transducer and activator of transcription (JAK/STAT) pathway, induced by Interleukin-6 (IL-6), have been found to promote myoblast fusion (Trenerry et al., 2011).

Other pathways, including the insulin/IGF-1 signaling pathway and the PI3K/Akt pathway, also regulate their differentiation and function (Gardner et al., 2012; G. Wang et al., 2018). Despite significant advancements in understanding the process, the intricate molecular choreography governing myogenic cell fusion remains not fully deciphered.

1.2.6. Syncytiotrophoblast cell fusion

The syncytiotrophoblast, a multi-nucleated layer in the placenta, is formed and maintained through a complex process known as trophoblast fusion. This process involves the continuous merging of single-nucleated cytotrophoblast cells from the placental villi, which results in the formation of the placental barrier. This barrier is critical for nutrient exchange, gas exchange, and waste removal between the maternal and fetal circulations (Pfeffer & Pearton, 2012; Renaud & Jeyarajah, 2022). One key facilitator of trophoblast fusion is syncytin, a class I fusogen. Syncytin is a unique protein encoded by the human endogenous retrovirus-W (HERV-W) (Mi et al., 2000). Its primary role is to mediate the fusion of cytotrophoblasts, leading to the formation of the syncytiotrophoblast layer. Overexpression of syncytin has been implicated in the progression of certain cancers and autoimmune diseases, highlighting the importance of tightly controlled syncytin, expression during trophoblast fusion (Bjerregaard et al., 2006; Fei et al., 2019; Giménez-Orenga & Oltra, 2021).

1.2.7. Macrophage fusion

Macrophages, versatile components of the immune system, have an extraordinary capability that sets them apart from other immune cells: the ability to fuse together. This fusion capacity enables them to form specialized structures, such as Langerhans giant cells (LGCs), foreign-body giant cells (FBGCs) and osteoclasts, which play significant roles in various physiological and pathological processes (Pereira et al., 2018). For example some multinucleated macrophages have enhanced phagocytic capabilities, FBGCs can form in response to foreign bodies that are too large to be engulfed by single

macrophages, and osteoclasts have increased mitochondrial activity, as they are the primary cells responsible for the energetically taxing process of bone resorption and are essential for bone remodeling and maintenance (Ahmadzadeh et al., 2023; Kodama & Kaito, 2020).

Fusion of macrophages is a complex process triggered by specific cytokines, such as interleukin-4 (IL-4) for FBGCs, interferon (IFN) -γ for LGCs and receptor activator of nuclear factor kappa-B ligand (RANKL) inducing osteoclastogenisis (Ahmadzadeh et al., 2023; Novack & Teitelbaum, 2008; Pereira et al., 2018). This process is thought to involve the upregulation of certain fusion mediators, like E-cadherin and cluster of differentiation 47 (CD47) (X. Han et al., 2000; Helming & Gordon, 2009; Mbalaviele et al., 1995). Moreover, protein tyrosine phosphatase PTP-PEST, which interacts with and dephosphorylates various cytoskeleton-associated proteins, is believed to play a role in regulating cellular functions critical to fusion, such as migration, adhesion, proliferation, and transformation (Rhee et al., 2013). In addition to their primary roles in the body's defense against pathogens and bone remodeling, in certain contexts, fused macrophages can paradoxically stimulate tumor growth, underscoring the complexity of their role in health and disease.

1.2.8. Cancer cell fusion

First identified over a century ago, cancer cell fusion plays a pivotal role in the creation of polyploid giant cancer cells (PGCCs) within tumors (Carter, 2008; Parris, 2013; Pawelek, 2005). PGCCs are formed through cell fusion, emerging larger than regular cells, and demonstrating characteristics akin to those of cancer stem cells (CSCs), expressing markers that are typically found in both normal cells and stem cells, and also possess the ability to form tumors (Carter, 2008; Herbein & Nehme, 2020; Najafi et al., 2019). Intriguingly, it has been observed that chemotherapy may inadvertently promote cell fusion, thereby leading to an increased potential for drug resistance (Bjerregaard et al., 2006).

Human endogenous retroviruses (HERVs) have been suggested to play a role in the formation of PGCCs. For instance, under the influence of arsenic trioxide treatment, colon cancer cell lines fuse to form PGCCs via Syncytin-1 expression (Li et al., 2021). Oncoviruses such as Kaposi's sarcoma virus and Hepatitis B virus are also implicated in the induction of PGCC formation (Herbein & Nehme, 2020). For most oncoviruses that contribute to the formation of PGCCs, the mechanism typically involves virally induced dysregulation of mitotic division. However, the human papilloma virus 16 (HPV16) might be an exception to this rule. The HPV16 E5 viroporin protein is known to induce cell fusion and PGCC formation, and has been shown to influence the development of early cancerous lesions in the cervix (Cullen et al., 1991; Delespaul et al., 2019; Hu et al., 2009; Shirasawa et al., 1987). Besides cell fusion, E5 performs numerous other functions and further study is warranted to determine if cell fusion contributes to the oncogenic potential of HPV16 (Gutierrez-Xicotencatl et al., 2021). The formation of PGCCs often corresponds with highly malignant and invasive cancers, contributing to poor patient outcomes (Herbein & Nehme, 2020).

While there are limited examples supporting the notion that cell fusion results in highly malignant cancer, recent studies have illuminated the potential role of cell fusion in facilitating metastases. Several promising hypotheses have emerged suggesting that cell fusion may serve to amplify the aggressiveness of cancerous growths. Cancer heterotypic hybrid cell formation is a cell fusion phenomenon in which cancer cells fuse with non-cancerous cells in the tumor microenvironment (Gast et al., 2018; Tretyakova et al., 2022). This process can occur in various types of cancer cell types, including breast cancer, prostate cancer, and melanoma and tumor cell scan fuse with various types of cell types including mesenchymal cells and leukocytes (Bjerregaard et al., 2006; Chitwood et al., 2018; Danila et al., 2007; Gauck et al., 2017; Lartigue et al., 2020; Xue et al., 2015). Tumor cells can also fuse with macrophages to acquire immune evasion by presenting macrophage surface markers (Dietz et al., 2021; Gast et al., 2018). Macrophage cancer hybrids form the majority of the circulating tumor cell population and the number of macrophage cancer hybrids correlates with cancer stage and disease

outcome. The exact mechanisms and consequences of macrophage and cancer cell fusion are not fully understood, but it is thought to play a role in the progression and metastasis of certain types of cancer with cancer hybrid cells seeding new metastases. These cell fusion events can also lead to the creation of CSCs which are highly resistant to chemotherapy and radiotherapy and can lead to tumor recurrence and metastasis (Ding et al., 2012; Gauck et al., 2017).

1.3. The PI3K-Akt pathway

1.3.1. Phosphatidylinositol-3-Kinase Isoforms and Function

Phosphoinositide 3-kinases (PI3Ks) comprise a crucial family of enzymes that dictate the course of numerous cellular processes, including cell growth, proliferation, survival, and metabolism. They catalyze the transformation of phosphatidylinositol lipids into phosphorylated phosphoinositides, functioning as secondary messengers in an array of cellular signaling pathways (Bilanges et al., 2019; Deng & Liu, 2022; Fruman et al., 2017). These enzymes are divided into three distinct classes (I, II, and III) based on their substrate specificity and structural attributes. The eight known PI3K isoforms are dispersed across these classes. Class I PI3Ks are heterodimeric complexes that consist of a catalytic subunit (p110) and a regulatory subunit (p85). The regulatory subunits act as stabilizers and modulators of the catalytic subunits, regulating their kinase activity. Meanwhile, class II and III PI3Ks are monomeric enzymes that assemble into tetrameric complexes (Bilanges et al., 2019; L. Duncan et al., 2020; M. Zhang et al., 2020).

Class IA PI3Ks are activated downstream of plasma membrane-bound receptors, such as receptor tyrosine kinases and G protein-coupled receptors (GPCRs). Activation occurs via recruitment to the plasma membrane through binding of the SH2 domains in the regulatory subunit to tyrosine-phosphorylated proteins (Deng & Liu, 2022; Vanhaesebroeck et al., 2012). Once activated, the catalytic subunits of class IA PI3Ks phosphorylate phosphatidylinositol 4,5-bisphosphate (PIP(4,5)) at the plasma membrane to generate the lipid secondary messenger phosphatidylinositol 3,4,5-trisphosphate (PIP(3,4,5)). Class II and III PI3Ks primarily regulate membrane trafficking and indirectly control signaling. Class II PI3Ks can phosphorylate the 3’ prime position of either

phosphatidylinositol (PIP) and PIP(4) to produce PIP(3) or PIP(3,4) whereas Class III PI3Ks exclusively phosphorylates PIP to generate PIP(3) (Bilanges et al., 2019; Vanhaesebroeck et al., 2012).

The cellular concentrations of PIP(3,4,5) and PIP(3,4), which at most comprise less than 0.01% of phospholipids within the cell (Ebner et al., 2017; Ijuin & Takenawa, 2012). PIP(3,4,5) and PIP(3,4) concentrations are meticulously regulated by an array of phosphatases, such as the inositol lipid 3-phosphatase PTEN and various 5-phosphatases, including Src homology 2 (SH2)-containing inositol phosphatase 1 and 2 (SHIP1, SHIP2) inositol polyphosphate-4-phosphatase type I A and B (INPP4A, INPP4B) (Heinke, 2022; Posor et al., 2022; Vanhaesebroeck et al., 2012). PTEN converts PIP(3,4,5)and PIP(3,4) into PIP(4,5)and phosphatidylinositol 4-phosphate (PIP(4)), respectively (Martini et al., 2014). Concurrently, 5-phosphatases sequentially dephosphorylate PIP(3,4,5), generating PIP(3,4), PIP(3), and PIP, ultimately leading to the cessation of PI3K signaling. This intricate network of enzymes underscores the complexity of phosphoinositide regulation and its integral role in cellular function and homeostasis.

.

1.3.2. PI3k activation and signal transduction

Receptor Tyrosine Kinases (RTKs) are a family of cell surface receptors that play a crucial role in cellular signaling by transmitting extracellular signals to the interior of the cell. Upon binding of a receptor ligand, RTKs homodimerize or heterodimerize and autophosphorylate, which leads to the activation of downstream signaling pathways. One of the downstream pathways activated by RTKs is the PI3K pathway (Deng & Liu, 2022; Lemmon & Schlessinger, 2010). There are three ways in which RTKs can activate PI3K. The first method involves the direct binding of the p85 subunit of PI3K to the phospho-YXXM motifs on the activated RTK (M. Zhang et al., 2019). The second method is mediated by Growth Factor Receptor-bound Protein 2 (GRB2), which preferentially binds to the phospho-YXN motifs of the RTK (Lowenstein et al., 1992; Ogura et al., 1999). GRB2 can bind to the scaffolding GRB2-associated-binding protein (GAB), which in turn

can bind to p85 and activate PI3K (Jiang & Ji, 2019; M. Zhang et al., 2019). The third method of RTK-mediated activation of PI3K occurs via the binding of RTKs to Ras. GRB2 binds to and activates Son of Sevenless (SOS), which then activates Ras. Ras, in turn, activates p110 independently of p85, leading to the activation of PI3K. GRB2 can also exist in a large complex that contains SOS, Ras, and GAB or other scaffolding proteins, which brings these activators into close proximity to p110 subunit of PI3K (Cuesta et al., 2021; Krygowska & Castellano, 2018).

The enzyme's catalytic and regulatory subunits interact in various ways to maintain low enzymatic activity levels under normal conditions. Specifically, the catalytic subunit's helical, kinase, and C2 domains make contact with the p85-N-SH2 domain, while its C2 domain interacts with the p85-iSH2 domain (T. O. Chan et al., 2002; Kano et al., 2019; Sun et al., 2010). These additional connections serve to inhibit the enzyme's activity in the absence of external signals. However, when the regulatory subunit binds to phosphotyrosines, its SH2 domains release these inhibitory contacts and reposition the enzyme dimer near the cell membrane (Deng & Liu, 2022). This enables the enzyme to access its substrate and receive further inputs from Ras and other signaling components. The two isoforms of the PI3K catalytic subunit, p110α and p110β, have different modes of activation. While p110α interacts with Ras, a small GTPase protein, p110β is activated by Rac1 and cell division control protein 42 (Cdc42, which are also small GTPases (Bilanges et al., 2019; Deng & Liu, 2022; Martini et al., 2014). This distinction in activation mechanisms highlights the diversity in how different signaling pathways are regulated by the PI3K pathway and may have implications for developing targeted therapies for diseases where these isoforms play a role.

1.3.3. Phosphatidylinositol (3,4,5)-triphosphate

Phosphatidylinositol (3,4,5)-trisphosphate (PIP(3,4,5)) is a phospholipid molecule that is of utmost importance in cellular signaling and membrane organization (Manna & Jain, 2015; Riehle et al., 2013; Salamon & Backer, 2013). The class IA phosphoinositide 3-kinases (PI3K) phosphorylate phosphatidylinositol (4,5)-bisphosphate (PIP2) to produce

PIP(3,4,5). PIP(3,4,5) serves as a membrane organizer and has multiple functions that significantly impact the physical properties of the plasma membrane.

The regulation of membrane curvature is a complex process that involves the participation of various molecules. PIP(3,4,5) is one such molecule that plays a crucial role in the formation of membrane structures such as invaginations and protrusions. These structures are essential for several cellular processes, including endocytosis, exocytosis, and cell migration. The negatively charged head group of PIP(3,4,5) recruits positively charged regions of proteins, thereby facilitating the recruitment of proteins such as dynamin, Epsin, and BAR-domain proteins (Basquin et al., 2013; Coutinho-Budd et al., 2012; Goldenberg & Steinberg, 2010; Itoh et al., 2001). These proteins are known to possess the ability to bend the membrane, thus contributing to the regulation of membrane curvature (Lemmon, 2008). For protein recruitment, PIP(3,4,5) serves as a docking site for proteins containing specific lipid-binding domains, such as the PH (pleckstrin homology), FYVE, and PX domains (Banerjee et al., 2010; Lemmon, 2007). Examples of proteins recruited by PIP(3,4,5) include Akt (a serine/threonine kinase), phospholipase C-γ (PLC-γ), and guanine nucleotide exchange factors (GEFs) for the Rho family GTPases (Carretero-Ortega et al., 2010; P.-W. Chen et al., 2022; H.-S. Li et al., 2003; Mahankali et al., 2011).

In relation to the remodeling of the actin cytoskeleton, PIP(3,4,5) has the ability to enlist and activate proteins that are involved in actin cytoskeleton remodeling, such as Rho family GTPases (e.g., Rac, Rho, and Cdc42) and their downstream effectors, namely, WASP (Wiskott-Aldrich syndrome protein) and WAVE (WASP-family verprolin-homologous protein). These modifications in the actin cytoskeleton can result in changes to the shape and tension of the plasma membrane, which can subsequently impact cellular processes such as adhesion, migration, morphogenesis, and actin based membrane protrusions (Bretschneider, Anderson, & Ecke, 2009; Chang et al., 2005; Jiménez et al., 2000; Takahashi & Suzuki, 2011; Zhou et al., 2020).

PIP(3,4,5)triggers multiple signaling pathways, showcasing its diversity in cellular functions. For instance, PIP(3,4,5) recruits and activates Akt (Protein Kinase B),

influencing cell survival and growth. It also facilitates the membrane recruitment of PDK1 (3-Phosphoinositide-Dependent Protein Kinase 1), which in turn activates Akt and other kinases. Additionally, PIP(3,4,5) interacts with proteins such as Rac1 and Cdc42, affecting cell motility and shape. Therefore, PIP(3,4,5) serves as a signaling nexus, directing an array of cellular processes.

1.3.4. Akt isoforms, activating phosphorylations, and known functions

The Akt family, consisting of three highly homologous isoforms—Akt1, Akt2, and Akt3—plays a critical role in the regulation of numerous cellular processes (Hinz & Jücker, 2019; J. Wang et al., 2018). These serine/threonine kinases have been extensively studied due to their involvement in cell growth, proliferation, survival, and metabolism (Yudushkin, 2019). Dysregulation of Akt signaling has been implicated in several pathological conditions, including cancer, diabetes, and neurological disorders. To better understand the diverse functions and regulation of Akt isoforms, this background section will provide an overview of their structural features, activation mechanisms, phosphorylation patterns, and known roles in physiological and pathological contexts.

All three Akt isoforms share a highly conserved structure, comprising an N-terminal pleckstrin homology (PH) domain, a central kinase domain, and a C-terminal regulatory domain. Despite their structural similarities, the isoforms exhibit distinct tissue expression patterns and substrate specificities, suggesting unique roles in cellular processes (J. Wang et al., 2018). Akt1 is ubiquitously expressed, whereas Akt2 is predominantly found in insulin-responsive tissues, and Akt3 expression is mainly restricted to the brain and testes (Hinz & Jücker, 2019). Akt activation occurs through a complex signaling cascade initiated by growth factors, cytokines, and other extracellular stimuli. Key components of this cascade include receptor tyrosine kinases, PI3K, and PDK1. The binding of growth factors to their cognate receptors leads to PI3K activation, which in turn generates PIP(3,4,5). PIP(3,4,5) recruits both Akt and PDK1 to the plasma membrane, facilitating Akt phosphorylation by PDK1 and subsequent full activation by

mammalian target of rapamycin complex 2 (mTORC2)-mediated phosphorylation (Yudushkin, 2019).

The phosphorylation dynamics of Akt isoforms are crucial for their activation and downstream signaling. Akt is typically phosphorylated at two key residues: the activation loop within the kinase domain (Thr308 in Akt1, Thr309 in Akt2, and Thr305 in Akt3) and the hydrophobic motif within the C-terminal regulatory domain (Ser473 in Akt1, Ser474 in Akt2, and Ser472 in Akt3) (Yudushkin, 2020). Isoform-specific phosphorylation events and their implications for substrate specificity and signaling outcomes are still being explored (Gao et al., 2014). Substrates of Akt include the forkhead box proteins (FOXOs), which upon phosphorylation by Akt are inhibited from promoting apoptosis and cell cycle arrest, and glycogen synthase kinase 3 beta (GSK-3β), which is involved in glycogen synthesis and when phosphorylated by Akt is inactivated, promoting cell survival and growth (Manning & Toker, 2017; Song et al., 2005; Yudushkin, 2020). Another key substrate of Akt is the mechanistic target of rapamycin (mTOR), a protein that regulates cell growth, cell proliferation, and protein synthesis. When Akt phosphorylates mTOR, it enhances its activity, promoting protein synthesis and cell survival (Manning & Toker, 2017; Song et al., 2005; Yudushkin, 2020).

1.4. Macropinocytosis

1.4.1. Macropinocytosis overview

Eukaryotic cells are capable of internalizing different types of cargo by plasma membrane ruffling and forming vesicles in a process known as endocytosis. The most extensively characterized endocytic pathways are arguably endocytosis by clathrin-coated pits, lipid raft/caveolae-mediated endocytosis and phagocytosis (Doherty & McMahon, 2009). A fourth is macropinocytosis (MaPi), defined as the nonselective endocytic process driven by the actin cytoskeleton and involving internalization of extracellular fluid, solutes, and membrane into large vesicles (0.2 to as many as 5 μM in diameter) known as macropinosomes (Kay, 2021). Its functions are manifold; in addition to the “eating and drinking” observed in life forms such as the soil dwelling

eukaryotic amoeba *Dictyostelium discoideum* (Kay et al., n.d.), MaPi is observed in phagocytes, T cells, B cells, and neurons subserving antigen presentation, nutrient sensing, cell migration, and signaling. Given the capacity of macropinosomes, it can also serve as a means of host cell entry by viruses and bacteria (García-Pérez et al., 2003; Mañes et al., 2003). In addition, rapid plasma membrane remodeling as well as change in overall cellular volume can occur by internalization of large membrane patches into macropinosomes (Donaldson et al., 2009; Freeman et al., 1979).

1.4.2. Immune defense and macropinocytosis

MaPi is also involved in immune defense, as it allows immune cells such as macrophages to take up and eliminate pathogens, such as bacteria and viruses (BoseDasgupta & Pieters, 2014). More importantly, MaPi by both dendritic cells and macrophages samples the environment for foreign proteins enabling presentation of oligopeptide fragments to major histocompatibility (MHC) complex class I and class II molecules (A et al., 2006; Canton, n.d., 2018; Lim et al., 2012). MHC I and MHC II peptide complexes are recognized by CD8+ (cytotoxic) and CD4+ (helper) T cells, respectively to initiate T cell response against a pathogen. In distinction from transformed cells in which MaPi is induced, MaPi observed in macrophages appears more constitutive in nature. The exact degree to which MaPi serves as a source of foreign proteins versus the more traditional phagocytosis is currently unclear (Canton, 2018). In addition to macrophages and dendritic cells, MaPi is also observed in B cells (Charpentier et al., 2020; García-Pérez et al., 2003) as well as recently being shown to be an important source of extracellular proteins and amino acids helping fuel mTORC1 enabled T cell activation (Lim et al., 2012).

1.4.3. Nutrient uptake and macropinocytosis

It was originally thought that mammalian cells exclusively used transmembrane transporter proteins and complexes and traditional endocytosis to acquire bulk nutrients for the supply of components for cellular synthesis as well as energy. It has since been

appreciated that this may not exclusively be the case. Indeed, much of the energy and chemical matter existing in the extracellular space is comprised of complex macromolecules, for example in proteins rather than individual amino acids. These can serve as important nutrient sources but are clearly ill suited for cellular entry by bespoke transporters. Rather, the comparatively large macropinosomes may carry such macromolecules from the immediate cellular environment, targeting them to the lysosome where hydrolases break them down into their constituent amino acids, lipid and carbohydrate parts thereby creating an intracellular source of energy and anabolism (Palm, 2019).

1.4.4. Cancer and macropinocytosis

The study of cancer has been instructive with the realization that activating point mutations in oncogenes, such as the RAS (Rat sarcoma virus) small GTPase, dramatically stimulate cancer cell MaPi both *in vitro* (Bar-Sagi & Feramisco, 1979) and *in vivo* (Commisso, 2019; Seguin, n.d.). Members of the RAS family, (HRAS, KRAS, and NRAS) are the most frequently mutated oncogenes in common human tumours including lung, colorectal, and pancreatic cancer. Activating KRAS mutations are observed in 84% of all RAS-mutant cancers and are observed in nearly 100% of the usually fatal pancreatic ductal adenocarcinoma (Waters & Der, 2018). It was demonstrated that, analogous to the axenic (i.e. not living on live prey) variant slime mold *Dictyostelium*, the increased MaPi serves as a critical nutrient delivery pathway in cancer cells (Commisso et al., 2013; Lambies & Commisso, 2022) with the ensuing lysosomal degradation of macropinocytosed extracellular proteins (Lawrence & Zoncu, 2019) supplying an important source of nutrients and energy in what are frequently harsh environments.

1.4.5. Mechanism of macropinocytosis induction by receptor tyrosine kinase activation of ras

In addition to illuminating the potential anabolic role of MaPi in cancer cell “feeding”, cancer studies have revealed the interplay between MaPi and cell signaling. In this

regard, although sharing common mechanisms of action, MaPi can either be induced (e.g. by growth factors in cancer and other cells) or constitutive (e.g. in macrophages and dendritic cells). In reality, Ras-mutant tumor cells, as exemplars of inducible cells, normally express low levels of MaPi; to macropinocytose they need epidermal growth factor (EGF) binding to the tyrosine kinase receptor EGFR (Araki et al., 2007; Nakase et al., 2015). In addition to EGF, platelet derived growth factor (PDGF), macrophage colony stimulating factor (M-CSF) and the chemokine CXCL12, have all also been shown to induce MaPi in a variety of cells (Lambies & Commisso, 2022).

Ras is next activated by the liganded EGFR or another receptor tyrosine kinase (RTK) through exchange of bound guanosine diphosphate (GDP) guanosine triphosphate (GTP) (Simanshu et al., 2017).The Ras guanine exchange factor (GEF) Son of Sevenless (SOS) and growth factor receptor bound protein 2 (Grb2) both then bind to phosphotyrosine residues on activated RTKs. The ensuing translocation of this complex to the plasma membrane brings SOS in close contact with Ras, leading to its conversion to the GTP-bound, active state. The regulatory p85 subunit of PI3-kinase then binds to phosphotyrosine residues on the RTK (e.g. EGFR), which induces a conformational change that relieves autoinhibition of the p110 catalytic subunit (Krygowska & Castellano, 2018). Simultaneously, recruitment of PI3-kinase to RTKs brings the enzyme together with its substrate lipid PIP2 in the cytosolic leaflet of the plasma membrane. Translocation of PI3-kinase to the plasma membrane is further supported by interaction of its Ras-binding domain with activated Ras (Gupta et al., 2007). In this fashion, RTKs recruit PI3-kinase to the plasma membrane through binding directly to the regulatory p85 subunit, and indirectly through activation of Ras.

1.4.6. The molecular underpinnings of macropinocytosis

Although the exact mechanism of MaPi initiation is not known, it appears the binding of GTP-Ras to the Ras-binding domains of PI3K catalytic subunits especially p110α may fuel local generation of PIP(3,4,5) rich patches (Porat-Shliom et al., 2008). Such a PIP(3,4,5) domain could direct dendritic actin polymerization to the extending lip of

macropinocytic cups by recruiting a ring of the SCAR/WAVE complex and thus activating the actin related protein (Arp) 2/3 complex. Much of what we know about the ensuing process comes from the soil dwelling eukaryotic amoeba *Dictyostelium*, where both MaPi and the closely related cell migration related pseudopod formation have been intensively studied (Veltman et al., 2012).

The actin geometry in macropinocytic cups can be viewed through the lens of actin waves, closed structures with a ring of actin polymerization encircling a central PIP(3,4,5) domain, a subset of which will progress to MaPi (Bretschneider, Anderson, & Ecke, 2009; Gerisch et al., 2019a; Veltman et al., 2016). Cryo-electron microscope tomography shows that the central area of the wave largely consists of actin filaments parallel to the membrane packed more densely than elsewhere in the membrane while the tip of wave contains a branched or dendritic actin network (Jasnin et al., 2019). The dendritic network is largely generated by the Arp2/3 complex, recruited by the SCAR/ WAVE. Arp2/3 can be found at 70° junctions between fibers, generating novel fibers that point predominantly outwards toward the membrane and possibly are a source of outward force as they extend (Kay et al., 2022). The accumulation of the SCAR/WAVE and Arp2/3 complexes at the periphery of PIP(3,4,5) patches provides a general mechanism for forming cups in the plasma membrane, not only in MaPi but also in circular dorsal ruffles and in phagocytosis (Veltman et al., 2014).

When viewing this process in terms of our FAST protein cell fusion pathway, *Dictyostelium* work emphasizes the importance of the signaling axis of Ras, Ras-activated PI3K, and the protein kinases Akt and serum and glucocorticoid-regulated kinase (SGK) together with associated regulators neurofibromin 1, PTEN, mTORC2, and PDK1 in MaPi. Specifically, activation of mTORC2 and substrates of the Akt family kinases, along with the PI3K that catalyze the conversion of PIP2 into PIP(3,4,5), can be found at the growing edge of the nascent macropinosome cup, in addition to Ras and Rac family GTPases (Kay et al., 2022; Williams et al., 2019). Furthermore, deletion of PI3K, double deletion of the Akt and SGK protein kinases, or deletion of either of their activators PDK1 and TORC2,

all block MaPi, and as I determined they similarly inhibit p14 mediated cell fusion (Kay et al., 2022; Veltman et al., 2014).

1.4.7. Macropinocytosis fission

MaPi is a form of endocytosis characterized by the formation of macropinosomes, cellular compartments enclosed by the plasma membrane. While the process bears similarities to other endocytic pathways, the membrane fission mechanism in MaPi is less well understood. Technological advancements in live microscopy have, however, proposed multiple potential mechanisms for macropinosome closure. In each case, the closure of a macropinosome results from plasma membrane fission, creating a distinct vesicle separate from the cell's cytoplasm. This final step shares features with membrane fusion as it requires merging different regions of the plasma membrane. A variety of proteins have been implicated in this process. For instance, the activation of C-terminal-binding protein/brefeldin A ADP-ribosylated substrate (CtBP1/BARS) by p21-activated kinase (Pak1) is known to mediate membrane curvature. CtBP1/BARS is also necessary for MaPi cup closure and the deactivation of Rac1 which is essential in the formation of the macropinocytotic cup and membrane ruffles.(Liberali et al., 2008; Yoshida et al., 2009, 2015). The original proposed mechanism of MaPi fission involves a "purse-string" approach, where a contractile ring made predominantly of polymerizing actin proteins encircles the intended fission area (Buckley & King, 2017; King & Kay, 2019). As the contractile ring contracts, akin to a closing drawstring, it draws the two membrane edges closer, eventually leading to their pinch-off potentially by a dynamin like protein and the formation of two separate membranes (King & Kay, 2019). Some intermediate stages in membrane fission bear similarities with membrane fusion. Both processes, for instance, involve the formation of hemifused or partially divided structures composed of highly curved membranes (Mattila et al., 2015). However, despite the similarity in protein utilized and intermediate, the critical difference lies in the outcomes: membrane fusion results in the merging of two membranes, while fission leads to their separation.

1.5. Rationale and objectives

FAST proteins exhibit minimalistic structures and operate within the cellular milieu, suggesting that they may co-opt host machinery for cell fusion. Kinases play a vital role as signaling control hubs within cells, and thus, utilizing medium content screens to investigate which kinases are essential for FAST-mediated fusion serves as an efficient preliminary step in identifying the cellular components that act as cofactors for fusion. Through the identification of necessary kinases, such as PI3K and Akt, and by analyzing the indispensable downstream signaling mediators and spatiotemporal localization of their signaling during cell fusion, this study was able to identify MaPi as a necessary process for fusion. The subsequent question that arises is whether the involvement of these kinases in fusion and MaPi is unique to FAST proteins or if other fusogens, both structurally similar and dissimilar to FAST proteins, also rely on this process.

To achieve the desired outcomes of this study, several objectives have been outlined. First, we will investigate the necessary kinases, such as PI3K and Akt, in FAST-mediated fusion, which will help us understand the cellular components involved in the fusion process. Next, we aim to determine the indispensable downstream signaling mediators and spatiotemporal localization of their signaling during cell fusion, allowing us to gain insights into the mechanisms that drive the fusion event. Furthermore, we will establish the role of MaPi in FAST protein-mediated cell fusion, shedding light on the cellular processes that facilitate fusion. Finally, our goal is to examine whether the relationship between the identified kinases, fusion, and macropinocytosis is unique to FAST proteins or if it is shared by other fusogens with different structural features, thereby broadening our understanding of the factors that govern cell fusion across various fusogens. By addressing these objectives in a systematic manner, this study aims to contribute significantly to the existing knowledge of cell fusion processes and their underlying mechanism.

A

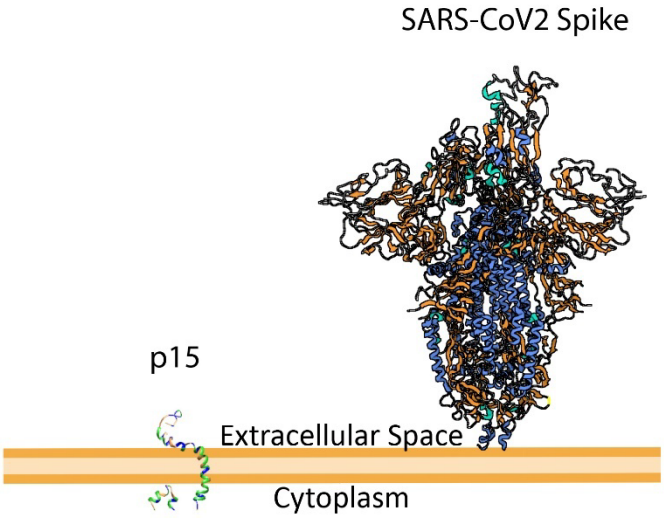
SARS-CoV2 Spike
p15
Extracellular Space
Cytoplasm

B

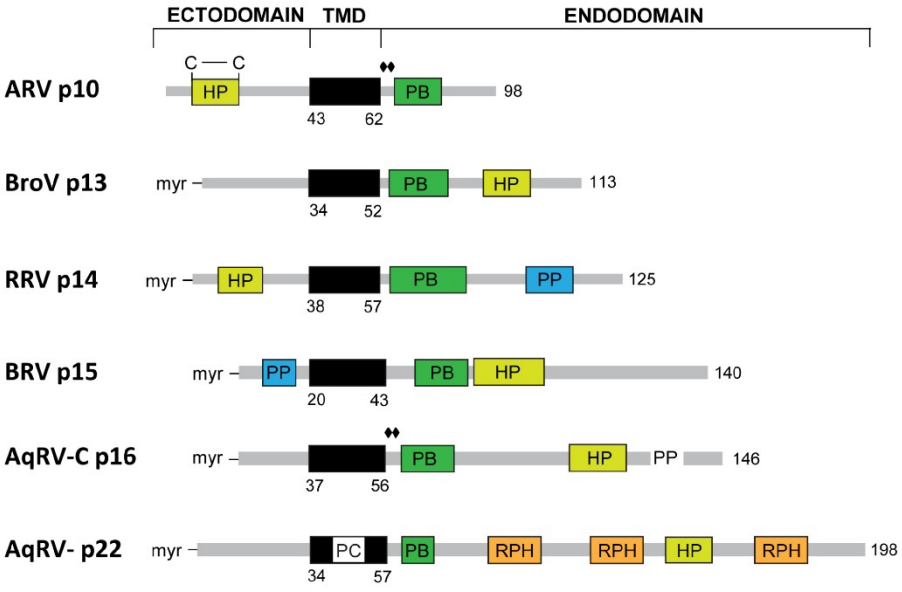
ECTODOMAIN
TMD
ENDODOMAIN
ARV p10
C — C
HP
PB
98
43
62
BroV p13
myr
PB
HP
113
34
52
RRV p14
myr
HP
PB
PP
125
38
57
BRV p15
myr
PP
PB
HP
140
20
43
AqRV-C p16
myr
PB
HP
PP
146
37
56
AqRV- p22
myr
PC
PB
RPH
RPH
HP
RPH
198
34
57

1.6. Figure 1: Comparative analysis of p14 FAST protein and SARS-CoV-2 Spike protein.

A. Schematic representation of p14 FAST protein (left) and SARS-CoV-2 spike protein (right) embedded in a cell plasma membrane. The p14 FAST protein contains a fusion peptide region and a transmembrane domain, which are essential for its fusogenic activity. In contrast, the SARS-CoV-2 spike protein exhibits a more complex structure, with a receptor-binding domain responsible for recognizing and binding to host cell receptors, a fusion peptide region facilitating the fusion process, a heptad repeat region promoting the structural rearrangement necessary for membrane fusion, and a transmembrane domain anchoring the protein in the viral membrane. These distinct structural features determine their respective cell-cell fusion mechanisms and efficiencies. **B.**Diagrammatic representation of the fusion-associated small transmembrane (FAST) protein family, which is encoded by orthoreoviruses and aquareoviruses, as adapted from the work of Boutilier and Duncan in 2011 and Marta Ciechonska, 2014. Each protein within this family incorporates a singular transmembrane domain (TMD), as designated by the amino acid residues highlighted underneath. FAST proteins include p10 from avian and Nelson Bay reovirus (ARV and NBV), p13 from Broome reovirus (BroV), p14 from reptilian reovirus (RRV), p15 from baboon reovirus (BRV), and p16 and p22 from group-C and group-A Aquareovirus (AqRV-C and AqRV). All contain a cytoplasmic region abundant in basic amino acids, depicted in green, and a hydrophobic section, colored in yellow. Additionally, RRV p14 includes a "FLiPS" motif, displayed in red. The RRV p14 also houses a poly-proline (PP) helix within its endodomain, shown in blue. Conversely, BRV p15 possesses the PP helix within its ectodomain. All FAST proteins are modified by acylation, either through the N-terminal myristic acid (myr), seen in RRV p14, BRV p15, and AtRV p22, or by the attachment of two palmitic acids (represented as diamonds) situated adjacent to the membrane in the endodomain of ARV and NBV p10. Furthermore, AtRV p22 features three regions abundant in arginine, proline, and histidine (RPH), denoted in orange. The length of each protein is indicated at the right end of each depiction.

A

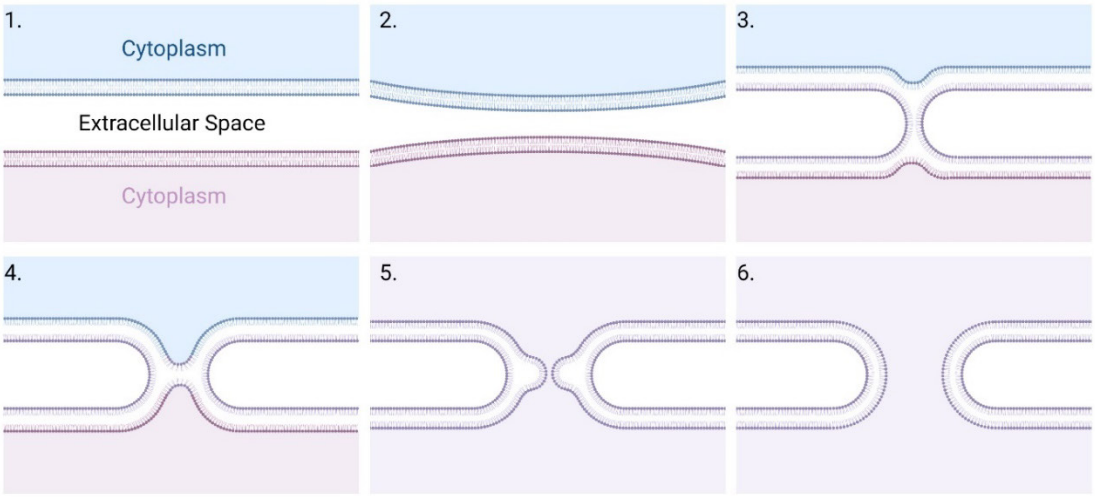
1.
Cytoplasm
Extracellular Space
Cytoplasm
2.
3.
4.
5.
6.

B

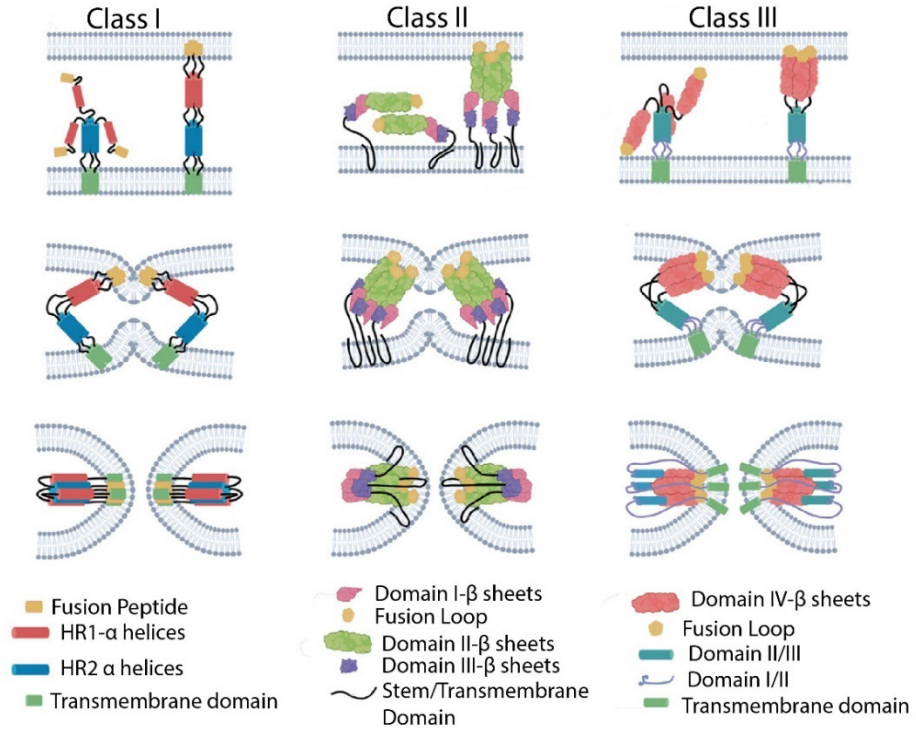
Class I
Class II
Class III
Fusion Peptide
HR1-α helices
HR2 α helices
Transmembrane domain
Domain I-β sheets
Fusion Loop
Domain II-β sheets
Domain III-β sheets
Stem/Transmembrane Domain
Domain IV-β sheets
Fusion Loop
Domain II/III
Domain I/II
Transmembrane domain

1.7. Figure 2. Models of the mechanisms of membrane fusion by Enveloped Virus Class I, II, & III fusion proteins.

This description has been adapted from the work of Sapir and colleagues (Sapir, Avinoam et al., 2008). **A.** A series of schematics illustrating the six stages of cell-cell fusion intermediates: **(1)** Cell-cell adhesion, in which proteins on the surface of two cells interact, enabling the cells to establish a close contact; **(2)** Tight membrane apposition, wherein the plasma membranes of the two cells are brought into close proximity, preparing them for fusion; **(3)** Hemifusion stalk formation, during which the lipid bilayers of the two cells begin to merge at the point of contact; **(4)** Hemifusion diaphragm formation, where the outer leaflets of the lipid bilayers have fused, while the inner leaflets remain separate, creating a thin barrier between the cells' cytoplasm; **(5)** Fusion pore formation, in which a small aqueous channel is established between the two cells, allowing for limited exchange of cellular contents; and **(6)** Fusion pore expansion, whereby the fusion pore enlarges, permitting the mixing of cytoplasmic contents and resulting in complete cell-cell fusion. This stepwise process facilitates efficient cell-cell fusion mediated by the p14 FAST and SARS-CoV-2 spike proteins. **B.** The diagram illustrates the structures of Class I, II, and III viral fusogens. Fusion peptides or loops are highlighted in orange. The Class I fusogen includes HR1 alpha helices in red and HR2 alpha helices in blue, along with a green transmembrane domain. In Class II, the fusogen structure comprises Domain I beta sheets colored in pink, Domain III beta sheets in purple, and Domain II beta sheets in green. The Class III fusogen exhibits a distinct Domain IV in globular red and Domain I/II presented in green. The structure prior to fusion in class I enveloped virus fusogen comprises two alpha-helical domains, which hide the N-terminal fusion peptide. Once the protein is activated, it results in the formation of coiled coil domains and reveals the fusion peptide. This, combined with its interaction with the host membrane and the folding back of the fusion protein, leads to a close approach of the membranes and the mixing of lipids. The pre-fusion structure of the class II enveloped virus fusogen consists of beta-sheets positioned tangent to the plasma membrane. Each monomer's apex contains internal fusion loops. When activated, the fusion loops are exposed, and the fusion proteins form a trimer, interact with the host membrane, and fold back. This sequence brings the membranes into close proximity. The fusogens in class III enveloped viruses contain fusion loops akin to those in class II fusogens, but instead of being embedded in beta-sheets, these are attached to alpha-helices.

Chapter 2: Materials and Methods

2.1. Cell Lines

The entire cultivation process was executed at 37°C with an atmosphere containing 5% CO_2. General cultivation saw cells grown until they reached 80% confluence, after which they were divided in a 1:5 ratio every 48 hours (h). However, the growth procedure for C2C12 mouse muscle myoblasts was different; these were allowed to grow until 60% confluence was achieved and were then divided in a 1:20 ratio every other day.

The growth medium varied based on the cell type. Quail muscle fibroblast (QM5) cells were cultured in a 199 medium, complete with Earle's salts (Invitrogen) and supplemented with 10% heat-inactivated fetal bovine serum (FBS) (Invitrogen). Vero cells were also grown in the same 199 medium combined with Earle's salts but supplemented with 5% FBS. On the other hand, HT1080, HeLa and human embryonic kidney (HEK) cells were grown in Dulbecco's modified Eagle medium (DMEM) that was enriched with 10% FBS and 25 mM HEPES.

2.2. Primary antibodies:

Primary antibodies: The polyclonal anti-RRV p14 rabbit antiserum has been previously described (Corcoran and Duncan, 2004). Additional primary antibodies utilized in this study include monoclonal anti-Akt and anti-phospho-Akt(473) antibodies, obtained from Cell Signalling (Catalog 9272, 4060), anti-phospho-AKT(308) (Cell Signaling #13038), anti-PKC-Alpha (PKCalpha Cell Signaling 2056), anti-Sin1 (Cell signaling 12860), Phospho-SinT87 (Cell Signaling 14716), Myomerger (R&D AF4580), and MHCII antibodies. We also used the monoclonal SARS-CoV2 Spike (ELabBiosciences #E-AB-V1006), pS6 (Cell Signaling, 2211s), S6K (Cell Signaling, 2217ss), and 4EBP (Cell Signaling, 9644)antibody in the experimental procedures.

Secondary antibodies: Polyclonal anti-rabbit horseradish peroxidase (HRP) and anti-mouse HRP were purchased from Cell Signaling Technologies. Polyclonal anti-rabbit Alexa Fluor 647 antibody was obtained from Thermofisher Scientific.

2.3. Plasmids

The research conducted for this study was greatly facilitated by several generously donated plasmids. John Cooper (Washington University in St. Louis) gifted us with two plasmids, BOB-LCK-GFP and pBOB-LCK-tdTomato, which were designated as Addgene plasmids #118738 and #118739 respectively (RRID:Addgene_118738 and RRID:Addgene_118739). We received the pcDNA3-PH(Akt)-GFP plasmid from Craig Montell (UC Santa Barbara) (Addgene plasmid #18836, RRID:Addgene_18836), which we subsequently cloned into a pljm1 backbone to create the HeLa-TRE-p14-rTA3 (TetOn-p14-HeLa). Additionally, David Sabatini (Massachusetts Institute of Technology) provided us with the Raptor_1 and Raptor_2 shRNA plasmids (Addgene plasmid #1857 and #1858, RRID:Addgene_1857 and RRID:Addgene_1858, respectively), as well as the Rictor_1 and Rictor_2 shRNA plasmids (Addgene plasmid #1853 and #1854, RRID:Addgene_1853 and RRID:Addgene_1854, respectively).

To perform Sin1 knockdown, we utilized Addgene plasmids #13483 and #13484, denoted as mSin1 shRNA#1 and mSin1 shRNA#2, respectively. The PKC shRNA plasmids V2LHS_170435 and V3LHS_318575 from the GIPZ library were used, along with the NSshRNA from the same library. Eric Pringle (Dalhousie University) contributed the Sars-Cov2 Spike plasmid in pcDNA3, pLJM1-B*-BSD-ACE2 (for the 293A-ACE2/TMPRSS2 cells), and PLJM1-Bpuro-TMPRSS2. The pLVX-Mymg (Myomerger) and pBabe-X-Tmem8c (Myomaker) plasmids were gifts from Douglas Millay (University of Cincinnati), subsequently cloned into pLJM1-B-Puro-TRE and pLJM1-B* by Nichole McMullen (Dalhousie University).

Plasmid constructs containing RRV p14, p14 G2A, p14C88, and BRV p15, as described in previous literature (Dawe and Duncan 2002, Corcoran and Duncan 2004, Noyce, Taylor et al. 2011), were also used. Additionally, the pLJM1-B*-Puro-TRE-p14-mRuby2 construct was cloned by Nichole McMullen from pcDNA3-p14 mRuby2-Lifeact-7, a gift from Michael Davidson (Addgene plasmid #54674, RRID:Addgene_54674). Nichole McMullen also contributed the previously undescribed pLJM1-B*-BSD-PH(AKT)-GFP domain and PLJM1-B*-BSD-eGFP plasmids. The pLJM1-B*-puro-tre-p14 construct was

produced by Katie Proudfoot (Dalhousie University), and rtTA3 plasmids to control dox induction were supplied by Craig McCormick (Dalhousie University).The collective contributions of these researchers have significantly aided the progress of our study.

2.4. BRV p15 kinome inhibitor and siRNA fusion screens

For the BRV p15 Kinase inhibitor and siRNA fusion screen, HT1080 cells were transfected with pcDNA3.1-Tre-p15 and pLenti-CMVrtTA3-hydro and maintained under hygromycin and puromycin selection. For the siRNA screen, 2.5 x 10^3 cells per well, and for the kinase inhibitor screen, 5 x 10^3 cells per well were seeded into 384-well dishes. 24 hours post-seeding, the kinase inhibitor screen was initiated by exposing cells to 258 distinct small molecule kinase inhibitors, in triplicate, at concentrations of 0.025, 0.25, and 2.5µM. Alongside this, cell fusion was triggered with a doxycycline (DOX) treatment (5 µg/ml).

The siRNA screen involved reverse transfection of 2130 unique siRNA sequences, targeting 710 kinases. To execute this, Lipofectamine reagent and siRNA, pre-distributed in the 384-well plate, were independently diluted in Opti-MEM reduced serum medium. After a brief incubation, the two solutions were mixed gently and incubated for an extra 20 minutes at room temperature, facilitating the formation of siRNA-Lipofectamine complexes. The complexes were then evenly distributed across each well. Next, the HT1080 cells, in appropriate growth medium, were added to the wells ensuring immediate exposure to the complexes. Post-seeding, the plate was placed in a humidified incubator set at 37°C and 5% CO2. Following a 36-hour incubation period for gene silencing, p15 expression was induced using a doxycycline treatment.

For both screens, 24 hours after doxycycline induction cells were fixed with 4% paraformaldehyde for 20 minutes. Subsequently, staining was performed using CellMask deep orange for cytoplasm and Hoescht 33342 for nuclei, in accordance with the manufacturer's instructions. The Opera high content screening system captured 15 images per well using a 20x objective air lens. For fusion quantification, the Columbus software automated the process of counting nuclei per cell. Syncytial cells with over 4 nuclei were classified as having undergone fusion. Treatments resulting in over a 33%

decrease in total nuclei count, compared to untreated controls, were excluded from the final analysis.

2.5. Lentivirus production and generation of cell lines

Lentivirus particles were produced by co-transfecting HEK293T cells with packaging plasmids psPAX2 and pMD2.G and the appropriate lentiviral expression plasmid. The various lentiviral expression plasmids are as follows: pLJM1-Akt(PH)-GFP, pLJM1-B*-Puro-TRE-p14, pLJM1-B*-Puro-TRE-p14-mRuby2, pLenti-CMV-rtTA3-hygro, pLenti-CMV-rtTA3-BSD, pLJM1-B*-Puro-TRE-Mymg, pLJM1-B*-BSD-Tmem8c or shRNA vector. Supernatants were harvested 48 to 72 h post-transfection and filtered through 0.45 µm filters (Millipore).

Cells were seeded in 6-well dishes at density of 50,000 and 24 h later were transduced with serial dilutions of lentivirus containing the vectors listed above. Subsequently, cell lines were placed under antibiotic selection for 72 h then transferred to 175 cm^2 cell culture flasks and allowed to divide until 70% confluent, then trypsinized and frozen in cell culture media with 10% dimethyl sulfoxide (DMSO) and kept in liquid nitrogen.

2.6. Cell fusion experiments

Stable cell line with a DOX inducible p14 (TetOn-p14) was created by transducing HeLa cells with pLJM1-B*-Puro-TRE-p14 and pLenti-CMV-rtTA3-hygro as described above. For cell fusion experiments, 1.5 x 10^5 TetOn-p14 HeLa cells were seeded in 12 well dishes and the next day were induced to fuse with doxycycline (5 µg/ml) for 5 h and then treated with small molecule inhibitors for 9 h in the presence of doxycycline. Cells were then fixed with 4% paraformaldehyde and stained with wheat germ agglutinin (WGA) - Alexa 594 and Hoechst. Images were acquired with the 10x objective on the Axio observer microscope. To minimize variation arising from user bias, the same 5 regions within each well were selected for imaging using Zen Blue sample carrier setup. The ImageJ Stardist nuclei detection plugin was used to automate syncytial and total nuclei

identification and quantification after syncytia were manually annotated. The fusion index was then calculated by the ratio of syncytial nuclei (nuclei in cells containing greater than 4 nuclei) to total nuclei within a field of view. The relative fusion index within an experiment was calculated as the ratio of the mean (5 fields of views) treatment fusion index to the vehicle control treated fusion index. The mean of the relative fusion index of 3 independent experiments was used for the final quantitation of a relative fusion index.

For cell fusion experiments involving shRNA knockdown of PKC-alpha or Rictor+Raptor, cells were maintained in DMEM supplemented with 10% FBS and 1% penicillin-streptomycin solution (all from Thermofisher Scientific). For lentiviral transduction, cells were seeded at a density of 1 x 10^5 cells per well in 6-well plates and incubated with the lentivirus-containing medium in the presence of 8µg/ml Polybrene (Sigma-Aldrich) for 24 h. After 24 h of transduction, the medium was replaced with fresh DMEM containing 2µg/ml puromycin (Thermofisher Scientific) and blasticidin (Thermofisher Scientific) to select for successfully transduced cells. Puromycin selection was carried out for 72 h, after which surviving cells were further expanded. TetON-p14 HeLa cells with RICTOR, RAPTOR, PKC alpha and Scrambled shRNA. Cells were then trypsinized and seeded in 12 well plates, allowed to incubate overnight and then treated with doxycycline to induce pexpression. 12 h later cells were fixed and fusion quantified with the same protocol outlined above.

2.7. Selection and verification of knockdown cells

Knockdown efficiency of RICTOR, RAPTOR, and PKC alpha genes was confirmed by Western blot analysis. For Western blot, cells were lysed and protein concentrations were determined by BCA Protein Assay (Biorad). Equal amounts of protein were loaded on SDS-PAGE gels, transferred to PVDF membranes (Biorad), and probed with specific antibodies against RICTOR, RAPTOR, PKC alpha, and Coomassie blue protein stain as a loading control. All western experiments were performed n≥2.

2.8. Cell fusion assays

Mouse C2C12 myoblasts were cultured in Dulbecco's Modified Eagle Medium (DMEM), supplemented with 10% fetal bovine serum (FBS) and 1% penicillin-streptomycin. Cells were maintained at 37°C in a humidified atmosphere of 5% CO_2. When the cells reached about 60% confluence, differentiation was induced by switching the medium to DMEM supplemented with 2% horse serum (HS). The medium was changed every 24 h. The treatment group received BYL719 at a concentration of 1µM and 2.5µM. BYL719 was dissolved in DMSO and added to the medium every 24 h, immediately after the medium change. The control group received the same volume of DMSO without BYL719. Three days post-differentiation, cells were fixed with 4% paraformaldehyde for 15 minutes and then permeabilized with 0.1% Triton X-100. Nuclei were stained with DAPI and myotubes were stained with an anti-myosin heavy chain (MHC) antibody followed by an Alexa Fluor-conjugated secondary antibody. Images were captured using a fluorescence microscope. The fusion index, representing the degree of myoblast fusion into myotubes, was calculated as the number of nuclei within MHC-positive cells divided by the total number of nuclei. At least five random fields were counted for each condition in each experiment.

Fusion experiments were conducted using transfected p14 and p14 mutants in HT1080, HeLa, Vero, A549 cells and SARS-CoV2 spike protein in HEK293A-ACE2/TMPRSS2 cells. Cells were transfected with 1 µg of DNA and 3 µl of Lipofectamine (Invitrogen) per well Lipofectamine 2000 (Thermofisher Scientific) in cell line appropriate medium supplemented with 10% FBS. Cells were fixed using methanol and stained with Wright-Giemsa stain following the manufacturer's protocol. Syncytial nuclei were counted in five fields of each well at 10X magnification, and images were captured using a Nikon Diaphot TMD microscope under bright field illumination.

2.9. Exogenous addition of PIP(3,4,5) to cultured cells

This study employed a synthetic, cell-permeable derivative of PIP(3,4,5) and PI3P, provided by Echelon Biosciences. The PIP(3,4,5) (pip3) solution was freshly prepared in a

buffer composed of 150 mM NaCl, 4 mM KCl, and 20 mM HEPES (pH 7.2). The solution was resuspended by either bath sonication or vigorous vortexing to ensure uniform mixing. A mixture was prepared using 300µM of the phospholipids and 100µM of freshly prepared histone, also supplied by Echelon. This mixture was incubated at room temperature for 5 minutes.

Subsequently, the mixture was diluted to 1/10th of its original concentration using a modified HBSS buffer. This diluted mixture was immediately applied to TetOn-p14-HeLa cells that had previously been treated with DOX (5 µg/ml). TetOn-p14-HeLa cells were seeded in 24 well cell culture plates at a density of 2×10^4cells per well and cultured overnight. Cells are treated with DOX and fresh cell culture media, 8 h later cells were treated with vehicle control or BYL 719 (2.5µM) in combination with the addition of media containing alone, PIP(3,4,5) (7.5µM) or PIP(3) (7.5µM). Cells were then fixed and fusion quantified 6-8h post treatment.

2.10. Pore-forming assay

HeLa cells were stained with Cellmask Deep red according to the manufacturer's instructions and 1 x 10^4 cells were seeded with 1 x 10^4 HeLa transduced with Tre-p14, rTA3, and GFP per well in a 96 well plate. 24 h later cells were treated with doxycycline (5µg/ml) and 5 h later treated with vehicle control and small molecule inhibitors. At 10 h post fusion induction, cells were fixed with 4% P.F.A. and stained with Hoechst and WGA-Alexa-555 according to the manufacturer's protocol. Images were captured on the Axio Observer on the 20x objective. 8 images were captured per well and cells positive for both cytoplasmic stains were counted and binned by number of nuclei within the cell (1, 2-4, 5-7, or >8 nuclei per cell. Vehicle controls and treatments were performed in triplicate.

2.11. Dextran uptake

For the fixed-cell dextran uptake assays, HeLa cells transduced with Tre-p14 and rTA3 were utilized. These cells were initially seeded in 96-well optical bottom Corning plates at a density of 1.2 x 10^4 cells. To induce p14 expression, a treatment with doxycycline was performed. Following 9 h post-induction, cells underwent pre-treatment with the designated drugs for a period of 1 hour. Subsequently, a concentration of 1 µg/ml of dextran-70kDa-Alexa 488 was introduced to the cells and left to incubate for 30 minutes. Upon completion of the incubation period, cells were thoroughly washed three times with Hanks' Balanced Salt Solution (HBSS). Next, cells were stained with Hoechst and fixed using 2% paraformaldehyde for a duration of 20 minutes. Imaging of the cells was performed on the Axio Observer, capturing 18 fields of view per condition with 20 z-stacks and a 500nm spacing. Utilizing a 40x objective, images were captured in two independent experiments using pre-selected areas within each well.

The quantification of dextran uptake was carried out utilizing the software tool CellProfiler. This image analysis software was used to measure the integrated intensity of dextran fluorescence per nuclei. CellProfiler's flexible, modular pipeline system allowed for the customization of analysis to accommodate the specific characteristics of our dextran uptake images. Firstly, the images were loaded into the software. The identification of individual cells was then achieved by segmenting the Hoechst stained nuclei and the cell boundaries. The software then facilitated the measurement of mean dextran fluorescence within the segmented cell areas. These measurements were exported into a spreadsheet for further analysis.

2.12. Live Cell imaging

Cell lines expressing fluorescent tags were seeded into 4 compartment 35mm dishes at a density of 6 x 10^5 cells. Cells were cultured in FluoroBrite imaging medium supplemented with 2mM glutamine, 100 U/ml pen-strep and 10% FBS. Cells were imaged on the Zeiss Z1 Observer spinning disk microscope on either 63x or 100x oil immersion objectives.

2.1.1. PH(Akt)-GFP Translocation

TetOn-p14 HeLa cells transiently transduced with PH(Akt)-GFP were incubated in phenol red-free DMEM and imaged using a spinning disk microscope (Zeiss) with a 63x oil immersion objective. The cells were maintained at 37°C and 5% CO_2 using a live-cell imaging chamber (Tokai Hit, Shizuoka, Japan). Cells were treated with DOX (5 µg/ml) at 0h and then media was replaced at 9 h with, fresh media containing either vehicle control, Dox (5 µg/ml), Dox+ BYL719 (1µM) or+ EIPA (20µM). Images were acquired every 2 minutes for 16 h using excitation/emission wavelengths of 488/510 nm for GFP. Z-stacks were acquired at 1µm intervals, and a maximum intensity projection was used for analysis.

The images were processed and analyzed using ImageJ software. Briefly, the GFP fluorescence intensity at the plasma membrane was measured using 1um wide region of interest (ROI) of starting at the cell edge. The mean fluorescence intensity of the plasma membrane was calculated by averaging the intensity values along the line-scan. The background fluorescence was subtracted from the mean fluorescence intensity. The PIP(3,4,5) levels were calculated by normalizing the Akt(PH)-GFP fluorescence intensity at the plasma membrane to the total Akt(PH)-GFP fluorescence intensity in the cell. The data were analyzed using GraphPad Prism software and presented as mean ± standard error mean (SEM). Statistical significance was determined using one-way ANOVA followed by Tukey's post hoc test. A p-value of less than 0.05 was considered statistically significant.

2.1.2. LCK-GFP and LCK-tdTomato live cell imaging

HeLa cells expressing LCK-GFP and LCK-tdTomato were imaged using the spinning disk microscope equipped with appropriate excitation/emission settings to separately capture the signals from GFP (488 nm excitation, 509 nm emission) and tdTomato (554 nm excitation, 581 nm emission). Z-stack images were captured at a step size of 0.5 µm to adequately resolve the entire cellular volume.

Raw image data were loaded into ChimeraX (UCSF). To improve visualization and reduce background noise, the images were median filtered with a radius of one voxel. A 3D surface model of each cell population was created using the "surface" command. The voxel threshold for surface creation was manually adjusted to best represent the observed structures. Different colors were assigned to the LCK-GFP and LCK-tdTomato labeled cells for clear differentiation. The 3D models were visualized using the default lighting and shading in ChimeraX.

For volumetric rendering, the raw z-stack images were imported into Arivis Vision4D software. The 3D volume rendering mode was selected in the "Visualization" tab. This software allows interactive exploration of the volumetric dataset in real time. Similar to ChimeraX, different colors were assigned to LCK-GFP and LCK-tdTomato channels, and the voxel intensity thresholds were manually adjusted to optimally visualize the cell populations.

The fusion events between the LCK-GFP and LCK-tdTomato labeled cell populations were identified as regions where the two different fluorescence signals co-localize. This was achieved by applying the "blend" function in both ChimeraX and Arivis, which allows visualizing the overlay of the two fluorescence signals. Fusion events were analyzed by quantifying the volumetric overlap of GFP and tdTomato signals.

Chapter 3: Results

3.1. Results overview

I aimed to investigate the cellular cofactors essential for FAST-mediated cell-to-cell fusion. Previous research that identified annexin A1 as a crucial fusion cofactor strongly supported the involvement of FAST proteins in co-opting host proteins and pathways for cell-to-cell fusion. Since kinase and kinase-associated proteins play a central regulatory role, they are suitable targets for a limited number of interventions, such as siRNA or small molecule inhibition, to assess the involvement of a broad range of cellular processes in fusion.

To identify kinase signaling pathways that regulate p15 FAST protein-mediated syncytiogenesis, I developed an automated imaging assay to quantify cell-to-cell fusion in HT1080 cells (Fig. 3A and B) and evaluated the fusion function using the relative fusion index (Fig. 3C). Extensive pilot studies were first conducted to determine the optimal screen parameters, including cell plating density, fusion duration, and staining protocols. Concurrently, the Columbus software was trained to a computer vision algorithm to automate the counting of syncytial nuclei over nine fields of view using an Opera high-content screening microscope. To facilitate automatic segmentation the nuclei were stained with Hoechst, while the cell body was stained with Oregon green-CellMask (Fig. 3B).

Using the automated p15 cell-to-cell fusion assay, two high-content screens were conducted to evaluate the contribution to fusion of kinases and kinase-associated proteins. The first screen (Fig. 4) was a pharmacological screen comprising treatments with 165 well-characterized small molecule kinase inhibitors at three different concentrations (0.025, 0.25, and 2.5µM). The second screen (Fig. 5) was an siRNA knockdown screen targeting 710 kinases and kinase-related proteins using three unique siRNA sequences for each target. The use of two distinct screens, one inhibiting protein function and the other protein expression, aimed not only to provide corroboration but also to address the possibility of compensatory effects, which have previously been

reported for PI3K. For example, there are three isoforms of the p110 catalytic subunit of Class IA PI3K. If an individual p110 isoform is silenced with siRNA, it may not necessarily inhibit its isoform-specific function. This is because all p110 isoforms can produce PIP(3,4,5), making them only distinguishable by their activators. Therefore, in the absence of the silenced isoform, other p110 isoforms may bind with p85 and other regulatory factors, potentially performing compensatory functions. Conversely, isoform-specific pharmacological inhibition of p110 does not deplete the protein, which could still bind to p85 and block any compensatory function of another isoform (Weiss et al., 2007).

The kinase inhibitor screen was performed in triplicate, and three small molecule inhibitors generated high probability hits: PIK75 at two concentrations (2.5uM and 0.25μM), A443654 at 2.5uM concentration, and PHA767491 at 2.5uM. These inhibitors potently inhibited p15 syncytia formation without significantly decreasing cell proliferation and viability (Fig. 4A). PIK75 is a class IA PI3K inhibitor with specificity for the p110α isoform over the p110β (200-fold) and p110ɣ (~100-fold) isoforms (Knight et al., 2006; Y. Li et al., 2012). PIK75 has also been reported to inhibit DNA-PK (Knight et al., 2006). A443654 inhibits Akt, an effector kinase of class I PI3Ks, while PHA767491 inhibits Cdc7/Cdk9 (Y. Luo et al., 2005; Montagnoli et al., 2008).

Interestingly, none of the siRNAs targeting PI3K Class 1 isoforms (PIK3CA, PIK3CB, PIK3CD, or PIK3CG) or Akt isoforms (Akt1, Akt2, and Akt3) inhibited syncytiogenesis sufficiently to classify as a hit in the siRNA screen. However, several factors confounded this screen and data analysis. For example, the varying efficiencies of gene knockdown by the non-pooled siRNAs made it necessary to score hits from unique siRNAs that inhibited fusion by greater than 50% rather than the mean fusion inhibition of the three siRNAs with the same target. Further discussion on the reasons why the PI3K-Akt pathway was resistant to siRNA inhibition is outlined in the Discussion.

To reconcile the seemingly conflicting results from the drug inhibitor screen and siRNA screen regarding the role of PI3K-Akt signaling in p15-mediated cell fusion, a network enrichment analysis was performed on the siRNA dataset using Kinase

Enrichment Analysis 3 (KEA3) software (Kuleshov et al., 2021). The analysis used a database of known kinase interactions to identify central signaling kinases and networks from a subset of the kinome, consisting of 52 gene targets within the siRNA screen that inhibited p15 syncytiogenesis by 50% or greater (Fig 5A). Akt was found to be the most common downstream signaling kinase among the 52 siRNA targets (Fig. 5C). Based on this finding, the PI3K-Akt pathway was selected for further investigation as it is known to regulate actin remodeling at the plasma membrane, which is essential for myoblast, osteoclast, and FAST protein fusion.

3.2. Validation of PI3K-Akt Involvement in FAST fusion

I next sought to determine if PI3K-Akt signaling was required for FAST protein cell fusion in various cell types, or if it was p15 or cell type dependent. HT1080 cells were transfected with BRV p15, or RRV FAST protein p14 in the absence or presence of PIK75 (250 nM) or A443654 (100 nM) (Fig. 4B) and Vero and A549 cell lines were transfected with p14 and also treated with PIK75 and A443654 (Fig. 4C). Cells were then fixed and Giemsa stained, and five random fields of view were selected (n=3). Fusion inhibition was qualitatively assayed by visual inspection, with the absence of large syncytia (greater than 10 nuclei in a multinucleate) within the field of view being scored as significant fusion inhibition. The results showed that both PIK75 and A443654 significantly inhibited fusion of both p15 and p14 in H1T1080 cells, and of p14 mediated fusion in A549, Vero and HeLa cells (Fig. 4B-D).

For subsequent evaluations of inhibitor treatment or genetic silencing on p14 mediated cell fusion, fusogenicity was quantified using relative fusion index. The relative fusion index was calculated from five fields of view, using the Ziess Zen Blue plate map module to select the same relative position within each well for treatment- and vehicle-treated controls. To assist with quantification of fusion index a semi-automated protocol was developed in which syncytia with greater than 4 nuclei were manually annotated and the machine learning computer vision program Stardist was

used to quantify syncytial nuclei and total nuclei within a field of view (Schmidt et al., 2018).

To confirm the specificity of the p110α and Akt involvement in FAST-mediated fusion, two additional small molecule inhibitors of p110a and Akt were employed, BYL719 and MK2206, respectively, which inhibit through distinct mechanisms of action from PIK75 and A443654. PIK75 competitively inhibits p110α binding of the phosphatidylinositol substrate PIP(4,5), whereas BYL719 inhibits p110α by binding to the ATP acceptor site of p110α (Gobin et al., 2015; Zheng et al., 2011). A443654 associates with ATP binding pocket of Akt, inhibiting kinase function and dephosphorylation by PP25, while MK2206 binds the Trp-80 residue and allosterically inhibits Akt kinase function (Fig. 7) (T. O. Chan et al., 2011; Rehan et al., 2014). Treatment with BYL719 (1 μM) or MK2206 (1 μM) significantly inhibited p14 syncytiogenesis (Fig. 4D) and immunoblot analysis of lysates of HeLa-Tet-On-p14 harvested 13 hours post-induction with doxycycline revealed that BYL719 and MK2206 did not alter p14 protein levels (Fig. 4E). These results established for the first time the importance of PI3K-Akt signaling in FAST protein-mediated cell fusion and validated a reliable experimental model for further investigation of the underlying mechanisms involved.

3.3. System-wide assay of host pathways utilized by p14 in cell fusion using multiplexed antibody-paired detection assay

The results from our high-content loss-of-function screens and subsequent confirmation experiments suggested that PI3K-Akt signaling may be the only kinase pathway required for FAST protein-mediated fusion. However, due to the limitations of high content screens and the complexity of metazoan cell fusion programs, I conducted another system-wide experiment to identify the host pathways utilized by FAST proteins in cell fusion.

In collaboration with ActivSignal, a multiplexed antibody-paired (MAP) detection assay was employed to quantify changes in 26 canonical signaling pathways by measuring the expression or phosphorylation of 70 signaling proteins (Alexandrov et al.,

2019). Lysates from HT1080 cells transfected with p14 or pcDNA3 for 10 hours (n=2) were incubated with multiple antibody pairs targeting two distinct epitopes on their respective kinase, phosphatase, or other signaling protein. Prior to incubation with protein lysates, paired antibodies were each tagged with half of a nucleotide sequence barcode, and then the pooled antibodies (140 antibodies, 70 pairs) were incubated with protein lysate samples. Subsequently, samples were washed and treated with a proprietary DNA ligase, which would ligate the nucleotide sequences if they were in close proximity (i.e., both bound to the target protein through their conjugated antibodies). To quantify the signal, nucleotide barcodes were read by next-generation sequencing, and only reads with the correct full-length nucleotide barcode were quantified to minimize false-positive detection from non-antigen-specific binding.

Comparing MAP detection assay results from p14 and mock-transfected cells, it was found that p14 expression influenced only Akt Ser473 phosphorylation and H2AX expression among the 70 signaling proteins examined, with more than a 2-fold increase in both Ser473 phosphorylation and H2AX expression in comparison to mock-transfected samples (Fig. 7B). The upregulation of Akt phosphorylation at ser473 supports the results from the p15 kinome screen (Fig. 5). Although the DNA damage response protein H2AX may play a role in FAST protein-mediated fusion, it has been previously known to be upregulated in the context of SARS-CoV-2 fused syncytia as a result of micronuclei formation and dsDNA in the cytosol and may not be directly involved in the cell fusion process (Costa et al., 2022; X. Liu et al., 2022). Taken together, the siRNA and small molecule inhibitor screens, as well as the MAP assay, provided strong evidence that PI3K-Akt signaling is an important host cofactor for p14- and p15-mediated fusion.

3.4. p14-mediated cell fusion is dependent on p14 induction of PI3K(p110α) but not p110β production of PIP(3,4,5).

To better understand the involvement of the PI3K-Akt signaling pathway in FAST protein cell fusion, I investigated whether p14-mediated fusion relied on constitutive activity of the PI3K-Akt pathway or if p14 modulated PI3K-Akt signaling activity. To this end,

western blots of pAkt p473 lysates were performed from Tet-ON-p14 HeLa cells induced to express p14 for 13 hours with doxycycline or left untreated (Fig. 8A). Since an antibody to quantify PIP(3,4,5) was not available, pAkt473 was used as an indirect measure of upregulation of PIP(3,4,5) production. Results showed that p14-expressing Tet-ON-p14 HeLa cells consistently had higher levels of pAkt473 than Tet-ON-p14 HeLa cells not expressing p14, indicative of PI3K-Akt activation.

While there were other PI3K inhibitors with specificity toward other PI3K isoforms present within the small molecule inhibitor screen, only PIK75 inhibited syncytiogenesis. To confirm that p14 induction of the PI3K-Akt pathway was dependent specifically on the p110α isoform, two additional inhibitors were screened; the p110β inhibitor TGX221 as well as wortmannin, a pan-Class 1 PI3K inhibitor (Jackson et al., 2005; Powis et al., 1994). In HeLa Tet-On cells, p14-induced phosphorylation of AktS473 was inhibited by PIK75, BYL719, and wortmannin treatments, but not by TGX221 (Fig. 8A), which is consistent with p14 activating the PI3K(p110α)-Akt signaling axis. As expected, PIK75, BYL719, and wortmannin also had an inhibitory effect on cell fusion when evaluated with p14 (Fig. 8B).

To further emphasize the significance of PIP(3,4,5) and PI3K signaling in FAST protein fusion, the PI3K-Akt pathway was hyperactivated by inhibiting PTEN using bpV(OHpic), the phosphatase primarily responsible for PIP(3,4,5) depletion (Schmid et al., 2004). This strategy facilitated the manipulation of PIP(3,4,5) accumulation without interfering with p14 activation of PI3K(p110α). Treatment of Tet-On-p14 HeLa cells with bpV(HOpic) (10uM & 20μM) led to a dose-dependent increase in p14-induced syncytium formation and hyperactivation of the PI3K-Akt pathway, as evidenced by the dose-dependent increase in pAktS473 detected through western blotting of HeLa Tet-On-p14 cells (Fig. 9A&B). Collectively, these results support the notion that FAST proteins promote PIP(3,4,5) production and Akt signaling activation via PI3K p110α, and that this pathway is crucial for efficient FAST protein-mediated cell-cell fusion. Additionally, beyond its role in Akt activation in facilitating cell fusion, PIP(3,4,5) may directly recruit other proteins that contribute to the fusion process.

To further support the essential role of PIP(3,4,5) in FAST protein cell-cell fusion, we conducted an inhibition-rescue experiment (Fig. 9C). Tet-ON-p14 HeLa cells were induced to express p14 and then treated with BYL719 (1μM) at 5 hours post-induction, just prior to the onset of syncytium formation, to inhibit the p110α-dependent increase in PIP(3,4,5), followed by exogenous addition of PIP(3,4,5) or another phosphoinositide, PIP(3). The exogenous addition of PIP(3,4,5), but not PIP(3), partially rescued p14 fusion function as indicated by a significant increase in the fusion index relative to the BYL719 treatment alone.

3.5. Assay of PIP(3,4,5) levels confirms essential role in FAST protein cell-cell fusion

To investigate the role of PIP(3,4,5) in p14-mediated cell-cell fusion, I assayed relative PIP(3,4,5) levels using a PIP(3,4,5) biosensor PH(Akt)-GFP in Tet-ON-p14 HeLa cells. After inducing p14 expression with doxycycline treatment, cells were observed by time-lapse confocal microscopy with six Z-stacks spanning from the dorsal plasma membrane to ventral surface (Fig. 10A). The ratio of fluorescent plasma membrane-proximal PH(Akt)-GFP bound to PIP(3,4,5) compared to unbound PH(Akt)-GFP diffuse in the cytoplasm (F_{PM}/F_{cyto}) was quantified in each preselected mononucleated cell at the Z plane 1.5uM from the bottom of the cell. Results indicated a significant increase in the F_{PM}/F_{cyto} ratio at 8, 12, and 16 hours in p14-expressing cells, indicating a rise in PIP(3,4,5) plasma membrane concentration (Fig. 11B). In contrast, there was no increase in PIP(3,4,5) in Tet-ON-p14 HeLa cells not induced to express p14 with doxycycline. Furthermore, BYL719 treatment at 10h rapidly reduced the F_{PM}/F_{cyto} ratio to levels that were not significantly different from time 0h baseline or non-induced Tet-ON-p14 control cells, indicating the PIP(3,4,5) rise was p110α-dependent. Cells that fused were excluded from the above PH(Akt)-GFP ratiometric analysis of mononucleated cells, suggesting that the PIP(3,4,5) rise occurred before fusion. These results further substantiated the essential role played by PIP(3,4,5) and/or the PI3K-Akt signaling axis in p14-mediated cell-cell fusion.

3.6. Live imaging correlates spatiotemporal activation of PI3K-Akt with p14-induced cell fusion synapse formation

The PI3K-PIP(3,4,5)-Akt signaling axis plays a crucial role in the remodeling of the cytoskeleton and plasma membrane, as well as coordinating transcriptional and translation changes during cell fusion (Gardner et al., 2012; Matheny et al., 2015; Oikawa et al., 2012). In other forms of cell fusion, such as myoblast, osteoclast, and trophoblast multinucleation, multiple signaling pathways act in concert to coordinate differentiation from precursor cells to the mature multinucleated cell type (Podbilewicz, 2014). However, except for osteoclast fusion, if and how PI3K and Akt contribute directly to the mechanism of membrane fusion during syncytiogenesis remains unclear.

My previous live imaging results of PIP(3,4,5) showed that PI3K-Akt activation occurs prior to cell-cell fusion. In this study, I sought to correlate the activation of PI3K-Akt with p14-induced cell fusion using greater spatial and temporal resolution. To do so, I employed short interval 3D time-lapse microscopy of a population of HeLa cells stably expressing PH(Akt)-GFP and TetOn-p14-mRuby co-cultured with wild type HeLa cells. Using this approach, I observed PIP(3,4,5) in membrane ruffles and p14 both localizing to sites of cell-to-cell fusion immediately prior to fusion (Fig. 10 A). By quantifying the change of mean PH(Akt)-GFP fluorescence within a two regions of interest (ROI, shown with dashed line circles in Fig. 10A), one each in the cytoplasms of a PH(Akt)-GFP + p14-mRuby HeLa cell and the adjacent wild type HeLa, and identifying when fluorescent intensity equalization between the two cells occurs (shown with the red line in Fig. 10B), I was able to approximate the time of cytosolic mixing between the two cells following membrane fusion and pore expansion. The fusion synapse was seen in an expanded view and was identified by locating the initial disappearance of the cell border of the p14-mRuby cell. Both p14-mRuby and PH(Akt)-GFP in the transduced HeLa cell could be seen to localize to the fusion synapse immediately prior to the cytoplasmic mixing of the two cells (right panel, white arrow, Fig. 10B). The localization of both PIP(3,4,5) and p14mRuby to the fusion synapse prior to cytosolic mixing provided compelling evidence

that PI3K-Akt functions at points of cell-cell contact as part of the FAST protein cell fusion mechanism. These findings suggest that p14 plays a critical role in PI3K-PIP(3,4,5)-Akt signaling during cell fusion and provide insight into the molecular mechanisms underlying the fusion process.

3.7. Insights into the role of Akt phosphorylation and downstream mediators in cell fusion

To investigate the downstream effectors of Akt signaling and their role in cell fusion, I used genetic and small molecule kinase inhibitors to determine whether the Akt-phosphorylating protein complexes mTORC1 and mTORC2 are necessary for p14-mediated cell fusion (Fig. 7). TetOn-p14 HeLa cells were treated with torin-1, a small molecule inhibitor of mTORC1 and mTORC2, or rapamycin, an inhibitor of mTORC1, and the effects on syncytiogenesis and Akt phosphorylation were examined. Treatment with torin-1 resulted in a significant inhibition of p14-mediated cell fusion and AktS473 phosphorylation (Fig. 12B), while treatment with rapamycin had no effect on p14-mediated syncytiogenesis (Fig. 12A), suggesting that mTORC2 activity, but not mTORC1, is required for p14 fusion. Akt activation is also tightly regulated by PDK1 that phosphorylates Thr308 in Akt after binding to PIP(3,4,5) and prior to Ser473 phosphorylation by mTORC2 (Manning & Toker, 2017). In accordance, treatment of TetOn-p14 HeLa cells with BX795, a PDK1 inhibitor, significantly decreased both p14-induced AktS473 phosphorylation and the relative fusion index (Fig. 12C&D).

The involvement of mTORC2 in cell fusion was further investigated by performing a lentiviral transduction of HeLa cells with shRNA targeting the mTORC2 subunit Rictor or the mTORC1 subunit Raptor in p14 Tet-On HeLa cells. Protein knockdown was confirmed by western blotting (Fig. 13A), and quantifying the relative fusion index of the four cell lines showed that Rictor, but not Raptor, knockdown significantly inhibited cell fusion (Fig. 13B) and AktS473 phosphorylation (Fig. 13C). Furthermore, p14 induced phosphorylation of Thr86 in the Sin1 subunit of mTORC2 (Fig. 13D), which is known to be a substrate of Akt and enhance activity of mTORC2 as part of a positive feedback loop

between mTORC2 and Akt, and genetic knockdown of Sin1 decreased p14-mediated syncytiogenesis (Fig. 13E) (G. Yang et al., 2015). Thus, p14 expression activates mTORC2 to upregulate a PI3K-Akt signaling axis required for FAST protein-mediated syncytiogenesis.

mTORC2 phosphorylates a regulatory hydrophobic motif in the C-terminal tail of Akt, but also in other AGC kinases like protein kinase C alpha (PKCα) and SGK1 that are involved in actin remodelling and cell migration (Ballesteros-Álvarez & Andersen, 2021). To determine whether these other mTORC2 targets act in parallel with Akt to regulate cell-cell fusion, TetOn-p14 HeLa cells were treated with the SGK1 inhibitors EMD638683 and GSK-650394. These treatments did not significantly alter the relative fusion index (Fig. 14A). Similarly, shRNA knockdown of PKCα in TetON-p14 HeLa cells had no significant effect on the relative fusion index (Fig. 14C&D), suggesting Akt is the primary AGC kinase target of mTORC2 driving cell-cell fusion. However, treatment of cells with the conventional PKC inhibitor Go6976 resulted in a modest reduction in the relative fusion index in some experiments (Fig. 14B). Further experiments are required to determine whether PKCα, a calcium effector and important regulator of actin dynamics, is involved in FAST protein-mediated cell-cell fusion.

3.8. Akt activation precedes fusion and is not sufficient for syncytia formation, while PI3K-Akt signaling is critical for fusion pore expansion

My screens and pathway analyses demonstrated that p14 activates PI3K which in turn activates a PDK1-mTORC2-Akt signaling axis that is required for efficient FAST protein-mediated syncytiogenesis. Given that syncytia formation is the end stage of a multi-step cell-cell membrane fusion process, the fusion index I employed is an indirect measure of plasma membrane fusion. It was conceivable that the PI3K-dependent p14 mediated processes could occur after membrane fusion and pore formation. For example, PI3K and/or Akt could mediate the post-fusion pore expansion needed to allow nuclear transfer and syncytium formation or perhaps Akt signaling is activated in response to plasma membrane fusion and is needed to maintain survival of syncytia.

To determine whether Akt activation is required for membrane fusion and pore formation or occurs in response to membrane fusion, HeLa cells were transfected with the fusion-incompetent p14 mutant p14G2A or the fusion-defective mutant p14c88, a C-terminal truncation that retains some vestigial ability to induce formation of a few small syncytia (Fig. 15A) (Corcoran et al., 2006; Corcoran & Duncan, 2004). Western blot analysis of lysates from HeLa cells transfected with p14, p14G2A, and p14c88 showed comparable levels of pAktS473 phosphorylation, which were higher than mock-transfected HeLa cells (Fig. 15B), indicating PI3K-Akt signaling is not activated in response to cell-cell fusion. This was consistent with my previous demonstration that p14 upregulates PIP(3,4,5) expression in mononucleated Tet-ON-p14 HeLa cells prior to their fusion (Fig. 10).

To determine whether PI3K-Akt signaling is required for pore formation prior to syncytium formation, I developed a quantitative two-colour fluorescence fusion pore assay. TetOn-p14 HeLa cells labeled by GFP transduction were co-cultured at a 1:1 ratio with wild-type HeLa cells labeled with CellTracker Deep Red dye, p14 expression was induced with Dox, and cells were treated with the various small molecule kinase inhibitors starting just prior to the expected onset of cell-cell fusion and syncytium formation (~5-7 h post-induction). Fluorescence microscopy was then used to quantify cells that contained both CellTracker Deep Red and GFP, and these cells were binned by their number of nuclei (Purple arrows, Fig. 16A). Cells treated with BYL719, MK2206, or BX795 to inhibit PI3K, Akt or PDK1, respectively, all showed a dramatic decrease in the numbers of co-labeled cells of all sizes, relative to mock-treated, p14-expressing cells (Fig. 16B). A control population that were not induced to express p14 showed no co-labelled cells. The largest number of dual-coloured p14-expressing cells detected were mononucleated, consistent with the limited number of multinucleated cells at this early timepoint. These cells are likely the result of cytoplasmic mixing through a fusion pore that had either not yet undergone the fusion pore expansion necessary for multinucleated cell formation or had failed to expand and subsequently closed. As well as an overall decrease in dual-coloured cells of all sizes, cell populations treated with the

inhibitors all had a lower ratio of dual-labeled mononucleated cells to multinucleated syncytia when compared to control (Fig. 16B), further indicating that these inhibitors block syncytium formation upstream of fusion pore formation and implying the PI3K-Akt pathway is required for membrane fusion.

3.9. Is the PI3K-Akt pathway universally required by cell-cell fusogens?

Myomerger, a small protein that shares many features with the FAST proteins, mediates membrane fusion during metazoan myogenesis and myogenesis is known to be Akt-dependent (Gardner et al., 2012; Quinn et al., 2017). I was interested in determining whether this PI3K-Akt pathway I discovered to be required for efficient FAST-protein mediated cell-cell fusion was similarly required for cell-cell fusion mediated by myomerger. I used stably transduced HEK293A cells provided by Nichole McMullen. These cells constitutively express myomaker and express myomerger under TetOn-control. When induced, ~15-20% of the cell population fuses over 24 hours. As shown (Fig. 17A), treatment of these myomaker+TetOn-myomerger HEK293A cells with BYL719, PIK75 MK2206, torin-1 but not rapamycin downregulated syncytia formation (Fig. 17B). Western blot analysis of lysates from the same experiment revealed that dox-induction of myomerger expression in myomaker+TetOn-myomerger HEK293A cells increased AktS473 phosphorylation (Fig. 17C). Treatment with BYL719, PIK75, MK2206 and torin-1, but not rapamycin, inhibited both syncytium formation and myomerger-dependent AktS473 phosphorylation but did not significantly reduce myomerger protein expression. The p110α-Akt signaling pathway is therefore required for cell-cell fusion mediated by both FAST proteins and myomerger/myomaker. This provides the first evidence of PI3K(p110α) and mTORC2 involvement in myomerger fusion.

Similar results were obtained by Dr. Nandini Margam using similar kinase inhibitor and fusion function experiments in differentiating C2C12 mouse myoblasts undergoing primary myotube formation. At 3 days post-differentiation, AktS473 phosphorylation was elevated, and BYL719 treatment inhibited both multinucleation and Akt activation in a dose-dependent manner (Fig. 18A-C). We were unable to study

the effects of Akt inhibition on C2C12 myotube formation using MK2206 because of toxicity issues with long-term Akt inhibition (3 days). However, small molecules that activate Akt have been shown to increase myotube formation in C2C12 cells (W. Luo et al., 2019).

To assess whether the PI3K-Akt pathway was required by just small fusogens for cell-cell fusion, we transfected ACE2/TMPRSS2-transduced HEK293A cells with SARS-CoV2 Spike protein, a Class I fusion protein. Western blots revealed no significant change in Akt activation in cells expressing the enveloped virus fusion protein, and while AktS473 phosphorylation was inhibited by BYL719 and MK2206, Spike fusion activity was not inhibited (Fig. 19). Nichole McMullen obtained similar results using VSV G protein, where the above inhibitors had no effect on fusion (personal communication). It would appear that activation of, and reliance on, a PI3K-Akt pathway is feature of the small fusogens, not the enveloped virus fusogens.

3.10. Membrane ruffling and macropinocytosis are critical for FAST protein mediated cell fusion.

As previously mentioned, during time-lapse microscopy observations of HeLa TetOn-p14-mRuby cells transduced with PH(Akt)-GFP, I noticed an increase in PIP(3,4,5) and p14-enriched plasma membrane ruffles (Fig. 20 A). Additionally, I observed the formation of large, µm-sized endocytic vesicles at these membrane ruffles (Fig. 20A white arrows). These vesicles contained p14-mRuby within their membrane, and the PIP(3,4,5) biosensor associated transiently with the vesicle, rapidly losing signal as the vesicle moved toward the center of the cell. Notably, live cell imaging observations revealed that both ruffling and the formation of large endocytic vesicles are qualtitatively upregulated in HeLa TetOn-p14-mRuby cells expressing p14 (Fig. 20A).

The large vesicles observed were the size of macropinosomes, and since PI3K-Akt signaling is known to play a crucial role in both cell membrane ruffling and MaPi, I explored the possibility that the induction of MaPi serves as the functional role of PI3K-Akt signaling in p14 protein-mediated cell fusion. To investigate this, I treated p14-

TetOn-HeLa cells with a variety of inhibitors targeting individual components of the macropinocytotic pathway (Fig. 20B). Ethyl-isopropyl amiloride (EIPA), a sodium/hydrogen exchange inhibitor, is the most widely used MaPi inhibitor, selectively blocking MaPi without affecting other forms of endocytosis. EIPA works by reducing cytoplasmic pH at the plasma membrane, consequently blocking Rac1-actin polymerization of membrane ruffles and MaPi (Koivusalo et al., 2010). The GTP-binding protein ADP-ribosylation factor 6 (Arf6) is essential for macropinosome closure but not membrane ruffling, and it operates downstream of PI3K (Williamson & Donaldson, 2019). Arf6 was targeted by the indirect inhibitor NAV 2729 and the direct inhibitor secinH3 (Benabdi et al., 2017; Hafner et al., 2006). Additionally, macropinosome closure, but not membrane ruffling or actin polymerization, was inhibited by blocking microtubule polymerization with nocodazole (Leyden et al., 2021).

As demonstrated in Figure 21A, treating p14-TetOn-HeLa cells with all the above MaPi inhibitors significantly impeded cell fusion, suggesting that MaPi is a necessary process for cell fusion. Moreover, the inhibition of p14-mediated fusion with Arf6 inhibitors and nocodazole suggests that macropinosome closure, rather than just membrane ruffles, plays a critical role in cell-cell fusion. Using the PH(AKT)-GFP translocation assay, which measures changes in PIP(3,4,5) concentration at the plasma membrane, I determined that treatment with EIPA did not inhibit p14 mediated PIP(3,4,5) production and therefore MaPi was not upstream of PI3K-Akt activation (Fig. 21B).

To confirm and further investigate the role of p14-induced MaPi in cell-cell fusion, I employed two common assays for MaPi, the cellular uptake of fluorescent high molecular weight dextran, and uptake of fluorescent latex beads. Compared to control p14-TetOn-HeLa cells, dox-induction of p14 expression increased the uptake of both unconjugated latex beads dyed with high molecular weight dextran (Fig. 22 A) and Oregon green (Fig. 23 A) by over 2-fold as measured by integrated intensity per nuclei to account for variable cell density (Fig. 22B & Fig. 23B). Moreover, increased cellular uptake of the 70kDa dextran was significantly reduced when cells were treated to inhibit

PI3K (BYL719&PIK75) and MaPi (EIPA), but not when clathrin-mediated endocytosis was inhibited using PITSTOP2 (Fig. 22B). Additionally, treatment of cells with the p110α inhibitor PIK-75 blocked the p14-induced uptake of uncoated latex beads labeled with Oregon Green (Fig. 23B). In contrast, treatment of p14-expressing cells with the PTEN inhibitor bpV(HOpic), which increased PIP(3,4,5) and cell-cell fusion (Fig. 11A), upregulated dextran uptake (Fig. 22B). These findings provide compelling evidence that MaPi is an effector function of p14-induced PI3K-Akt signaling and is required for p14-mediated cell-cell fusion.

3.11. Active macropinocytosis with the generation of macropinosomes is observed at time and points of cell-cell fusion

Having previously observed PIP(3,4,5)-positive membrane ruffles at sites of cell-to-cell fusion, it was likely that MaPi was occurring at the fusion synapse. Using the same logic from our studies on MaPi mediation of fusion, I aimed to capture MaPi facilitating p14-mediated cell-cell membrane fusion by employing live microscopy. Unfortunately, the temporal and spatial resolution of our previous imaging experiments was insufficient to capture the fast and subtle dynamics of plasma membrane fusion.

To improve these parameters, two bright fluorescent tags fused to the lymphocyte-specific protein tyrosine kinase (LCK) membrane-targeting domain were selected to provide consistent visualization of the membrane. These LCK tagged fluorophores enabled better visualization of the membrane compared to the tagged p14 and Akt constructs as higher expression of LCK-fluorophores did not induce cell death by either cell fusion or inhibition of the Akt survival pathways. Magnification was increased from a 63x to a 100x objective, and the Evolve camera with a 512x512 pixel chip was replaced with an Axiocam camera with a 1388x1048 pixel chip, reducing pixel scaling from 333nm to 63nm. To further enhance imaging quality, fewer z slices were captured, allowing for an increase in imaging frequency from 2-minute intervals to intervals of less than 1 minute.

With these optimized imaging conditions, live cell imaging was employed to capture fusion events between p14-Tet-On HeLa cells transduced with the membrane bio-label LCK-tdTomato and HeLa cells expressing LCK-GFP or left unlabelled to allow for further enhancement of imaging frequency (every 15s). Eight instances of cell fusion were captured, in which the point of plasma membrane fusion was clearly identifiable (within the z-stack and not obscured by overlapping membranes) with two examples shown (Fig. 24&25). In 6 out of the 8 instances membrane fusion coincided with or was immediately preceded by large vesicle formation proximal to the fusion synapse (Fig. 24). As shown in the supplemental video (Supplemental Video 1) and captured still images from the time series of this example experiment (Fig.25), membrane ruffles arising from p14-expressing cells were consistently observed prior to, and in the region of, cell-cell fusion events. In the captured cell fusion events, fusion did not occur at points or times of maximal penetration, where one plasma membrane projection extends into the opposing cell. A volumetric 3D rendering of one such event is shown in Figure 24A, depicting a p14-Tet-On HeLa cell expressing LCK-tdTomato (magenta) and an adjacent HeLa cell expressing LCK-GFP (yellow). The time and location of the cell-cell fusion event were identified within a 55-second window and a 3.5 µm range.

To quantify the loss of the intercellular barrier, I analyzed signal intensity of LCK-tdTomato and LCK-GFP along two parallel lines (grey and teal lines in Fig. 24B spaced 3.5 µm apart) that bisected the approximate location of plasma membrane apposition where cell fusion occurred. In Figure 24B, the upper grey and teal plot profiles [Right] display fluctuating signal intensities for each fluorophore, resulting from intracellular vesicle labeling by the LCK tag. A distinct maximum signal intensity is observed at the intact plasma membrane, followed by a sharp decline when the line passes into the opposing cell not expressing the respective fluorophore. For LCK-tdTomato, this occurs from left to right, while for LCK-GFP, it is from right to left.

As shown in Figure 24B right panel, the intensity profile along the grey line exhibits a rapid loss of the two distinct fluorophore peaks between the 0-second and 55-second images and then equalization of signal intensity along the length of the plot

profile, while distinct fluorophore maxmima remain in plot profiles of the teal line even at 110s. These results indicate that fusion occurs in the immediate vicinity of grey line intersection of plasma membrane between the two in the interval between images capture at 0s and 55s. Notably, a large vesicle was observed (white arrow, Fig. 24 C bottom panel, z-height = 0.7 µm) forming at 165 seconds near the site of plasma membrane fusion. Utilizing the improved resolution of our 3D imaging (Fig. 24 C, D), the appearance of a membrane ruffle from the LCK-tdTomato p14-Tet-On HeLa cell can be observed between 0 seconds to 55 seconds in the upper panel of Fig. 24 C from the complete volumetric (z-height 1.4 µm) rendering. In the volumetric rendering at 55 seconds, which bisects the cell at a z-height of 0.7µm (Fig. 244 C bottom row), one can observe a hollow within the ruffle, suggesting macropinosome formation. Subsequently, at 110 seconds and 165 seconds in the upper panel (Fig. 24C), ruffle collapse and the corresponding formation of a macropinosome can be observed. By using a 3D surface plot of both fluorophores, where height and color represent signal intensity, and centered on the macropinosome formation (50x50 pixels) (Fig. 24D), one can observe the presence of LCK-GFP signal in the lumen of the nascent macropinosome/membrane ruffle of the LCK-tdTomato Tet-On p14 HeLa cell at 55 seconds, which is concurrent with or precedes plasma membrane fusion.

In the surface plots at 165 seconds and 220 seconds, a distinct LCK-GFP signal (Fig. 24D, white arrow) can be seen within the dual-labeled LCK-tdTomato and LCK-GFP macropinosome. The persistence of the LCK-GFP signal within the macropinosome for more than one minute suggests that a portion of the plasma membrane of the LCK-GFP-expressing cell is being pinched off by the macropinocytotic action of the LCK-tdTomato cell. If the internalized membrane fragment was part of a membrane recycling pathway induced after fusion, the lateral diffusion of lipids (and fluorescently tagged membrane binding domains) within the fused membranes would have mixed. Furthermore, the presence of GFP signal but not tdTomato signal in the lumen of the macropinosome indicates that the plasma membrane associated with LCK-GFP was sequestered within the macropinosome prior to fusion with the LCK-tdTomato-expressing cell. In contrast,

plasma membrane and vesicles in the LCK-GFP expressing cell proximal to the fusion pore and not isolated prior to fusion are rapidly labelled with LCK-tdTomato (better visualized in composite images of Fig. 24 B white arrow).

Not only is this the first evidence of MaPi occurring at and concurrent with, or prior to cell fusion, but it also provides circumstantial evidence that through force exerted from the plasma membrane of a p14-expressing cell, membrane remodeling can be induced in an opposing cell. In this case, the exocytotic fission of a mono-labeled LCK-GFP vesicle inside a macropinosome demonstrates this effect.

3.12. Live cell imaging reveals macropinocytosis at the fusion synapse during p14-mediated cell-cell fusion

Membrane invaginations driven by actin-mediated membrane projections near sites of cell-cell fusion were first identified in *Drosophila* myogenesis, leading to the development of the actin protrusion-mediated membrane tension model for cell fusion (E. H. Chen, 2011). Subsequently, similar structures were observed in fusing osteoclasts, mammalian myoblasts, and during pathogen-induced cell-cell fusion. In line with these observations, innovative studies on artificial membranes and *Drosophila* myoblast fusion have demonstrated that increased membrane tension promotes fusion. However, high-resolution live imaging of cell-cell fusion in models where fusion occurs slowly over several days is challenging due to rapid induction of phototoxicity by laser exposure. Furthermore, the absence of tools to directly measure plasma membrane tension at subcellular resolutions during fusion has hindered the identification of conclusive evidence linking protrusive force from these membrane projections to increased membrane tension and cell fusion.

The potent fusogenic activity of FAST proteins, characterized by cell fusion events occurring over minutes to hours, provided a unique opportunity to perform high-resolution live cell imaging of the plasma membrane immediately before and after cell-cell fusion. Although quantitative measurements of membrane tension at the fusion synapse were not conducted, high-resolution imaging captured fusion events within

membrane ruffles. By examining the movement and deformation of the plasma membrane in both the invading and invaded cells at the site of cell fusion, just before the fusion process, insights were gained into the mechanism by which membrane tension is increased to facilitate fusion. Additionally, the relationship between membrane ruffles, macropinosome generation, and the sites at which these occur were characterized.

To this end, live cell imaging experiments of fusion events between TetOn-p14+LCK-Tdtom HeLa cells and LCK-GFP HeLa cells were conducted using Zeiss spinning disk confocal 3D microscopy of Z-stacks (z-slice = 4). Surface renderings were produced by thresholding the minimum signal intensity of LCK-tagged fluorophores associated with the plasma membrane, resulting in a more accurate view of the cell and membrane projections (Fig. 25 right column of A&A', bottom two rows of B). Transparent maximum intensity volumetric renderings of the acquired 3D images allowed for optimal visualization of macropinosome formation and cell to cell interface when viewed in conjunction with the surface projections (Fig. 25 left column of A&A', top two rows of B and C).

Figure 25 panel B illustrates the formation and closure of multiple macropinosomes (blue arrows), as well as their movement towards the cell center (orange arrows) following the collapse of membrane ruffles at the cell periphery. Notably, multiple macropinosomes can form from a single ruffle, and these ruffles do not necessarily arise at areas of cell-to-cell contact. The impact of macropinocytotic membrane ruffles from a p14-expressing cell on the plasma membrane topology of neighboring cells was also investigated. In the example video (Supplemental Video 2) and time series of still images (Figure 25 D), a multinucleated TetOn-p14+LCK-Tdtom HeLa cell (purple) was observed to form putative macropinocytotic vesicles, as depicted in the surface rendering of the bottom half of panel B of Figure 25. In panel C, a membrane ruffle travels along the cell periphery, undergoing periodic cycles of protrusive extension and retraction before reaching a mononucleated LCK-GFP HeLa cell (yellow). Panel D provides a zoomed-in time series view of the fusion synapse, visualizing

the deformation of the target LCK-GFP HeLa cell caused by a membrane ruffle emanating from the TetOn-p14+LCK-Tdtom HeLa donor cell, which ultimately results in cell-to-cell fusion.

At time 570.18s, the membrane ruffle encounters the plasma membrane of the mononucleated LCK-GFP cell. In the subsequent image, the area of cell-to-cell contact elongates as the ruffle travels along the edge of the yellow cell. Two macropinosomes can be observed forming at 670.8s, with the membrane of the LCK-GFP cell appearing to protrude towards the ruffle, as if being pinched by it. In the following acquisition, fusion can be observed having occurred between the two cells at the position of the upper macropinosome (Fig. 25, D, red arrow). Intriguingly, the initial plasma membrane fusion occurred at the macropinosome closure rather than the protrusive tips at the edge of the cup. Interestingly, the lower macropinosome continues to form successfully, as indicated by the orange arrow at 737.88 seconds. Notably, in determining the direction of force applied, it can be observed that the membranes at the fusion synapse deform towards the cytoplasm of the multinucleated p14-expressing cell as the membrane ruffle collapses and retracts in the seconds immediately preceding fusion. The deformation of the target plasma membrane (yellow membrane) was towards the cytoplasm of the retracting p14-expressing cell (purple membrane). These observations suggest the possibility that the activated MaPi process induced by p14 might generate membrane tension by pulling on an adjacent cell membrane, which could act in conjunction with or in place of the cellular protrusion model to facilitate cell fusion.

The formation of a macropinosome in the final image series supports the assertion that fusion synapse was an area of active MaPi. The combined results from live imaging experiments and those using MaPi inhibitors demonstrated that MaPi acts at the fusion synapse to facilitate p14-mediated cell-cell fusion, and at least some fusion events occur within the immediate vicinity of macropinosome formation. In conclusion, my results provide compelling evidence that p14 activates PI3K-Akt signaling that promotes membrane ruffling and MaPi, which plays a critical role in p14-mediated cell-cell fusion. In addition, my live imaging experiments provided insights into the dynamics

of plasma membrane fusion, showing that fusion can occur within a macropinocytotic cup rather than at the protrusive tip of invasive membrane protrusions, raising the intriguing concept that retraction forces might provide an alternate means to generate membrane tension and promote membrane fusion.

A

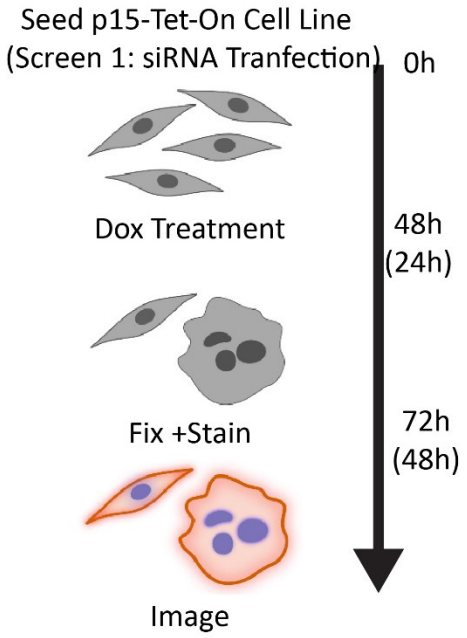

B

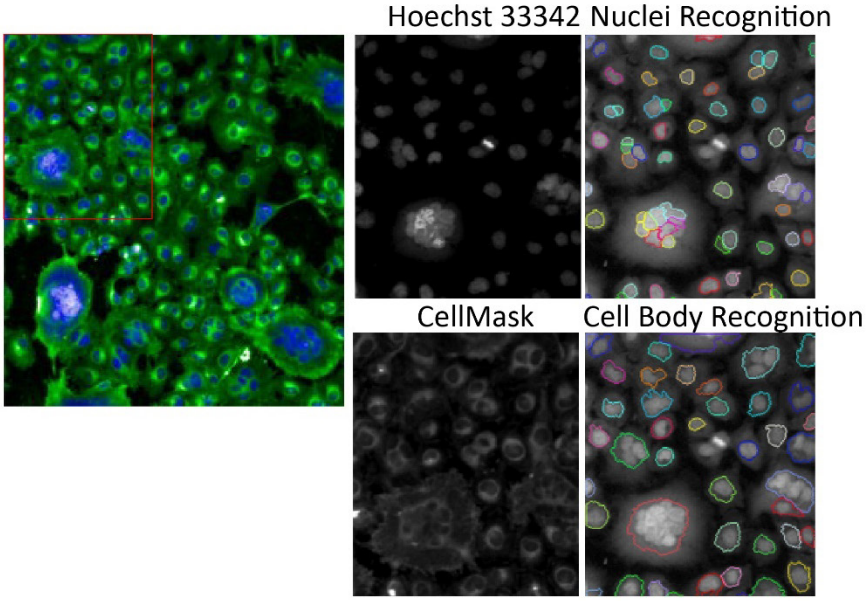

C

$$F_{Index} = \frac{Synyctial\ Nuclei}{Total\ Nuclei}$$

$$Relative\ F_{Index} = \frac{Treatment\ F_{Index}}{Vehicle\ Control\ F_{Index}}$$

3.13. Figure 3: Experimental protocol and quantification of cell fusion in HT1080 Tet-On-P15 cells.

A. Timeline of the experimental protocol for two screens of cell fusion in HT1080 Tet-On-p15 cells. Cells were incubated in 384-well plates and treated either with kinase inhibitors (24 h) at three different concentrations (0.025, 0.25, and 2.5 µM; n=165) or with siRNAs targeting 710 kinases and kinase-related proteins, each with three unique sequences (72 h total; siRNA 48h, Dox 24h; n=2130). Syncytial nuclei per well were counted after treatment. **B.** Representative fluorescence microscopy images of cells stained with CellMask (green) to visualize cell cytoplasm and Hoechst (blue) to stain nuclei. Cell and nuclei segmentation were performed using a unique algorithm in Columbus software. **C.** Equations used to quantify cell fusion: Fusion Index (F_{Index}) is the ratio of syncytial nuclei (cells with >4 nuclei) to the total nuclei within a field of view, providing a measure of the extent of cell fusion. Relative Fusion Index (Relative F_{Index}) is the ratio of the F_{Index} of a treatment group to that of a mock-treated control from the same experiment, enabling the comparison of cell fusion efficiency between treatment groups.

A

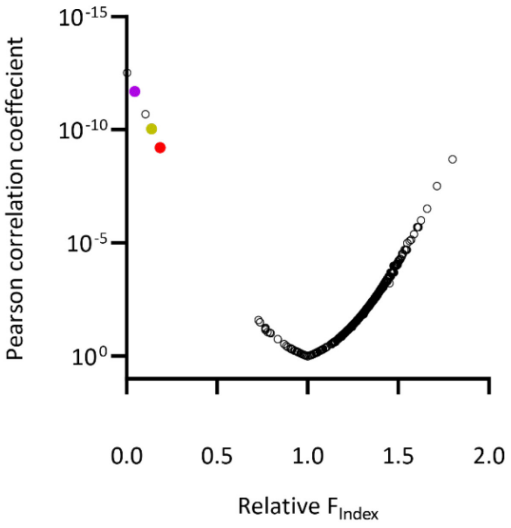
Pearson correlation coeffecient
10-15
10-10
10-5
100
0.0
0.5
1.0
1.5
2.0
Relative FIndex

B

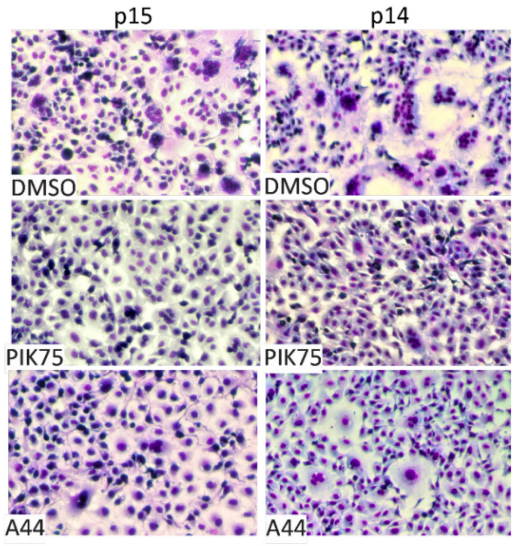
p15
p14
DMSO
DMSO
PIK75
PIK75
A44
A44

C

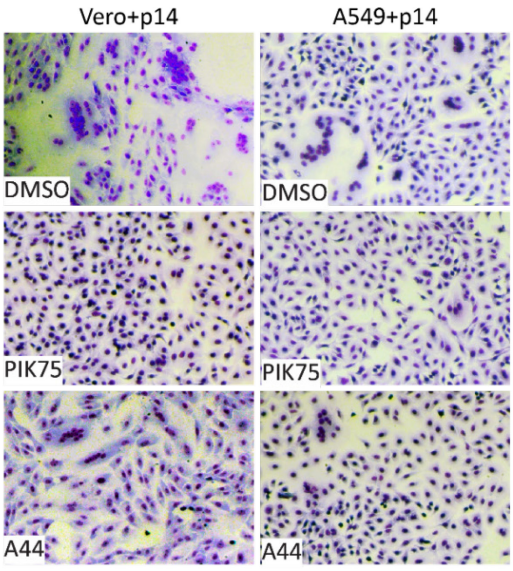
Vero+p14
A549+p14
DMSO
DMSO
PIK75
PIK75
A44
A44

D

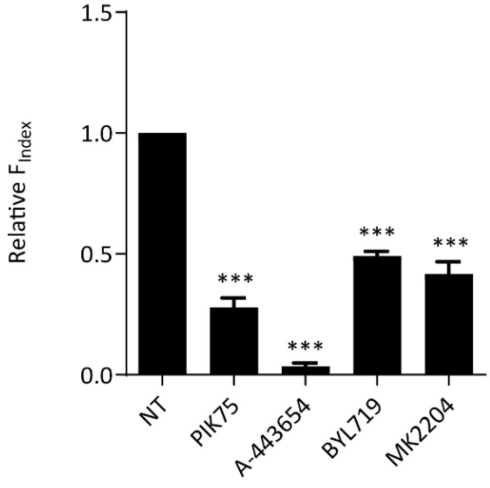
Relative FIndex
1.5
1.0
0.5
0.0
***
***
***
***
NT
PIK75
A-443654
BYL719
MK2204

E

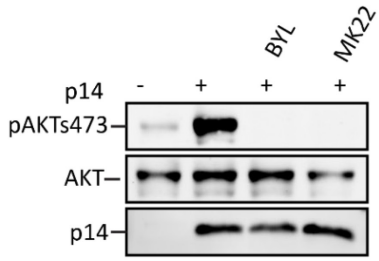
BYL
MK22
p14
-
+
+
+
pAKTs473
AKT
p14

3.14. Figure 4: Small molecule kinome inhibitors identify PI3K (P110α)-Akt pathway as necessary for FAST protein-mediated cell fusion.

A. Volcano plot of the kinase inhibitor screen, displaying the Relative F_{Index} on the x-axis, which represents the difference in Fusion Index between the treatment groups (165 drugs at 0.01, 0.1, and 10 µM) and the control group, and the negative log of the p-value of treatment vs. control on the y-axis. Three notable points are highlighted: Akt inhibitor A-443654 (1 µM; purple circle) and PI3K p110α inhibitor PIK-75 (0.1 µM; yellow circle and 1 µM; red circle &). **B.** Giemsa-stained HT1080 cells transfected with p14 and p15 fusogens alone (top row) or fusion inhibition with the p110α inhibitor PIK-75 (0.25 µM, middle row) or the Akt inhibitor A-443654 (0.25 µM; bottom row), demonstrating the impact of these inhibitors on cell fusion. **C.** Validation of hits in different cell lines: Giemsa-stained A549 and Vero cells transfected with p14 and treated with PIK75 or A443654, showing similar effects on cell fusion. **D.** Relative fusion index of HeLa cells transduced with a tetracycline-inducible p14 expression system, treated with doxycycline (5 µg/ml), and subsequently treated with either PI3K (p110α) inhibitors PIK75 (100 nM) or BYL719(1 µM) or Akt inhibitors A443654 or MK2206 (1µM) 5 hours post doxycycline induction of p14 expression. Cells were fixed and Giemsa-stained at 14 hours post induction, and the relative fusion index was measured to assess the impact of these inhibitors on p14-mediated cell fusion. **E.** Phospho-AktS473 and total Akt levels in TetOn-p14 HeLa cells, either untreated or treated with doxycycline (5µg/ml) and exposed to vehicle control, BYL719 (1µM), or MK2206 (1µM). Akt activation by p14 is blocked by inhibitors without affecting p14 expression.

A

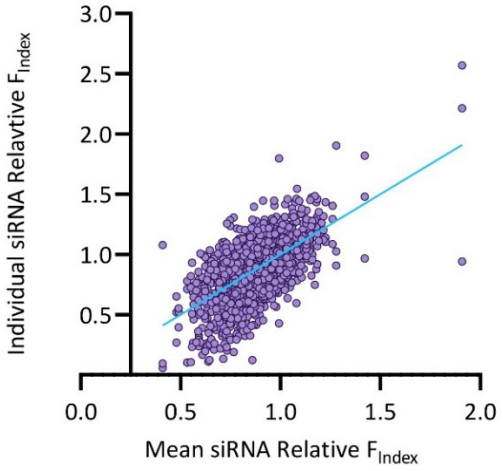
Individual siRNA Relavtive F Index
3.0
2.5
2.0
1.5
1.0
0.5
0.0
0.5
1.0
1.5
2.0
Mean siRNA Relative F Index

B

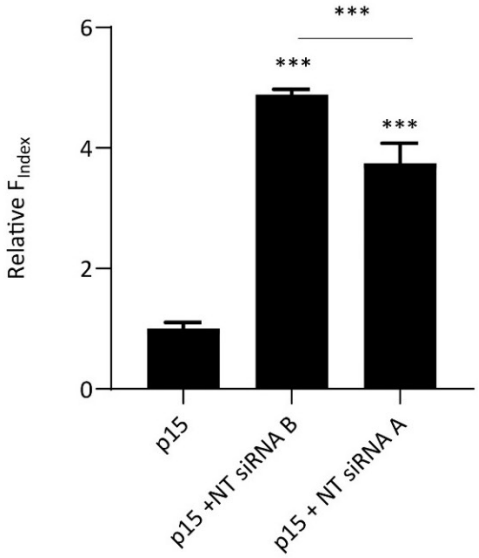
***
***
***
Relative F Index
6
4
2
0
p15
p15 +NT siRNA B
p15 + NT siRNA A

C

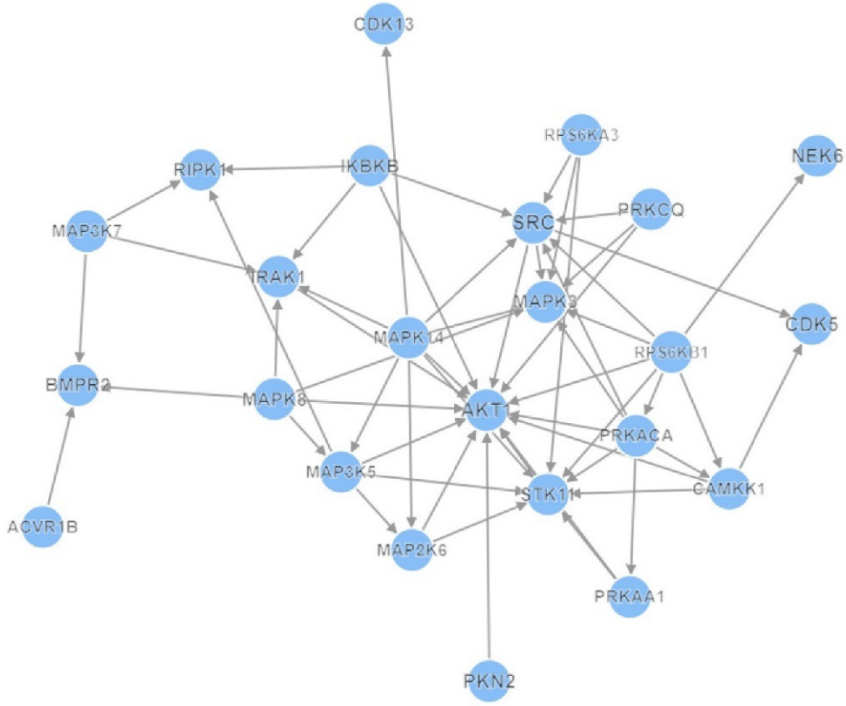
CDK13
RPS6KA3
NEK6
RIPK1
IKBKB
PRKCQ
SRC
MAP3K7
IRAK1
MAPK3
CDK5
MAPK14
RPS6KB1
BMPR2
MAPK8
AKT1
PRKACA
MAP3K5
CAMKK1
STK11
ACVR1B
MAP2K6
PRKAA1
PKN2

3.15. Figure 5: SiRNA screen targeting the kinome for modulators of syncytia formation In HT1080- TetOn-P15 Cells.

A. Cells were incubated in 384-well plates with siRNAs targeting 710 kinases and kinase-related proteins, each with three unique nucleotide sequences (72h total; siRNA 48h, Dox 24h; n=2130). Relative fusion index was determined for each unique siRNA (plotted on the y-axis) versus the mean of the three siRNAs targeting the same gene (x-axis). Notably, there was significant variation in fusion inhibition between the three siRNAs targeting the same gene. **B.** Relative Fusion Index of HT1080-Tet-ON-p15 cells transfected with either pcDNA3 or two non-targeting siRNAs for 48 hours, demonstrating that non-targeting siRNA transfection significantly increased fusion. **C.** Schematic of known interactions among the hits from the screen, identified by performing an siRNA network enrichment analysis of hits that significantly reduced cell-cell fusion (reduction in fusion >50%). The analysis was conducted using Kinase Enrichment Analysis 3 (KEA3), which utilizes libraries of known protein-protein interactions and kinase-substrate interactions to infer kinase signaling networks most likely to modulate a user-inputted subset of proteins (the "hits"). The schematic of the protein hits from the siRNA kinase screen of p15-mediated cell fusion reveals the most significant signaling networks converging upstream of Akt, highlighting the importance of these interactions in modulating cell-cell fusion.

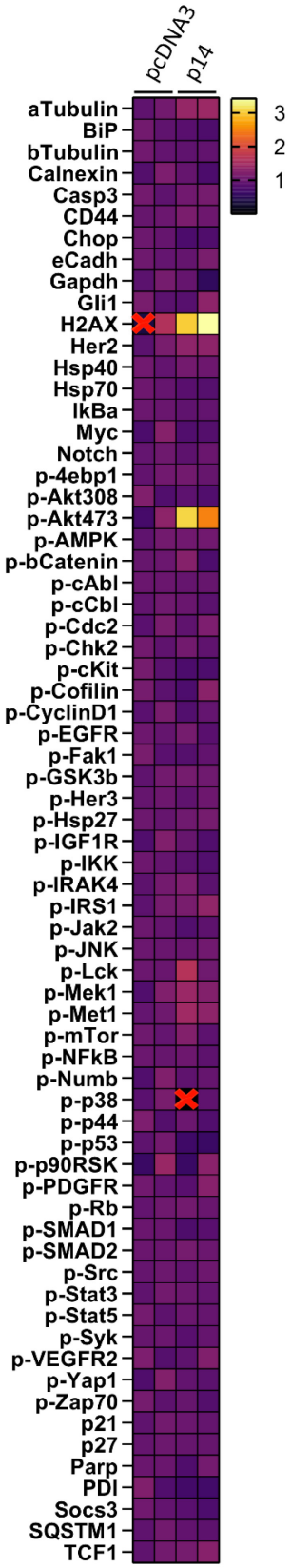
pcDNA3
p14
3
2
1
aTubulin
BiP
bTubulin
Calnexin
Casp3
CD44
Chop
eCadh
Gapdh
Gli1
H2AX
Her2
Hsp40
Hsp70
IkBa
Myc
Notch
p-4ebp1
p-Akt308
p-Akt473
p-AMPK
p-bCatenin
p-cAbl
p-cCbl
p-Cdc2
p-Chk2
p-cKit
p-Cofilin
p-CyclinD1
p-EGFR
p-Fak1
p-GSK3b
p-Her3
p-Hsp27
p-IGF1R
p-IKK
p-IRAK4
p-IRS1
p-Jak2
p-JNK
p-Lck
p-Mek1
p-Met1
p-mTor
p-NFkB
p-Numb
p-p38
p-p44
p-p53
p-p90RSK
p-PDGFR
p-Rb
p-SMAD1
p-SMAD2
p-Src
p-Stat3
p-Stat5
p-Syk
p-VEGFR2
p-Yap1
p-Zap70
p21
p27
Parp
PDI
Socs3
SQSTM1
TCF1

3.16. Figure 6: p14 selectively activates the PI3K(p110α)-Akt pathway, essential for p14 fusion activity.

A heat map of results from the ActivSignal Immuno-Paired-Antibody-Detection (IPAD) assay on lysates from HT1080 cell transfected with p14 or pcDNA3 for 10 hours. The IPAD assay the evaluates the activity of 20 canonical signaling pathways by quantifying 70 known signaling mediators (protein expression levels or phosphorylation status. The assay demonstrates p14 selectively increases Akt Ser473 phosphorylation and histone variant H2AX expression in HT1080 cells 10h post-transfection with pcDNA3 or p14 (n=2). No other pathways exhibited more than a 2-fold upregulation or downregulation.

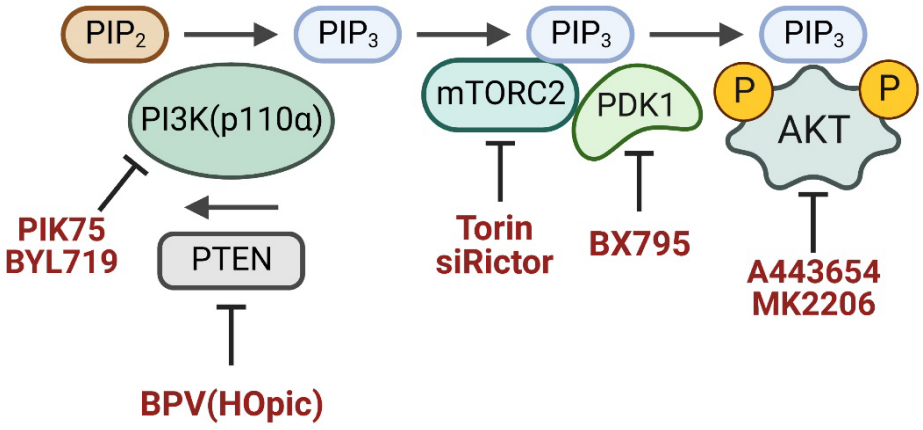

3.17. Figure 7: PI3K-Akt pathway function in cell-cell fusion mediated by FAST proteins.

The schematic illustrates the key components of the PI3K(p110α)-Akt signaling cascade and the role of this pathway in regulating cell-cell fusion mediated by FAST proteins. Small molecule inhibitors are used to modulate the pathway and investigate its impact on the fusogenic activity of FAST proteins. BpV(HOpic) inhibits PTEN, a phosphatase that negatively regulates the pathway. PIK75 and BYL719 selectively inhibit PI3K (p110α), which phosphorylates PIP2 at the 3' position, generating PIP(3,4,5). PIP(3,4,5) formation leads to the recruitment of PDK1, mTORC2, and Akt to the plasma membrane via their PH domains. BX795 targets and inhibits PDK1, a key kinase that phosphorylates and activates Akt. Torin-1 is a dual inhibitor of mTORC1 and mTORC2, with mTORC2 responsible for phosphorylating Akt at Ser473, a crucial step for Akt activation. Rapamycin specifically inhibits mTORC1, a central hub for transcriptional control downstream of Akt. MK2206 and A443654 directly inhibit Akt kinase function, suppressing its downstream effects on cell survival, proliferation, and metabolism.

A

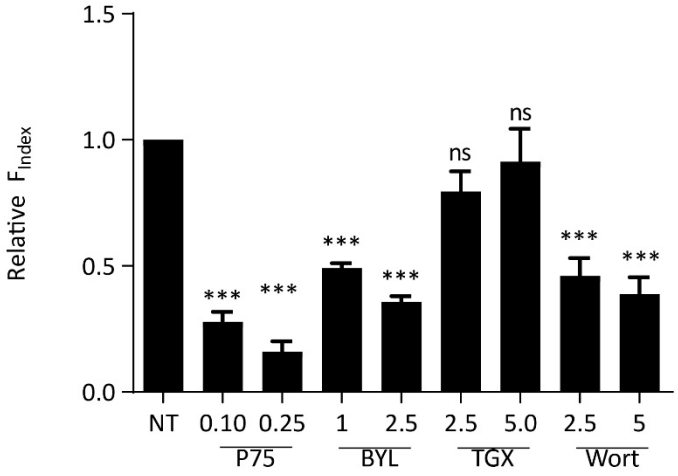

B

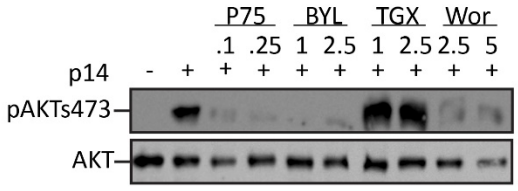

3.18. Figure 8: PI3K isoform p110α-dependent PIP(3,4,5) production is essential for p14-mediated cell fusion.

A. Inhibition of p110α by PIK-75 (P75), BYL719 (BYL), or the pan-PI3K inhibitor Wortmannin (Wort) results in a reduction of doxycycline-treated TetOn-p14 HeLa cell fusion (x-axis concentrations inμM), while the p110β inhibitor TGX-221 (TGX) does not have a significant impact. **B.** A similar pattern is observed in Akt Ser473 phosphorylation at the same μM concentrations, suggesting a strong correlation between the PI3K isoform p110α and its downstream signaling via Akt phosphorylation in modulating p14-mediated cell fusion.

A

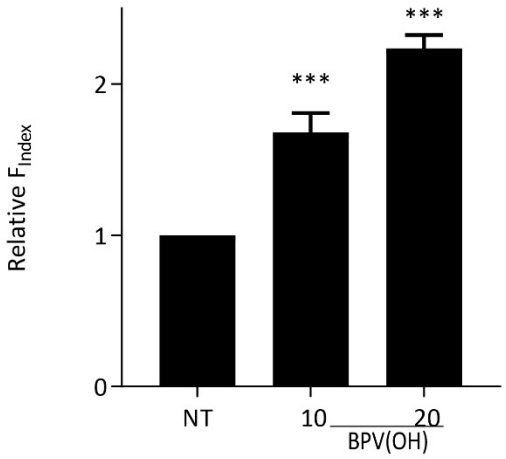
Relative F_Index
2
1
0
***
***
NT
10
20
BPV(OH)

B

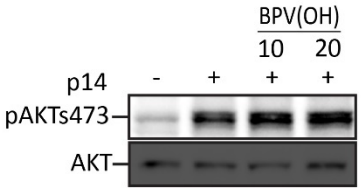
BPV(OH)
10
20
p14
-
+
+
+
pAKTs473
AKT

C

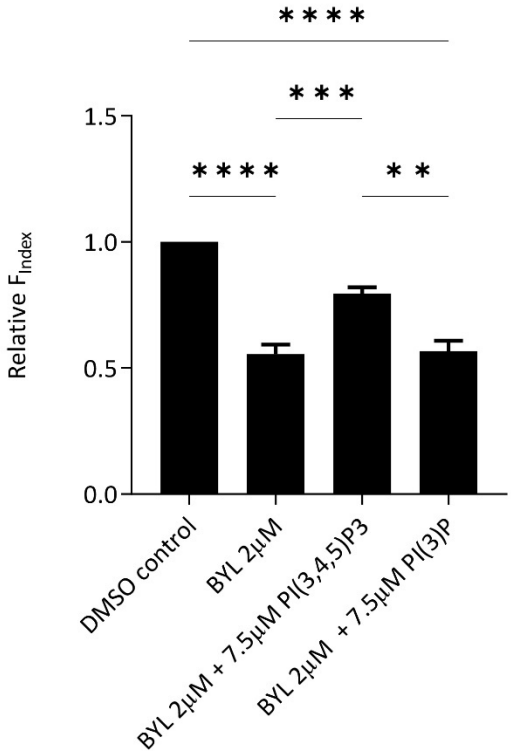
****
***
****
**
Relative F_Index
1.5
1.0
0.5
0.0
DMSO control
BYL 2μM
BYL 2μM + 7.5μM PI(3,4,5)P3
BYL 2μM + 7.5μM PI(3)P

3.19. Figure 9: PIP(3,4,5) production by p110α is essential for p14-mediated cell fusion.

A. Graph of the relative fusion index of TetOn-p14 HeLa cells at 13 hours post dox induction treated with bpV(HOpic) (concentrations in μM) 7 hours post dox induction of p14. **B.** Western blot of lysates from panel A. showing that bpV(HOpic) treatment increases p14-mediated Akt S473 phosphorylation **C.** Relative fusion index of TetOn-p14 cells treated with vehicle control, BYL719, BYL719 and PIP(3,4,5), or BYL719 and PIP(3) at 9 hours post dox induction and allowed to fuse for 3 hours. Inhibition of cell fusion by the PI3Kα inhibitor BYL719 (BYL) is partially reversed with the addition of PIP(3,4,5) but not PIP(3).

A

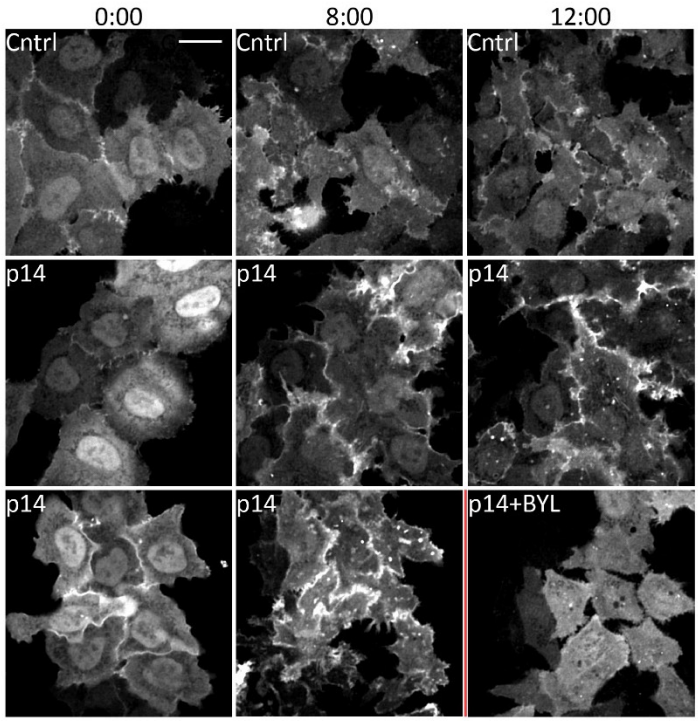
0:00
8:00
12:00
Cntrl
Cntrl
Cntrl
p14
p14
p14
p14
p14
p14+BYL

B

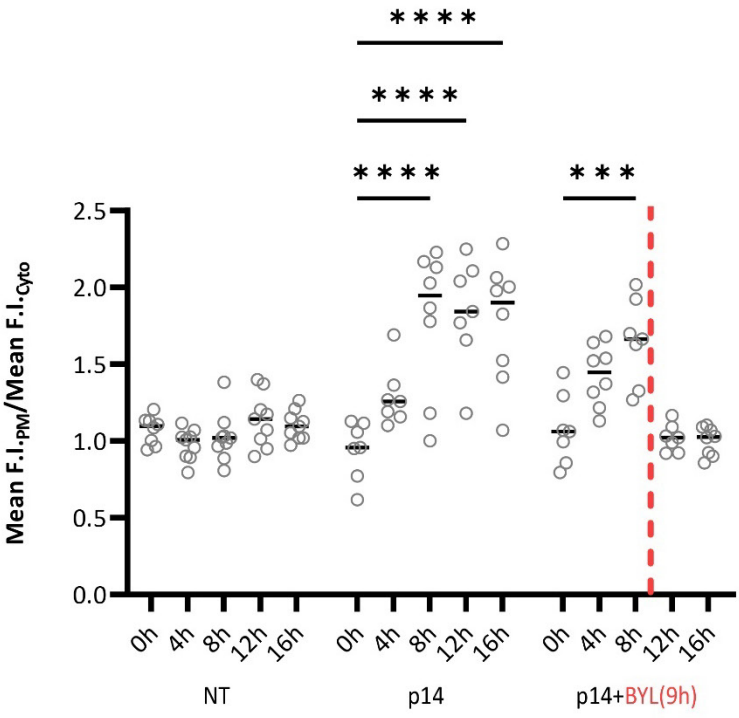
****
****
****
***
Mean F.I.PM/Mean F.I.Cyto
2.5
2.0
1.5
1.0
0.5
0.0
0h
4h
8h
12h
16h
0h
4h
8h
12h
16h
0h
4h
8h
12h
16h
NT
p14
p14+BYL(9h)

3.20. Figure 10: p14 expression induces PIP(3,4,5) production at the plasma membrane through PI3K (p110α) activation.

A. TetOn-p14 HeLa cells were transduced with the PIP(3,4,5)-binding pleckstrin domain of Akt tagged with GFP. Images depict untreated cells (top row), cells treated with doxycycline at time 0 (middle row), and cells treated with doxycycline at time 0 and the PI3Kα inhibitor BYL719 (1μM) at 9 h (bottom row) at timepoints 0, 8, and 12 h (1st, 2nd, 3rd columns, respectively). Scale bar = 25 μm. **B.** A graph displaying the cytosolic-to-plasma membrane ratio of PH(Akt)-GFP fluorescence intensity quantified in mononucleated cells at 0, 4, 8, 12, and 16 hours, providing a relative measure of PIP(3,4,5) concentration for the three treatments in (A). The time of BYL719 treatment is indicated by a dashed red line. These results demonstrate that p14 expression leads to an increase in PIP(3,4,5) production at the plasma membrane, which can be diminished by treatment with the PI3Kα inhibitor BYL719.

A

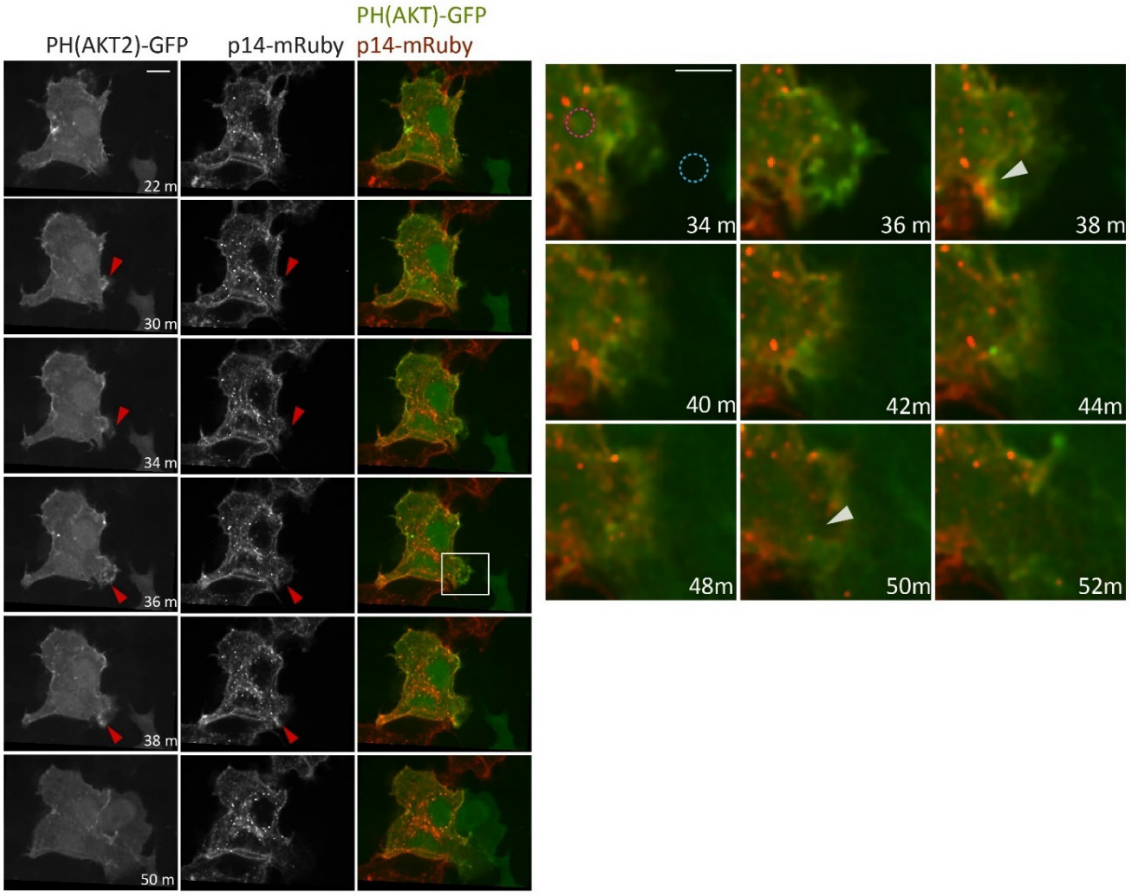
PH(AKT2)-GFP
p14-mRuby
PH(AKT)-GFP
p14-mRuby
22 m
30 m
34 m
36 m
38 m
50 m
34 m
36 m
38 m
40 m
42m
44m
48m
50m
52m

B

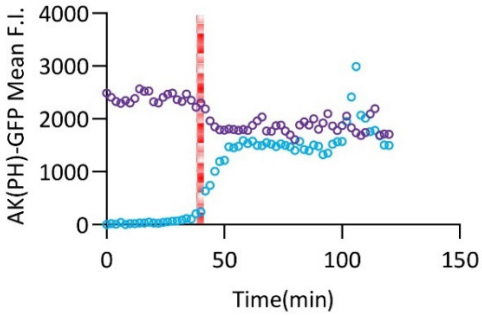
AK(PH)-GFP Mean F.I.
4000
3000
2000
1000
0
0
50
100
150
Time(min)

3.21. Figure 11: PIP(3,4,5) membrane ruffles and p14 localize to the fusion synapse prior to cell fusion.

A. Left panels show time-lapse images of a PH(Akt)-GFP (Green) and p14-mRuby (Red) transduced HeLa cell (left) adjacent to a non-transduced HeLa cell (right) 12h after doxycycline induction. The images display PH(Akt)-GFP and p14 localizing to the membrane in general and to the lower right cell fusion synapse (red arrow) in particular, during the 10 minutes preceding membrane fusion. Scale bar = 20µm. The enlarged boxed region in the cutout panel to the right shows p14 and PIP(3,4,5) at the site of cell-to-cell fusion immediately prior to cell fusion and transfer of the intracellular PH(Akt)-GFP signal between the PH(Akt)-GFP & transduced cell and adjacent non-transduced cells over time (assayed within the purple and blue circles shown in the top left panel). The white arrow indicates site of fusion pore expansion and PH(Akt)-GFP and p14-mRuby localization. Scale bar = 10µm. **B.** A graph depicting the PH(Akt)-GFP fluorescent intensity within the region of interest (ROI) in the p14-mRuby + PH(Akt)-GFP transduced HeLa cell (purple line from purple circle in panel A) and the non-transduced HeLa cell (blue line from blue circle in panel A). Fluorophore transfer following cell fusion is detected at approximately 40 minutes, as indicated by the vertical red line, after p14-mRuby and PH(Akt)-GFP localization to the point of fusion pore expansion.

A

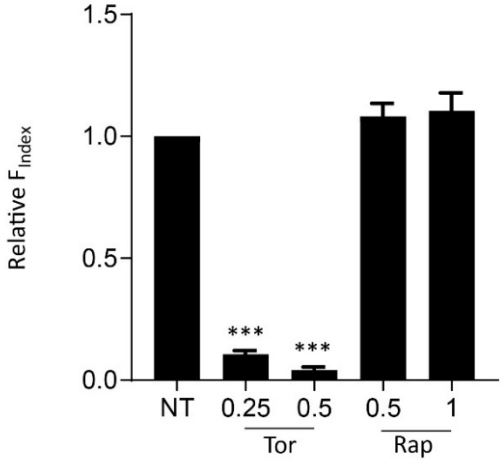
1.5
1.0
0.5
0.0
Relative F Index
***
***
NT
0.25
0.5
0.5
1
Tor
Rap

B

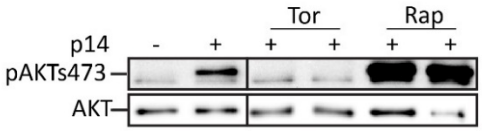
Tor
Rap
p14
-
+
+
+
+
+
pAKTs473
AKT

C

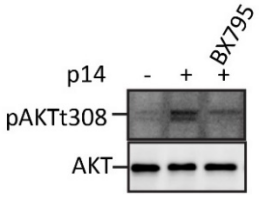
BX795
p14
-
+
+
pAKTt308
AKT

D

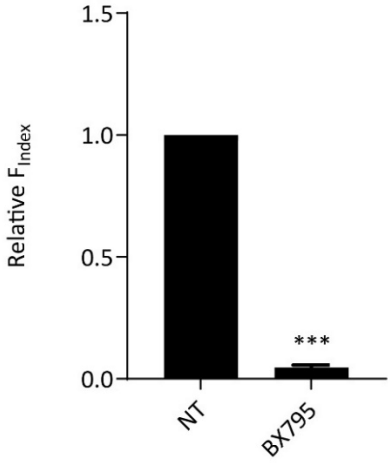
1.5
1.0
0.5
0.0
Relative F Index
***
NT
BX795

3.22. Figure 12. mTORC2 and PDK1 activation is necessary for p14 cell fusion.

A. Relative fusion indices for TetOn-p14 HeLa cells treated for 8 hours with mTOR kinase inhibitor Torin 1 (Tor) or mTORC1 inhibitor rapamycin (Rap), concentrations shown in µM at 5 hours post Dox induction. **B.** Immunoblots of TetOn-p14 HeLa lysates showing p14-mediated phosphorylation of Akt-S473 with the same treatment concentrations of mTOR kinase inhibitor Torin 1 (Tor) as panel A. **C.** Immunoblots displaying the effect of PDK1 inhibitor BX795 (2µM) on Akt-T308 phosphorylation in doxycycline-activated TetOn-p14 HeLa cells. Treatment with BX795 results in a decrease in Akt T308 phosphorylation. **D.** Relative fusion indices of doxycycline-activated TetOn-p14 HeLa cells treated with PDK1 inhibitor BX795(2µM) or vehicle control.

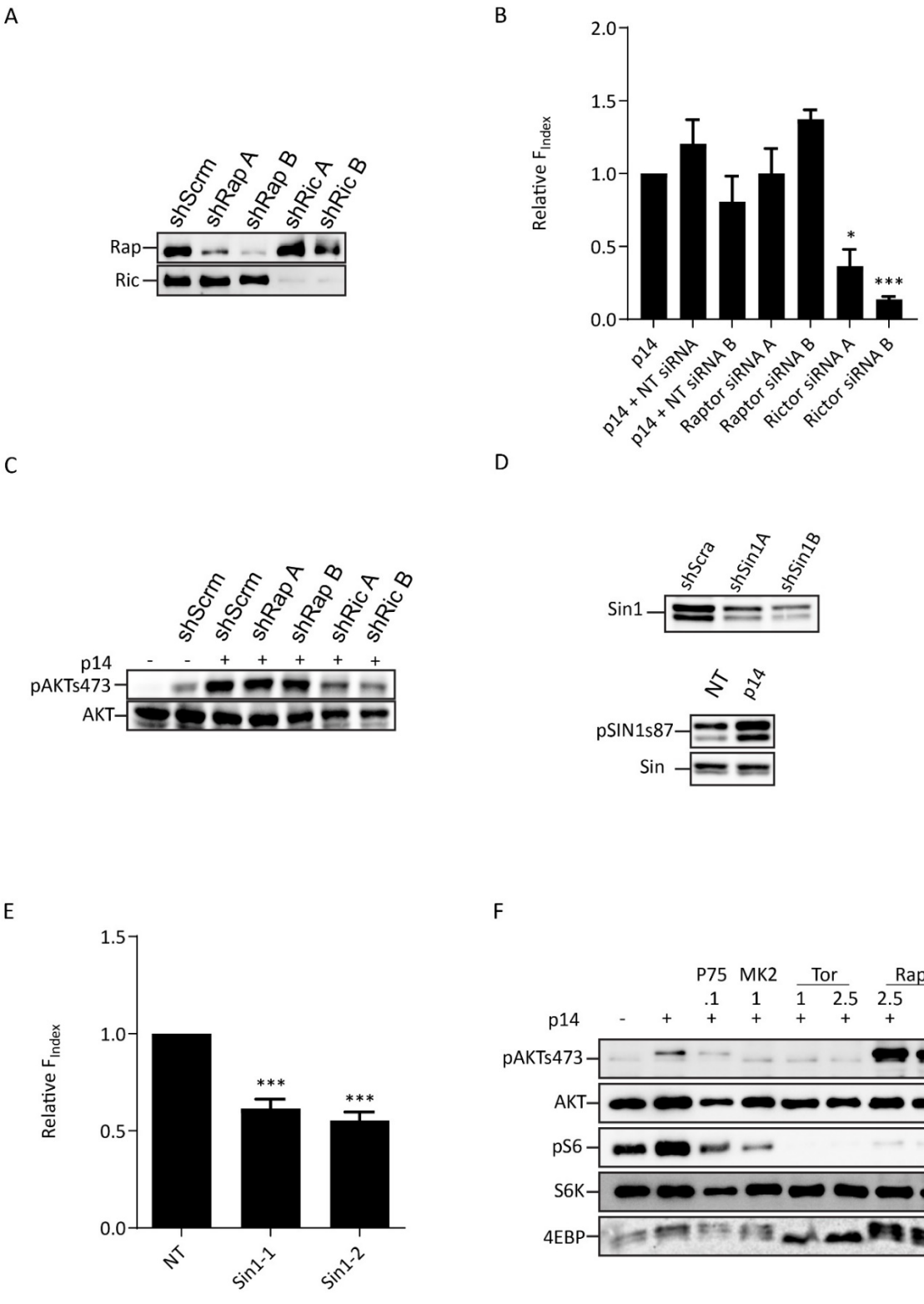
A
shScrm
shRap A
shRap B
shRic A
shRic B
Rap
Ric
B
Relative F Index
2.0
1.5
1.0
0.5
0.0
*
***
p14
p14 + NT siRNA
p14 + NT siRNA B
Raptor siRNA A
Raptor siRNA B
Rictor siRNA A
Rictor siRNA B
C
shScrm
shScrm
shRap A
shRap B
shRic A
shRic B
p14 - - + + + + +
pAKTs473
AKT
D
shScra
shSin1A
shSin1B
Sin1
NT
p14
pSIN1s87
Sin
E
Relative F Index
1.5
1.0
0.5
0.0
***
***
NT
Sin1-1
Sin1-2
F
P75 MK2 Tor Rap
.1 1 1 2.5 2.5 5
p14 - + + + + + + +
pAKTs473
AKT
pS6
S6K
4EBP

3.23. Figure 13. PI3K-mTORC2-Akt signalling does not activate mTORC1 to mediate p14 cell fusion.

A. Immunoblots showing lentiviral transduced shRNA knockdown of mTORC2 subunit Rictor and mTORC1 subunit Raptor in TetOn-p14 HeLa cells, with two distinct shRNAs for each target and a non-targeting shRNA as a control. Cells were treated with or without doxycycline (5µg/ml) for 14 hours before harvesting. **B.** Fusion quantification of TetOn-p14 HeLa cells transduced with non-targeting shRNA and two shRNAs each targeting Rictor or Raptor. Cells were treated with doxycycline (5µg/ml) for 13 hours before harvesting. **C.** Immunoblots revealing inhibition of Akt Ser473 phosphorylation in TetOn-p14 HeLa cells with Rictor knockdown, but not with Raptor knockdown, following 14-hour doxycycline treatment. **D.** Immunoblots showing lentiviral transduced shRNA knockdown of mTORC2 subunit SIN1 in TetOn-p14 HeLa cells, with two distinct shRNAs for the target and a non-targeting shRNA as a control and immunoblots revealing p14-mediated activation of SIN1, as indicated by phosphorylation at SIN1 T87 in TetOn-p14 HeLa cells treated with or without doxycycline. **E.** Fusion quantification of cells transduced with two shRNAs targeting SIN1. **F.** Immunoblots of phospho-Akt S473, Akt, phospho-p70S6 kinase beta-1 (pS6), p70S6 kinase beta-1(S6), and eukaryotic translation initiation factor 4E-binding protein 1 (4EBP1) from lysates of TetOn-p14 HeLa treated with vehicle control, PIK75, MK2206, torin-1 or rapamycin (concentrations in µM). The phosphorylation of S6 and the presence of multiple bands for 4E-BP1 represent distinct phosphorylation states of these proteins, which is indicative of mTORC1 activity. The number of bands for 4E-BP1 and their migration rates (as seen in their relative positions on the gel) are indicative of the different degrees of phosphorylation. These changes were shown to not correlate with alterations in the fusogenicity of p14 brought about by treatments with kinase inhibitors (Fig. 4D &12A).

A

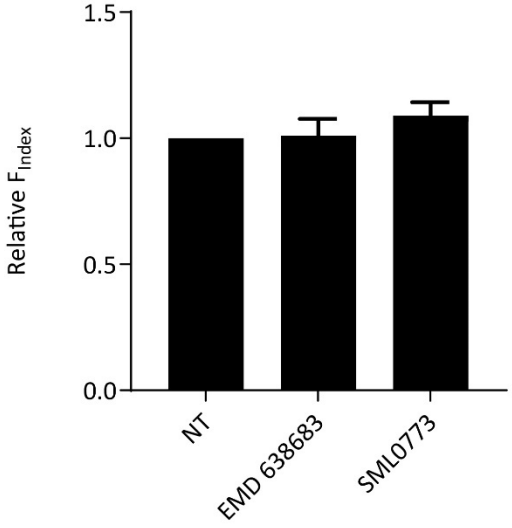
1.5
1.0
0.5
0.0
Relative F Index
NT
EMD 638683
SML0773

B

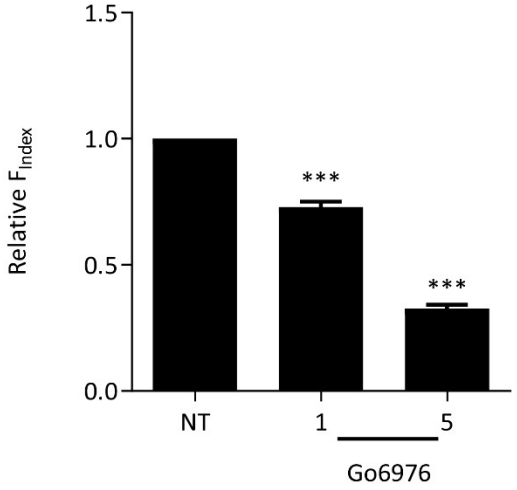
1.5
1.0
0.5
0.0
Relative F Index
***
***
NT
1
5
Go6976

C

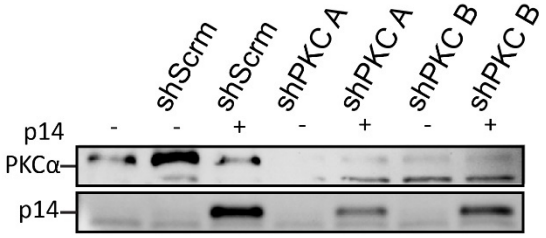
shScrm
shScrm
shPKC A
shPKC A
shPKC B
shPKC B
p14
- - + - + - +
PKCα
p14

D

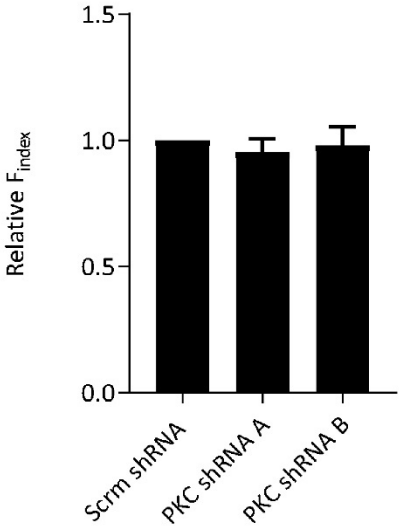
1.5
1.0
0.5
0.0
Relative F Index
Scrm shRNA
PKC shRNA A
PKC shRNA B

3.24. Figure 14. The AGC kinase PKC, but not SGK1, may be required for p14-mediated cell fusion.

A. The relative fusion index at 13 hours post dox induction and either not treated or treated with two SGK1 inhibitors, EMD 638683 and GSK-650394 for 8 hours, at the concentration of 10μM. **B.** The relative fusion index of TetOn-p14 HeLa cells using the same time course as A. and treated with the conventional PKC inhibitor, Go6976, at a concentration of 5μM. **C.** Immunoblots of TetOn-p14 HeLa cells stably transduced with one of two shRNAs knocking down PKCα or a scrambled shRNA control, with or without dox induction of p14 for 13 hours. **D.** Corresponding graph of relative fusion index showing no inhibition with PKC knockdown in TetOn-p14 HeLa cells.

A

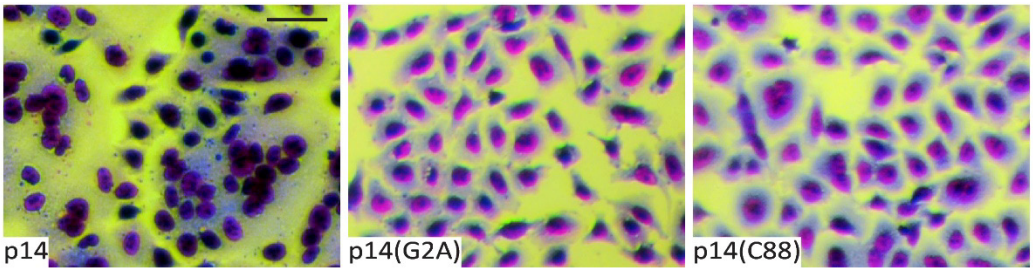

B

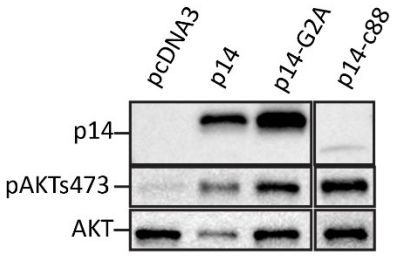

3.25. Figure 15. p14 activates Akt prior to cell fusion.

A. Micrographs of HeLa cells transfected with wild-type p14, and non-fusogenic mutants p14-G2A (point mutation that eliminates myristoylation motif) and cytoplasmic tail truncation p14Δ88-144 (p14c88). Cells were fixed and Giemsa-stained 14h post-transfection. **B.** Corresponding lysates were immunoblotted for p14, p14-G2A, and p14Δ88-144 (p14c88), AktS473 phosphorylation, and total Akt. The results show that expression of non-fusogenic mutants still activates Akt, suggesting that p14-mediated Akt activation occurs before, and is not a sequelae of, cell fusion events.

A

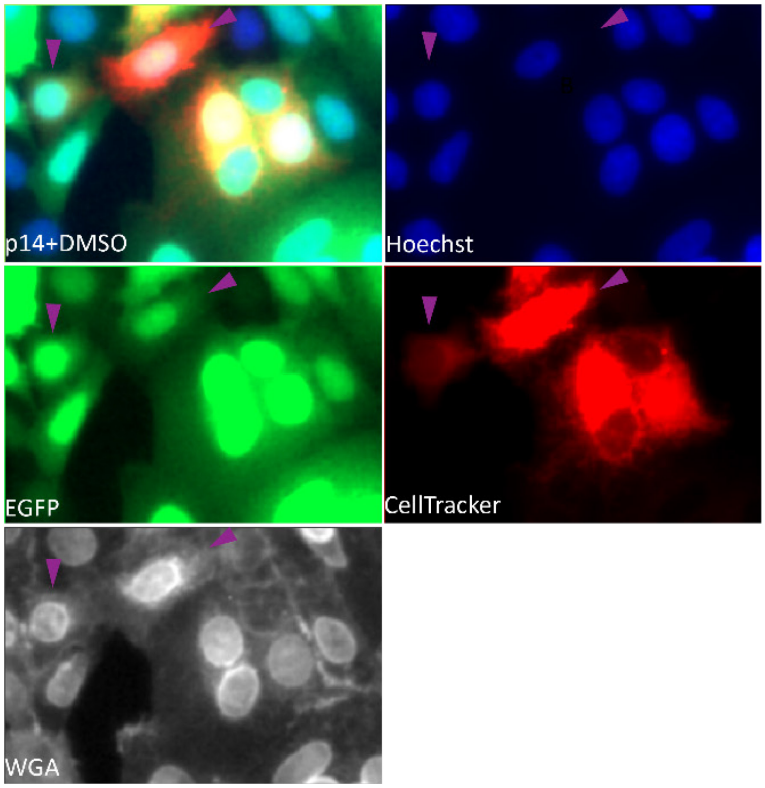
p14+DMSO
Hoechst
EGFP
CellTracker
WGA

B

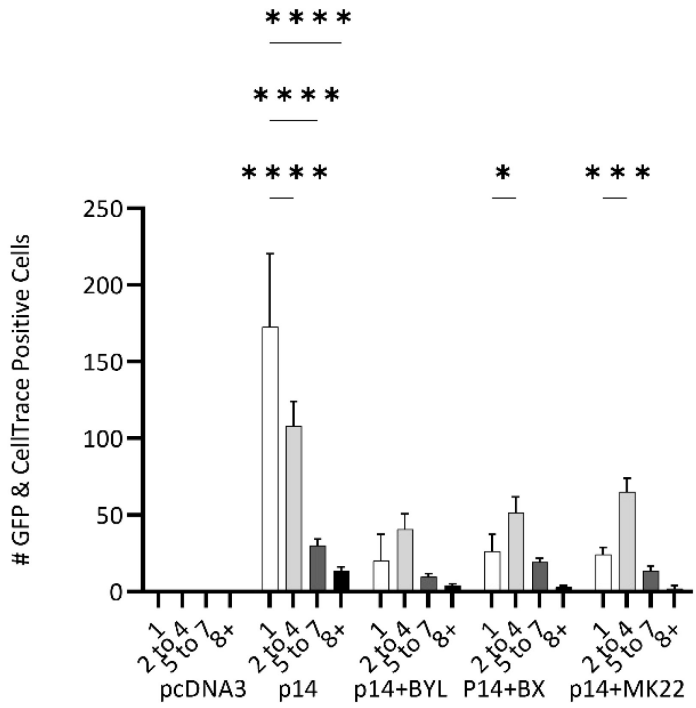
****
****
****
*
***
GFP & CellTrace Positive Cells
250
200
150
100
50
0
1
2 to 4
5 to 7
8+
pcDNA3
p14
p14+BYL
P14+BX
p14+MK22

3.26. Figure 16. p14-mediated activation of p110α-Akt is essential for the pore formation step during cell fusion.

A. Fluorescence micrograph depicting TetOn-p14 HeLa cells expressing GFP mixed with HeLa cells labeled with CellTracker Deep Red at a 1:1 ratio. p14 expression was induced by treating cells with doxycycline for 5 hours. Hoechst and WGA-555 were used to stain nuclei and cell borders, respectively. The number of nuclei within each cell containing both GFP and CellTracker Deep Red was quantified across 5 fields of view at 20x magnification (n=3) and grouped by nuclei count. Mononucleated cells (indicated by magenta arrows) exhibiting both fluorescent markers demonstrate fusion pore formation without the completion of subsequent fusion steps. **B.** Graph of the number cells positive for both fluorescent population markers (GFP and CellTracker Deep Red) binned by number of nuclei. Mixed populations were treated with BYL719 (1μM), BX795(2μM) and MK2206(2μM) 5 hours post dox induction and then fixed and dual color cells were counted 5 hours later. Cells co-stained with CellTracker Deep Red and GFP were manually identified and the quantification number of nuclei per dual color cell was automated.

A

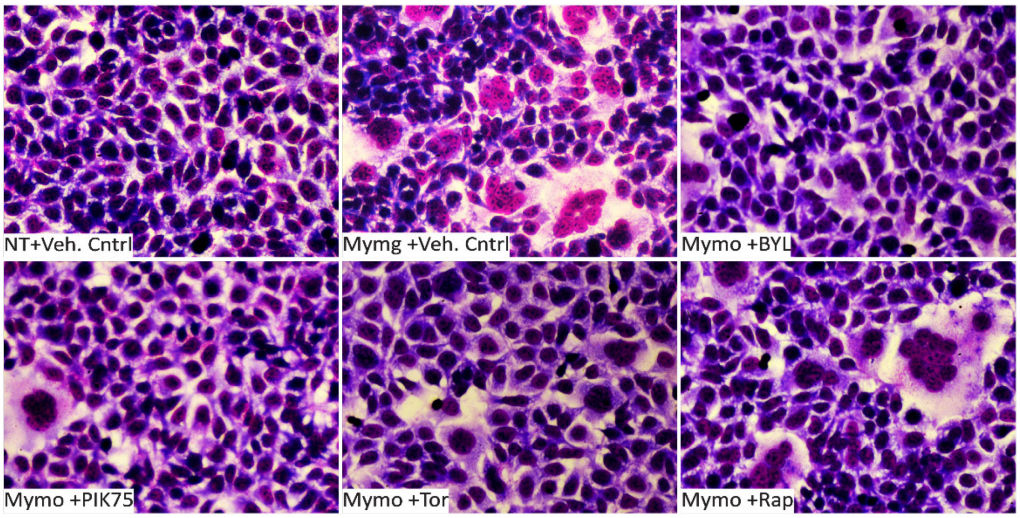
NT+Veh. Cntrl
Mymg +Veh. Cntrl
Mymo +BYL
Mymo +PIK75
Mymo +Tor
Mymo +Rap

B

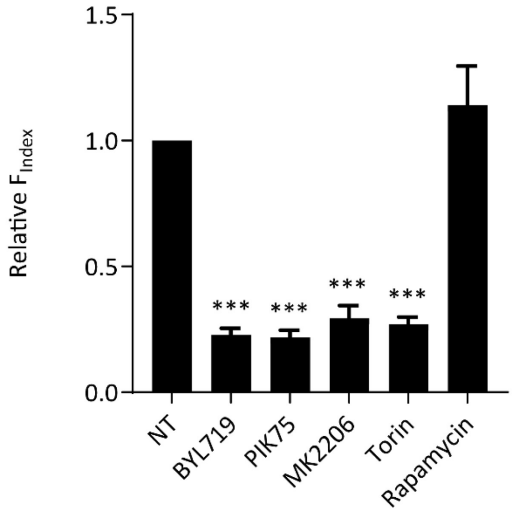
Relative F Index
1.5
1.0
0.5
0.0
***
***
***
***
NT
BYL719
PIK75
MK2206
Torin
Rapamycin

C

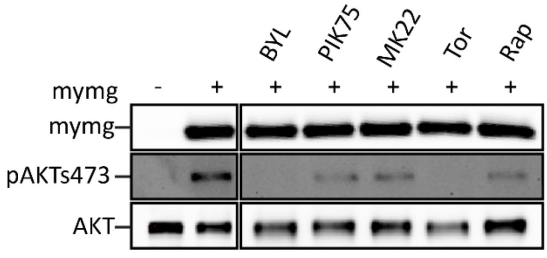
BYL
PIK75
MK22
Tor
Rap
mymg - + + + + + +
mymg
pAKTs473
AKT

3.27. Figure 17. Myomerger activates Akt prior to cell fusion.

A. Representative images of fusion in Geimsa stained Myomerger-Tet-On 293A (mymg) cells expressing Myomaker and treated with doxycycline (5µg/ml) for 24 hours alone or with BYL719 (1µM), PIK75 (100 nM), MK2206 (1µM), or rapamycin (500 nM) for 18 hours. **B.** Quantification of the relative fusion index for treatments described in Panel A. **C.** Western blot analysis of Akt Ser473 phosphorylation and total Akt in lysates from 293A Tet-On Myomerger cells.

A

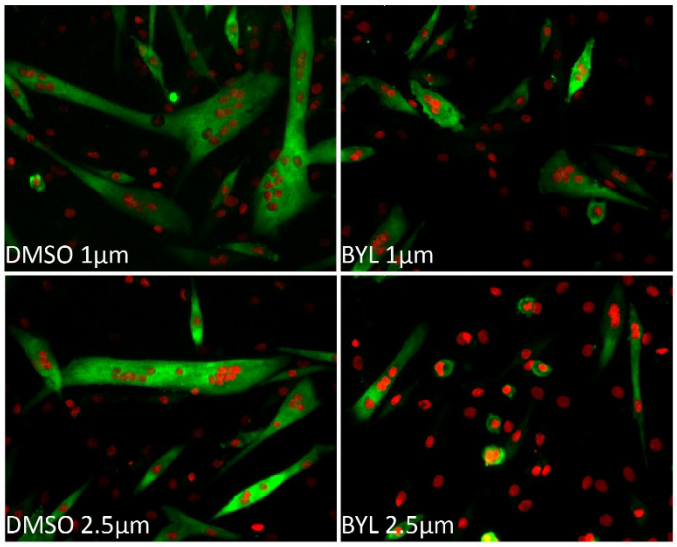
DMSO 1µm
BYL 1µm
DMSO 2.5µm
BYL 2.5µm

B

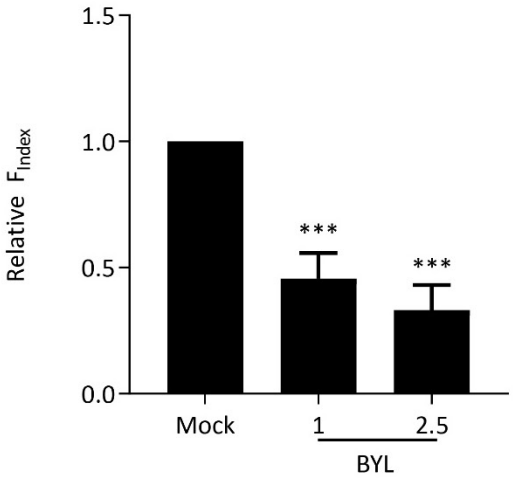
1.5
1.0
0.5
0.0
Relative F index
***
***
Mock
1
2.5
BYL

C

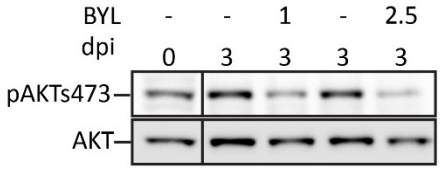
BYL - - 1 - 2.5
dpi 0 3 3 3 3
pAKTs473
AKT

3.28. Figure 18. C2C12 myogenic differentiation and fusion correlates with p110α-mediated Akt activation.

A. Fluorescent micrographs of C2C12 cells stained for MyoD (green) and nuclei (DRAQ5), treated with either vehicle control (DMSO) or BYL719 at two concentrations. **B.** Quantification of the relative fusion index of C2C12 cells, 3 days post-differentiation, treated daily with either BYL719 1µM (compared to DMSO 1µM) or BYL719 2.5µM (compared to DMSO 2.5µM) starting from day 1. **C.** Western blot analysis of phospho-Akt Ser473 and total Akt in C2C12 lysates collected at 0 days and 3 days post-differentiation, treated with either vehicle control (DMSO) or BYL719. The analysis shows an increase in pAkt S473 levels in vehicle control-treated C2C12 cells at 3 days post-differentiation compared to the BYL719-treated cells.

A

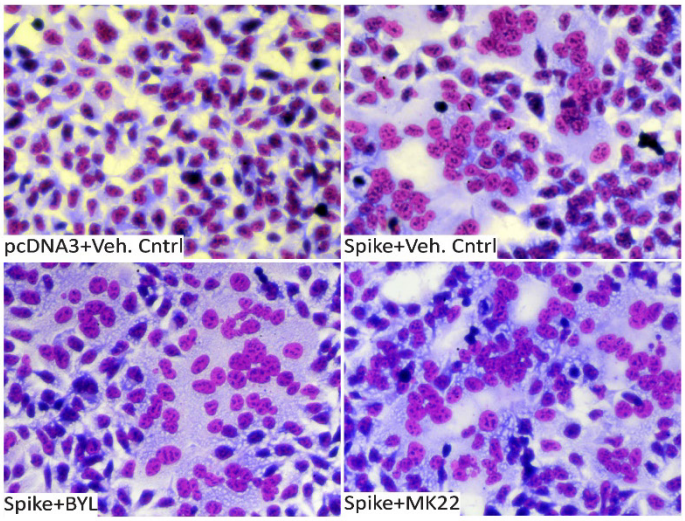
pcDNA3+Veh. Cntrl
Spike+Veh. Cntrl
Spike+BYL
Spike+MK22

B

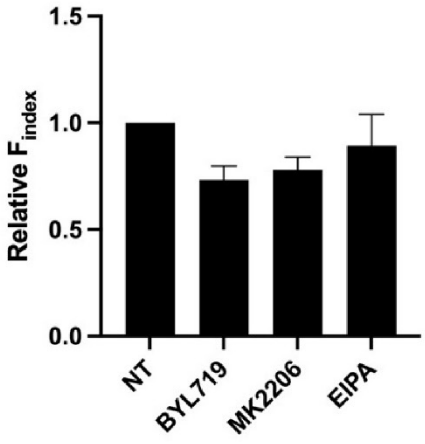
Relative F index
1.5
1.0
0.5
0.0
NT
BYL719
MK2206
EIPA

C

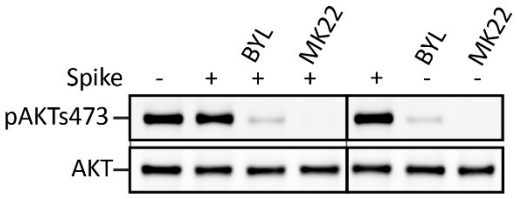
Spike
BYL
MK22
BYL
MK22
pAKTs473
AKT

3.29. Figure 19. SARS-CoV2 Spike-mediated cell fusion is not dependent on p110α activation of Akt.

A. Giemsa-stained images of 293A cells stably transduced with ACE2 and transfected with either empty vector (pcDNA3) or SARS-CoV2 Spike, and treated with vehicle control, BYL719 (1μM), MK2206 (1μM) or EIPA(10μM) 4 hours post-transfection and fixed at 10 hours post-transfection. **B.** Relative fusion index of PI3K and Akt inhibitor treatments shown in A. **C.** Western blot analysis of pAkt and total Akt in lysates from the same experiments in Panels A and B.

A

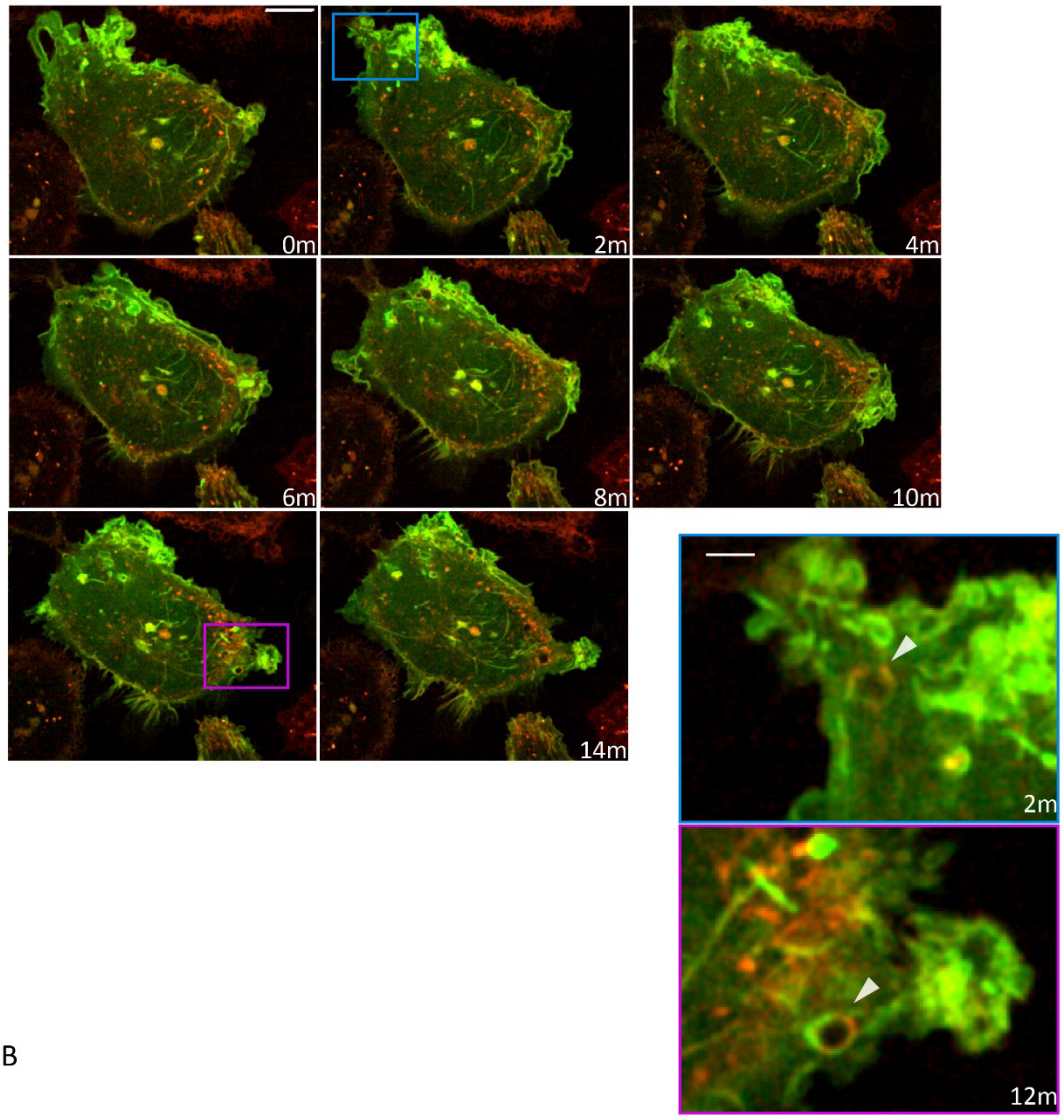
0m
2m
4m
6m
8m
10m
14m
2m
12m

B

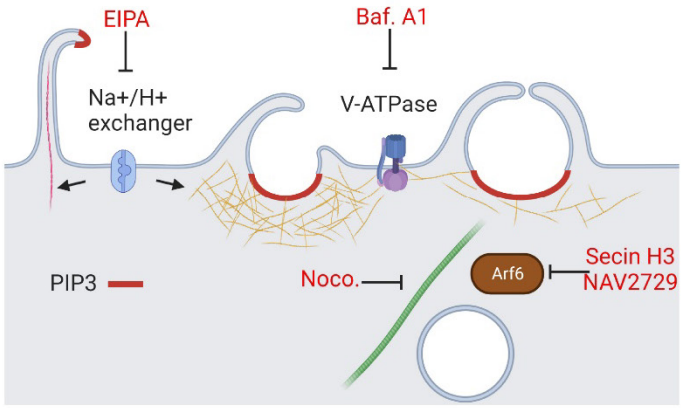
EIPA
Baf. A1
Na+/H+
exchanger
V-ATPase
PIP3
Noco.
Arf6
Secin H3
NAV2729

3.30. Figure 20. p14 is incorporated into large PIP(3,4,5) vesicles.

A. Time series of a PH(Akt)-GFP and p14-mRuby transduced HeLa cell 12 hours post doxycycline activation, displaying localized membrane ruffling. Scale bar = 15µM. In the insets of the two boxed areas (highlighted in purple and blue), large vesicles positive for PH(Akt)-GFP and p14-mRuby can be observed that resemble macropinosomes. Scale bar = 2µM. **B.** Diagram of the macropinocytosis pathway illustrating the targets of various inhibitors and their roles in the process; sodium/hydrogen exchange inhibitor ethyl-isopropyl amiloride (EIPA), cytohesin inhibitor SecinH3, ARF6 inhibitor NAV 2729, vacuolar H+-ATPase inhibitor bafilomycin A1, and tubulin-binding agent nocodazole. See text for details.

A

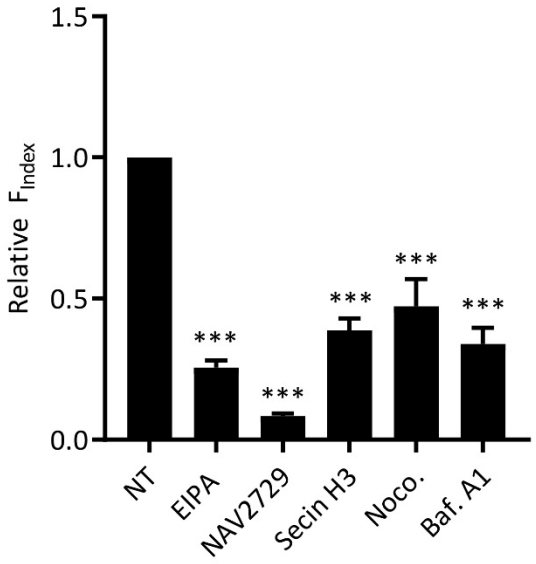
1.5
1.0
0.5
0.0
Relative F_Index
***
***
***
***
***
NT
EIPA
NAV2729
Secin H3
Noco.
Baf. A1

B

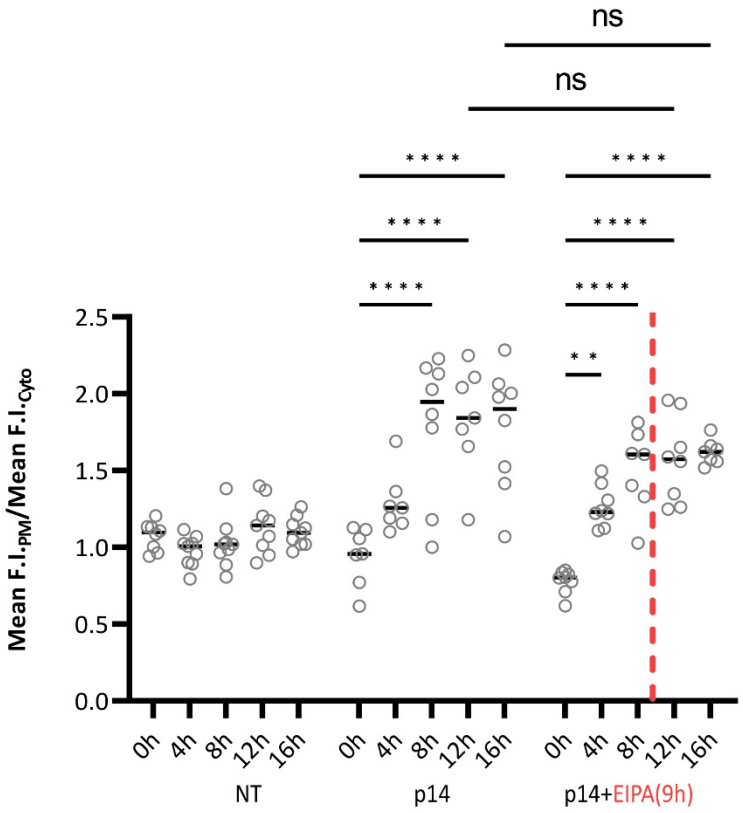
ns
ns
****
****
****
****
****
****
**
Mean F.I._PM/Mean F.I._Cyto
2.5
2.0
1.5
1.0
0.5
0.0
0h
4h
8h
12h
16h
NT
p14
p14+EIPA(9h)

3.31. Figure 21. The macropinocytosis pathway is essential for p14-mediated cell fusion.

A. Graph of the relative fusion indices of TetOn-p14 HeLa cells treated with the indicated five macropinocytosis inhibitors**.** The inhibitors utilized in the study include the sodium/hydrogen exchange inhibitor Ethyl-isopropyl Amiloride (EIPA, 30µM), cytohesin inhibitor SecinH3 (25µM), ARF6 inhibitor NAV 2729 (5µM), tubulin-binding agent nocodazole (1µM), and V-ATPase inhibitor Bafilomycin A1 (100nM). Following 5 hours post-induction, TetOn-p14 HeLa cells were pre-treated with these specific inhibitors for 8 hour and fusion index for each treatment was calculated. **B.** The graph illustrates the ratio of cytosolic-to-plasma membrane PH(Akt)-GFP fluorescence intensity, serving as a relative measure of PIP(3,4,5) concentration. TetOn-p14 HeLa cells transduced with the PIP(3,4,5)-binding pleckstrin domain of Akt tagged with GFP were treated with doxycycline at time 0 and EIPA (30µM) at 9 hours. Measurements were made at 0, 4, 8, 12, and 16 hours in mononucleated cells for the three treatments: No Dox, Dox, and Dox+EIPA. The application of EIPA is marked with a dashed red line. The results suggest that p14 expression prompts an upsurge in PIP(3,4,5) production at the plasma membrane, an effect that remains unabated by the EIPA treatment, a macropinocytosis inhibitor.

A

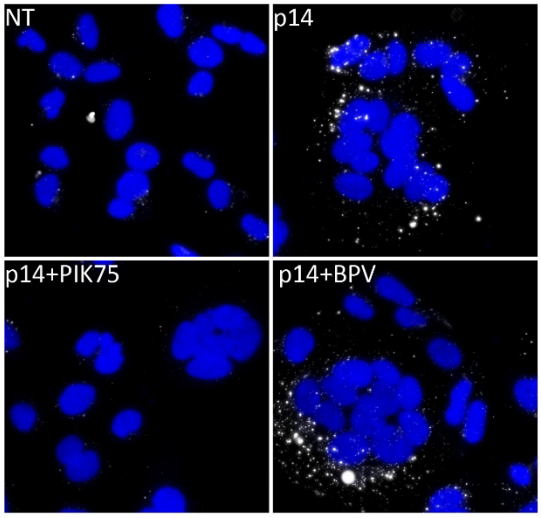
NT
p14
p14+PIK75
p14+BPV

B

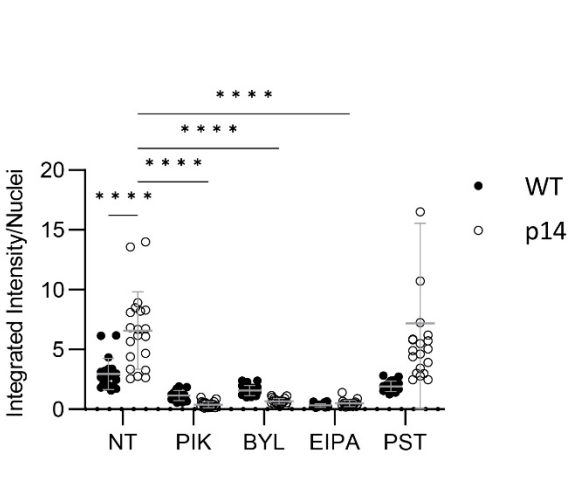
Integrated Intensity/Nuclei
20
15
10
5
0
****
****
****
****
NT
PIK
BYL
EIPA
PST
WT
p14

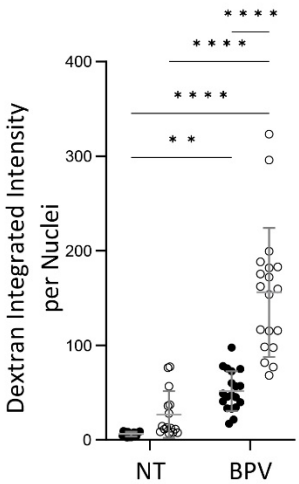
Dextran Integrated Intensity per Nuclei
400
300
200
100
0
****
****
****
**
NT
BPV

3.32. Figure 22. p14 increases high molecular weight dextran uptake in a p110α-dependent manner prior to cell fusion.

A. Micrograph showing fluorescent nuclei in blue (Hoechst) and high molecular weight dextran in white (70 kDa-dextran-TMR-Red) in doxycycline-activated TetOn-p14 HeLa cells 10h post induction. Cells were not-treated (NT) or treated with the PTEN inhibitor bpV(HOpic), 5μM), p110α inhibitor BYL719 (1μM), or macropinocytosis inhibitor EIPA (50μM). **B.** Quantification of high molecular weight dextran uptake in doxycycline-activated TetOn-p14 HeLa cells 10h post induction. Cells were treated for 1h with p110α inhibitors PIK75 (100nM) or BYL719 (1μM), macropinocytosis inhibitor EIPA (30μM), or endocytic inhibitor Pitstop2 (30μM) (left panel), or with bpV(HOpic)(5μM) (right panel) followed by incubation with 70 kDa-dextran-TMR-Red. Dextran uptake was normalized to the number of nuclei in the field of view as identified by Stardist nuclei segmentation software. Solid circles represent cells without p14 while open circles represent doxycycline-induced p14 cells. **C.** Same assay as in B with different y-axis range to demonstrate bpV(OHpic) increases in dextran uptake.

A

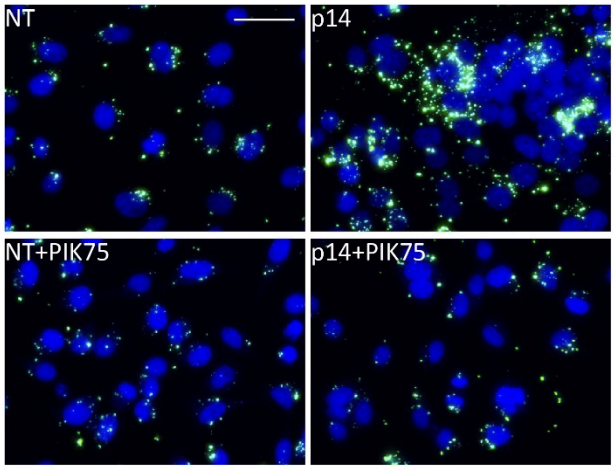
NT
p14
NT+PIK75
p14+PIK75

B

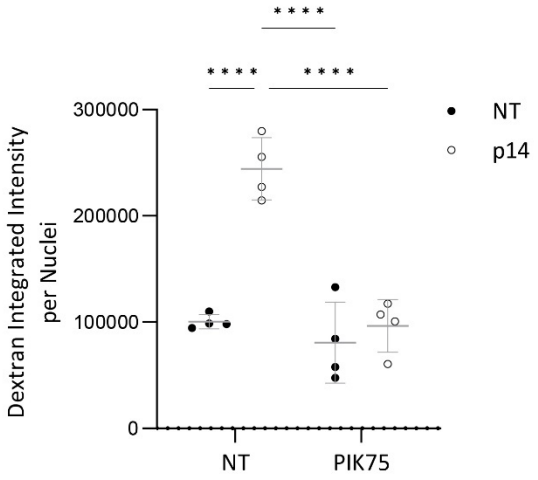
****
****
****
Dextran Integrated Intensity per Nuclei
300000
200000
100000
0
NT
PIK75
NT
p14

3.33. Figure 23. p14 increases latex bead uptake in a p110α-dependent manner.

A. Micrographs illustrating the uptake of latex beads (0.8μm) in doxycycline-activated TetOn-p14 HeLa cells HeLa cells were seeded and either induced to express p14 with doxycycline treatment (Dox+) or left untreated (Dox-). After 7 hours, the cells were treated with 100 nM PIK75 (PIK75+) or vehicle control (PIK75-) for 1 hour before incubation with latex beads for 4 hours in the presence of vehicle control or PIK75. Images were captured after washing out the latex bead-containing media. **B.** Graph showing the quantification of latex bead uptake in doxycycline-activated TetOn-p14 HeLa cells with or without PIK-75 treatment. Solid circles represent cells without p14, while open circles represent doxycycline-induced p14 cells.

A

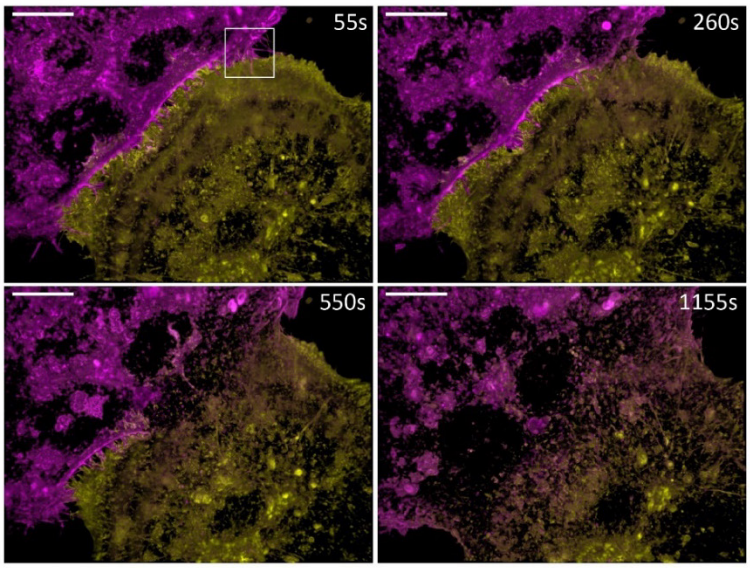
55s
260s
550s
1155s

B

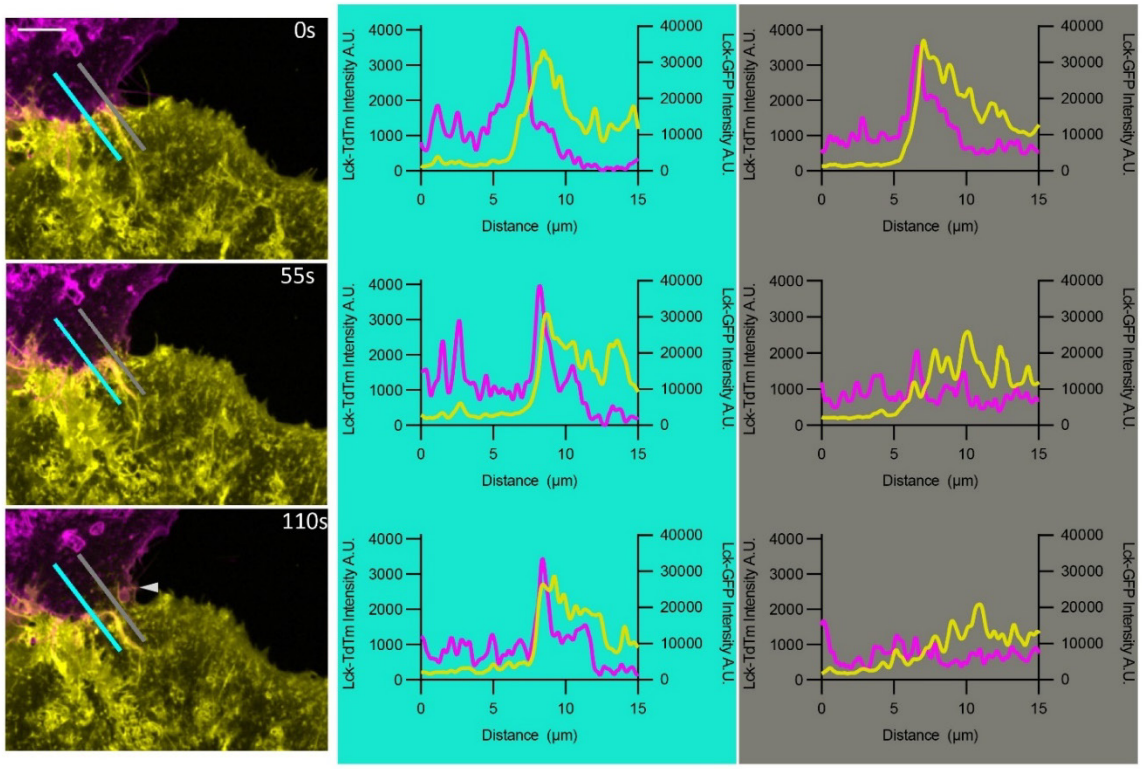
0s
55s
110s
Lck-TdTm Intensity A.U.
Lck-GFP Intensity A.U.
Distance (μm)

3.34. Figure 24. Active macropinocytosis with the generation of macropinosomes is observed at time and points of cell-cell fusion.

A. Volumetric rendering of a time series of a doxycycline treated TetOn-p14 HeLa cell expressing LCK-tdTomato (LCK-tdTom) (magenta) fusing with a LCK-GFP expressing cell (yellow) at 12h post doxycycline induction of p14. Scale bars = 20µM. **B.** Magnified images of the boxed region in panel A, with parallel teal and grey lines corresponding to the regions depicted in the accompanying fluorescence intensity plot profiles of the two fluors. Scale bars = 5µM. The time-dependent reduction in the peak intensity of the two distinct fluor peaks in the grey plot profiles from 55s to 165s, but not the teal plot profiles, corresponds with loss of the intact plasma membrane and equalization of the signals along the plot profile, indicating pore formation occurred where the grey bar transects the two membranes.

C

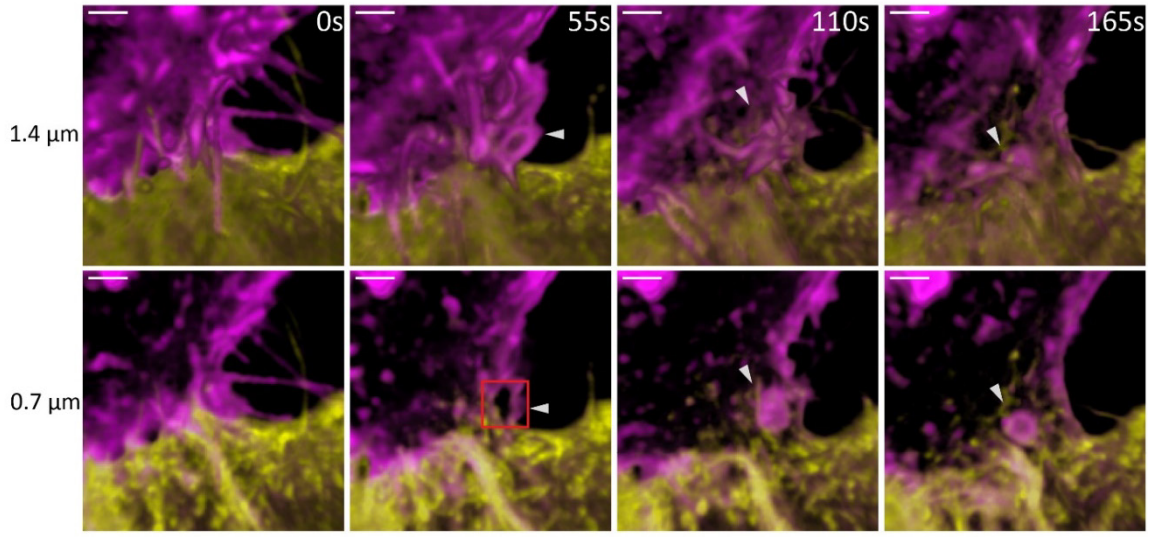
0s
55s
110s
165s
1.4 µm
0.7 µm

D

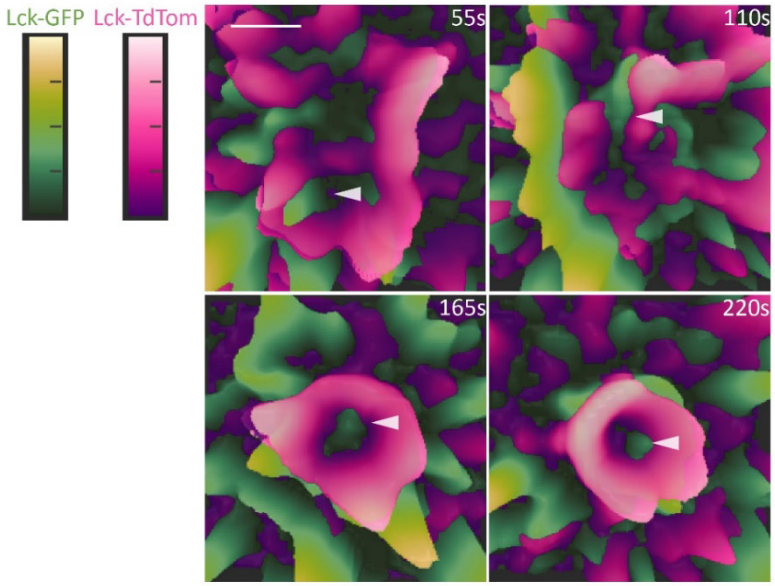
Lck-GFP
Lck-TdTom
55s
110s
165s
220s

Figure 24 (cont'd). Active macropinocytosis with the generation of macropinosomes is observed at time and points of cell-cell fusion.

C. Magnified images of the same region depicted in panel B, captured at the two indicated focal planes relative to the ventral cell surface. White arrowheads in the different timepoints indicate the same location in the respective focal planes and show the formation of a LCK-tdTom macropinosome at the fusion synapse containing a discrete LCK-GFP signal. **D.** Series of 3D surface plots (fluorescence intensity represented by peak height and color intensity) of the 50x50 pixel area centered on the macropinosome format of the lowest z plane. The formation of a LCK-TdTom macropinosome with a LCK-GFP signal localized within the cup and persisting in the lumen of the LCK-tdTom (white arrows) macropinosome, is an architecture consistent with the prefusion formation of macropinosomes wherein the LCK-tdTom expressing cell engulfs the GFP expressing cell before fusion pore formation and lipid mixing.

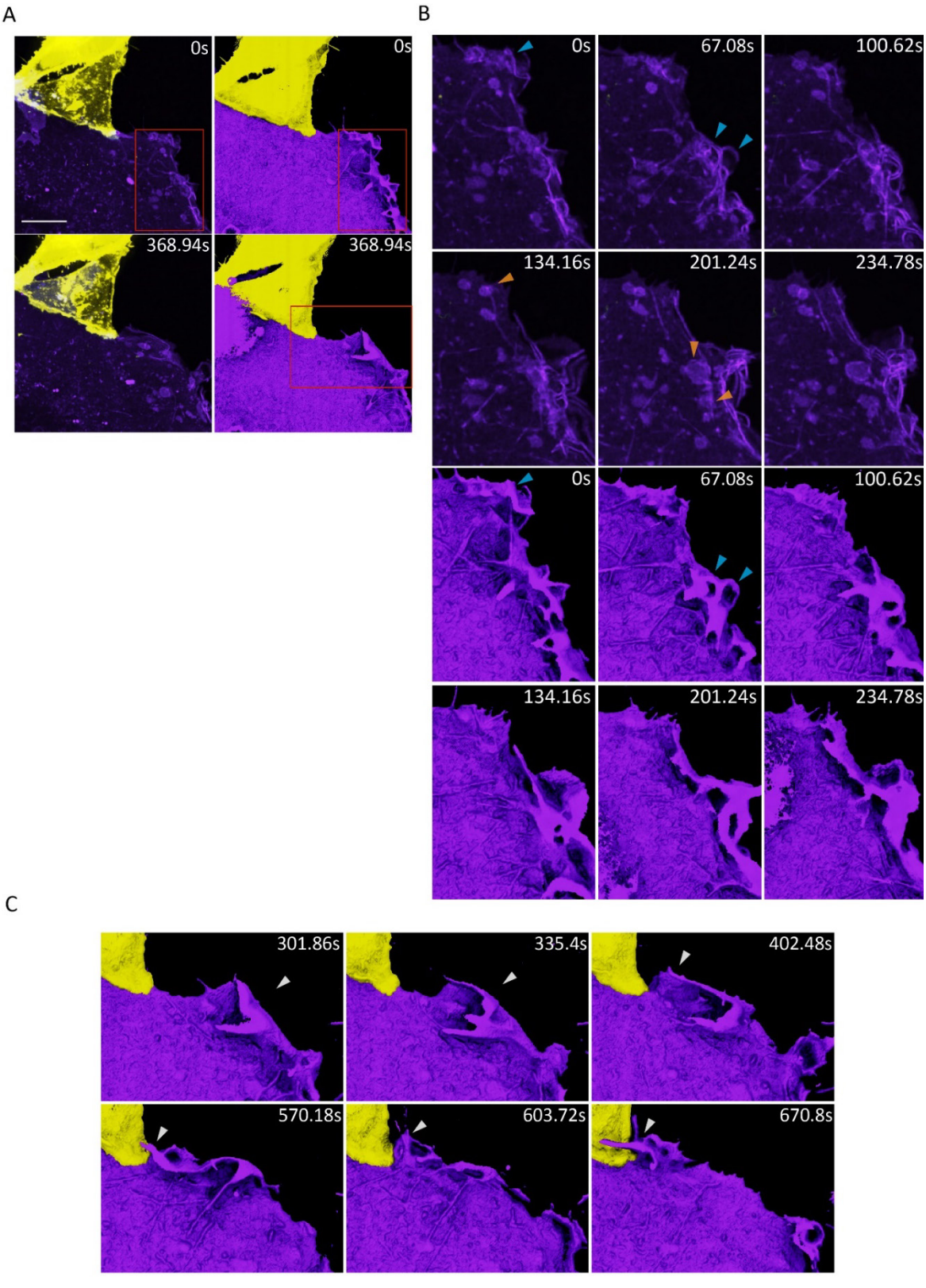
A
0s
0s
368.94s
368.94s
B
0s
67.08s
100.62s
134.16s
201.24s
234.78s
0s
67.08s
100.62s
134.16s
201.24s
234.78s
C
301.86s
335.4s
402.48s
570.18s
603.72s
670.8s

A’

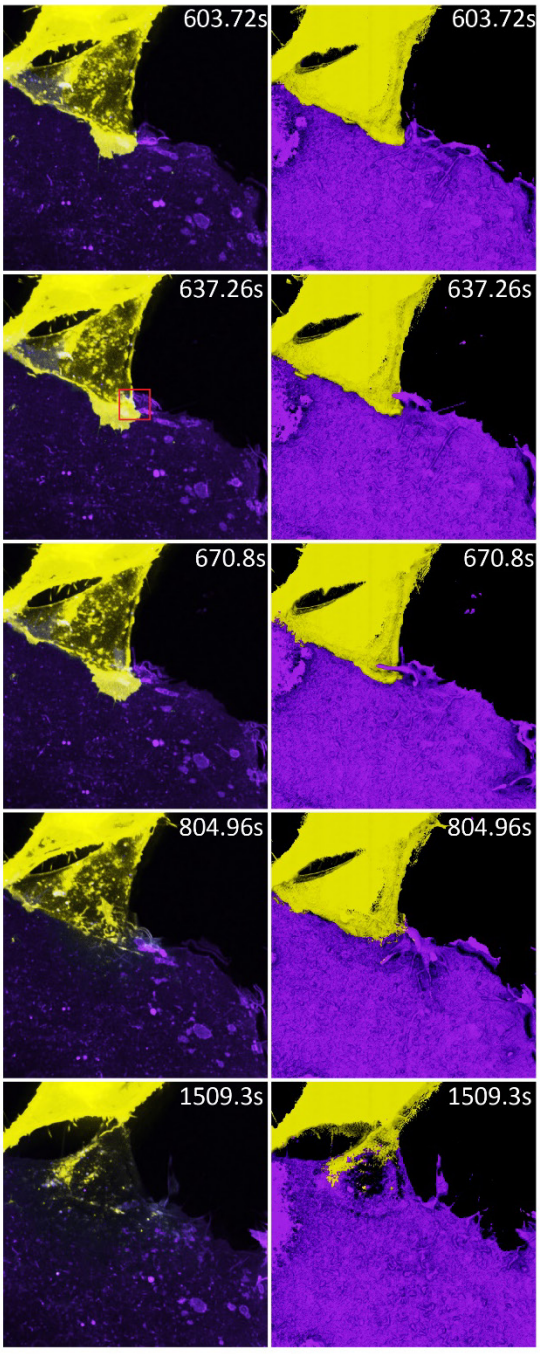
603.72s
603.72s
637.26s
637.26s
670.8s
670.8s
804.96s
804.96s
1509.3s
1509.3s

D

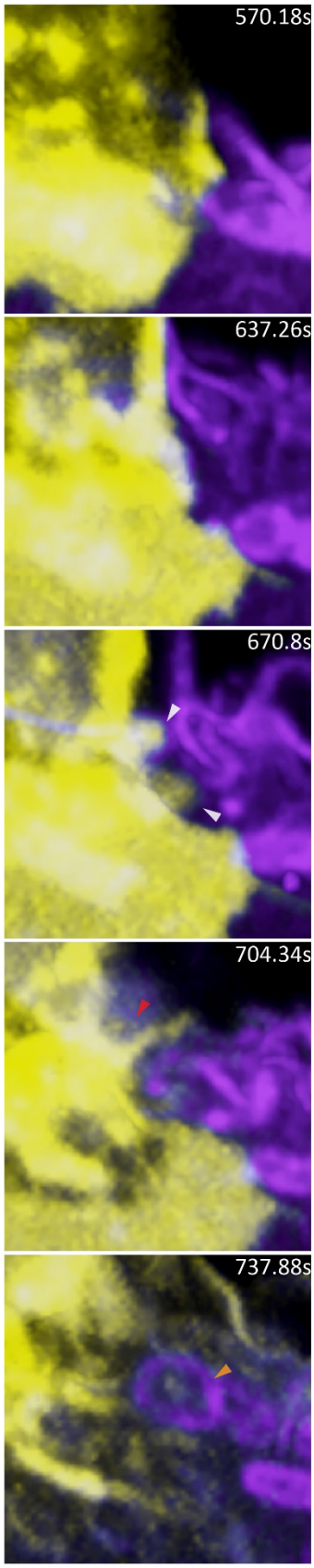
570.18s
637.26s
670.8s
704.34s
737.88s

3.35. Figure 25. Membrane ruffling and macropinocytosis cup formation precede membrane fusion at cell-cell fusion synapse.

A/A'. A time series of 3D-volumeric (A) and surface rendering (A') of a multinucleated LCK-tdTom TetOn-p14-HeLa syncytium (purple) fusing with LCK-GFP HeLa cell (yellow) not expressing p14. Image capture started at 12.5 hours post fusion induction (0 seconds) and then every 33.54 seconds taking 5 z-slices spaced 1.5 um apart. **B.** Cutout 1: Large vesicles (macropinosomes in max intensity projection; orange arrows) can be seen forming at the cell periphery of LCK-tdTom multinucleated cell from membrane ruffles (surface projection and max intensity projection; blue arrows) projecting upwards from the cell edge before fusing with the dorsal surface. **B.** A membrane ruffle travels along the edge of the syncytial cell from area of macropinosome formation toward LCK-GFP mononucleated cell, indicating macropinocytosis does not preferentially localize to sites of cell to cell contact. **C.** A cutout illustrating a membrane ruffle and the formation and closure of a macropinocytotic cup in LCK-tdTom containing and deforming the apposing LCK-GFP plasma membrane into the lumen of the macropinocytotic cup (white arrow) immediately prior to fusion at the fusion synapse and fluorophore transfer between cells (red arrow). A macropinosome (orange arrow) can be seen to originate from the same ruffle closure where fusion occurs confirming macropinocytosis occurs at points of cell to cell fusion.

Chapter 4: Discussion

4.1. Overview

The small size of the FAST proteins and their ability to robustly induce cell to cell fusion in nearly all cell types make them an excellent model for examining the minimal determinants of cell fusion. The use of "-omic" approaches was intended to provide a broad view of cellular cofactors needed for FAST protein-mediated cell-cell fusion while perhaps also providing some insights into more universal features of cell-cell fusion. Three different high-content assays, the siRNA and kinase inhibitor screens along with the MAC assay, all identified the PI3K-Akt pathway as a mediator of FAST protein-mediated cell-cell fusion (Fig. 28) This signaling hub is a central cellular signalling pathway with over 100 known substrates (Humphrey et al., 2013, 2015; Toker & Marmiroli, 2014), so merely identifying it as being required for FAST protein-mediated cell-cell fusion was not particularly informative. The breakthrough in our understanding of how this pathway promotes fusion synapse formation came from live cell imaging experiments and optimized dual colour fluorescence imaging protocols I developed.

Using a dox-inducible, p14 HeLa cell system, I could synchronize p14 expression and cell-cell fusion to allow 3D imaging over relatively short time frames. This allowed me to capture cell fusion at high-spatial and temporal resolution. I was also able to image macropinocytic vesicles that were dual-labeled for p14 and PIP(3,4,5) forming at the fusion synapse coincident with pore formation. Together, these results revealed for the first time that p14, via activation of PI3K-Akt signaling, upregulates MaPi pathways to promote cell-cell membrane fusion (Fig.28). Furthermore, collaborative studies indicated this pathway was also involved in myomerger-mediated syncytiogenesis (Fig. 26) and possibly during mouse myotube formation, but not during syncytium formation induced by diverse enveloped virus fusogens, suggesting a conserved mechanistic link between small protein fusogens. Intriguingly, time lapse image analysis showed fusion pore formation occurring in or immediately proximal to the macropinocytic cup and concurrent with retraction of the macropinocytic membrane to form a macropinocytic vesicle, suggesting a novel retraction mechanism rather than protrusion mechanism for

how actin-driven membrane deformations could induce the membrane tension needed for cell-cell fusion.

4.2. SiRNA and small molecules screens reveal the pi3k-akt pathway as a key regulator of fast-mediated cell fusion

An initial siRNA screen was conducted using multiple siRNAs to target numerous kinases. This medium-throughput screening method aimed to strike a balance between identifying potential hits and controlling costs. Kinases were targeted due to their central role in signaling networks and well-differentiated druggable nodes, such as individual kinases and well-characterized signaling cascades. This approach enabled the identification of pathways associated with rapid protein fusion, with multiple hits along a similar pathway reducing the likelihood of false positives. Additionally, kinases have been identified as mediators of various cell fusion forms (Omata et al., 2013; Weichert et al., 2016; H. Zhang et al., 2021).

However, no target gene in the p15-mediated fusion siRNA screen demonstrated greater than 60% fusion inhibition with all three siRNAs targeting that gene due to several confounding factors. For instance, cells transfected with the control non-targeting siRNA exhibited an increased rate of syncytiogenesis, complicating the standardization of results (Fig. 5B). Another factor complicating the analysis was that many kinases have multiple isoforms with similar structures. The removal of one isoform from the cellular environment can allow the remaining isoforms to compensate by binding interacting partners that they would normally be competitively inhibited from interacting with. For example, of the three Akt isoforms, *in vivo* studies indicate Akt2 is the primary isoform expressed in skeletal muscle and deletion of Akt2 decreases the myofiber area and fusion index (Gardner et al., 2012; Glass, 2011; Rommel et al., 2001). However, a single isoform of Akt is sufficient for myotube formation and over expression of Akt1 can restore function from loss of Akt2 (Gardner et al., 2012). In addition, studies on C2C12 fusion revealed that while pharmacological inhibition of PI3K isoform p110β results in a fusion defect, genetic knockdown leads to hyperactivation of p110α,

resulting in increased myotube size and nuclei number (Matheny et al., 2012, 2015). In my screen, each isoform of PI3K and Akt was individually targeted, making it challenging to assess the collective contribution of Akt to p15-mediated fusion.

Despite these limitations, the STRING network analysis and KEA3 identified subnetworks of kinase signaling that were overrepresented within these hits. Akt was found to be the most common downstream signaling kinase, which I subsequently confirmed is an essential kinase for efficient p14-mediated cell-cell fusion. STRING analysis of the hits compared to the targeted proteins in the screen revealed a significantly larger number of interactions between hits than would be expected by random chance (p=0.0202). This indicates that a protein signaling network is likely contributing to p15 fusion activity. Interestingly, p21-activated kinase 1 (PAK1) was identified as the highest scoring upstream kinase in the KEA3 analysis. PAK1 specifically contributes to myoblast fusion during muscle development by regulating the actin cytoskeleton, ensuring proper cell-cell contact for fusion (Joseph et al., 2017). In osteoclast formation during bone remodeling, PAK1 also regulates the actin cytoskeleton, aiding in the fusion of mononuclear precursors to form functional osteoclasts (Pereira et al., 2018). PAK1 is also known to be involved in other fusion events, including HIV-env fusion and *Cryptococcus neoformans* in cell fusion (Nichols et al., 2004; Pontow et al., 2004). It would be interesting to evaluate PAK1 relationship to the fusion-promoting PI3K-Akt signaling axis I identified and characterized.

While siRNA can effectively silence proteins, it may not always inhibit function to the same extent as drug inhibition. To validate the siRNA predictions and perform a more rigorous interrogation of kinase signalling in p15-mediated fusion we decided to perform an additional small molecule inhibitor screen. The small molecule kinome screen had a vastly reduced number of targets (165 vs 710 siRNA targets), and each drug was assayed at 3 concentrations in triplicate providing a robust dataset that also allowed detection of dose-dependent effects. Three small molecule inhibitors emerged as high probability hits from the inhibitor screen for their potent inhibition of p15 syncytia formation without causing a significant decrease in cell proliferation or viability: PIK75 at

concentrations of 2.5uM and 0.25uM, A443654 at 2.5uM concentration, and PHA767491 at 2.5uM (Fig. 4A).

PIK75 is a class IA PI3K inhibitor with specificity for the p110α isoform over the p110β (200-fold) and p110ɣ (~100-fold) isoforms (Knight et al., 2006; Y. Li et al., 2012). However, PIK75 has also been reported to inhibit DNA-dependent protein kinase (DNA-PK), an enzyme involved in DNA repair and V(D)J recombination (Liang & Blundell, 2023), hence a potential contribution of DNA-PK to p15 syncytia formation cannot be excluded. A443654 is an inhibitor of Akt, an effector kinase of class I PI3Ks [4], and previous studies implicate PI3K-Akt signaling in various cell fusion events (Jin & Woodgett, 2005; Oikawa et al., 2012). PHA767491 inhibits cdc7/cdk9, enzymes known to be involved in cell cycle regulation and transcription (Anshabo et al., 2021; Montagnoli et al., 2008). The involvement, if any, of these two kinases in cell fusion requires further investigation.

Of the four high-confidence hits from the kinase inhibitor screen, three identified the PI3K-Akt signaling axis as being necessary for p15 induced syncytiogenesis. This finding was corroborated by the MAC assay (Fig. 7B), which identified Akt and H2AX as the sole hits for inhibiting p14 fusion in the same cell line. The congruence of results from both the MAC assay and kinase inhibitor screen provided a high degree of confidence that these results warranted further investigation. The absence of other hits from these assays (aside from H2AX and cdk7/9) also pointed to the central role of PI3K-Akt signaling in both p15 and p14 fusion. Furthermore, the activation of PI3K-Akt by p14 strengthens the notion that PI3K-Akt signaling plays a more direct and significant role in the regulation of cell fusion events, rather than merely regulating cellular homeostasis.

Due to known off-target effects of small molecule inhibitors, such as PIK75 inhibiting DNA-PK, it was necessary to confirm PI3K-Akt involvement in p14-mediated cell fusion. Although genetic inhibition is ideal for this confirmation, pharmacological inhibitors of PI3K p110α and Akt were utilized instead. The kinase siRNA screen did not reveal significant fusion inhibition with any PI3K isoform or Akt isoform knockdown, which could be attributed to known issues with the genetic knockdown of single isoforms of p110 PI3K or Akt enabling non-physiological compensatory functions

(Arcucci et al., 2021). For instance, in C2C12 myoblast fusion, knockdown of p110β has been shown to hyperactivate p110α, resulting in increased Akt activation as well as myotube size and nuclei number. However, pharmacological inhibition of p110β with TGX221 hindered differentiation. (Jin & Woodgett, 2005). The specificity of p14-induced PI3K-Akt activation for the p110α isoform was confirmed by testing three additional inhibitors: BYL719 (p110α-specific), TGX221 (p110β-specific), and wortmannin (pan-Class 1 PI3K inhibitor). The results indicated that p14-induced AktS473 phosphorylation and fusion were inhibited by PIK75, BYL719 (p110α-specific), and wortmannin, but not by TGX221, supporting the notion that p14 activates the PI3K (p110α)-Akt signaling axis. p14 Tet-On HeLa cells were treated with A443654, a competitive inhibitor of substrate binding, and MK-2206, an allosteric inhibitor of Akt, to further investigate their role in fusion (Fig. 7A). The observed inhibition of fusion in both treatments indicated the necessity of Akt in p14-mediated fusion. Moreover, hyperactivation of the PI3K-Akt pathway induced by inhibiting PTEN with bpV(HOpic), which allowed manipulation of PIP(3,4,5) accumulation without directly affecting p14-mediated activation of PI3K(p110α), (Fig. 11A&B). further emphasized the significance of the PI3K-Akt signaling pathway in FAST protein-mediated syncytiogenesis.

Our investigation of fusion pore formation revealed that the PI3K-Akt pathway was required at or prior to pore formation. p14 expression in GFP-transduced HeLa cells resulted in cytosolic mixing with neighboring HeLa cells labeled with CellTracker Deep Red, without full fusion (Fig. 16A purple arrows). This was indicated by the presence of numerous dual-color mononucleated cells, suggesting that GFP can indeed diffuse between cells through fusion pores that have not yet expanded, or failed to do so. This observation was further corroborated by live-cell imaging, where we witnessed the transfer of GFP between cells for several minutes before the plasma membrane vanished (data not shown or reference a video). These results suggest that the fusion pores were sufficiently large to permit the transfer of GFP, thus validating our assay as a suitable method to investigate the role of PI3K-Akt signaling in fusion pore formation and expansion. Our study provides strong evidence that PI3K-Akt activation is not solely

a consequence of cell fusion but rather plays a vital role in the early stages of syncytium formation.

4.2 Understanding PI3K-Akt Dynamics in p14 Fusion Through the Lens of Other Fusion Models

Given the diverse functions of the PI3K-Akt pathway within cells, an examination of the existing literature on PI3K-Akt signaling regulation in other cell-to-cell fusion models provided valuable insights into the pathway's potential function in FAST protein fusion. The PI3K-Akt pathway has been associated with various fusion paradigms, performing distinct functions such as altering transcription and/or translation to differentiate fusion-incompetent cells into fusion-competent cells, as observed in myoblast fusion, or driving the formation of fusogenic invasive membrane projections at the fusion synapse in osteoclast fusion (E. H. Chen, 2011; Faust et al., 2019; Gardner et al., 2012). Guided by these contrasting models, we employed siRNA and inhibitor experiments to elucidate the necessary downstream effectors of PI3K-Akt signaling in FAST-mediated fusion, and live cell imaging to localize PI3K-Akt signaling and observe changes in cell morphology induced by this signaling. My results revealed that p14 mediated cell fusion, does not utilize the mTORC1 translation signaling hub critical for cell differentiation in myoblast fusion, and while p14 did induce membrane projections, their contribution to cell fusion is likely distinct from the protrusive force mechanism of invadopodia/podosomes previously described in osteoclast and Drosophila fusion.

To determine if p14-mediated fusion is distinct from myoblast fusion, we investigated whether p14 induces a myogenic-like differentiation program by drawing from the existing literature on downstream mediators of PI3K-Akt signaling in vertebrate myoblast cell differentiation. We employed inhibitor and siRNA approaches targeting the downstream mediator, mTORC1, which is required for C2C12 myotube formation and the expression of IGF-II and proliferation (Erbay et al., 2003; Rion et al., 2019). In mouse studies, satellite cells contribute a significant portion of myonuclei to mature myotubes through fusion, and p110α of PI3K signaling through mTORC1-cJun and FOXO

3a is necessary and sufficient for quiescence exit of adult muscle satellite cells prior to fusion (G. Wang et al., 2018).

However, our results revealed that p14-mediated fusion is not mTORC1 dependent, as evidenced by the lack of fusion inhibition by rapamycin treatment or Raptor shRNA knockdown, and the absence of a decrease in Akt S473 phosphorylation following rapamycin treatment in C2C12 cells. Additionally, while the mTORC1-pS6 pathway has been implicated in the regulation of myogenic differentiation by controlling the expression of key myogenic transcription factors such as MyoD, myogenin, and myocyte enhancer factor 2 (MEF2) (Lehka & Rędowicz, 2020; Yoon, 2017), the phosphorylation of S6, which was upregulated by p14 and inhibited by rapamycin (Fig. 13F) did not show a correlation with fusion as rapamycin treatment of TetON-p14 HeLa cells did not inhibit fusion (Fig. 12B). These findings further support the notion that p14-mediated fusion employs a distinct mechanism from that of myoblast differentiation (Gardner et al., 2012; Glass, 2011).

In contrast to the primarily transcriptional role of PI3K-Akt signaling in vertebrate muscle development, my study suggests PI3K-Akt signaling acts locally at points of cell-to-cell fusion. Specifically, we found that p14 activates PI3K, and the synergistic action of p14 and PI3K increases the proportion of syncytial nuclei to single cells within a cell population. The increase in Akt S473 phosphorylation coincides with the fusion-critical function of PI3K-Akt signaling, as PI3K-Akt signalling occurs prior to fusion in mononucleated cell (Fig. 9) and non-fusogenic p14 mutants induce Akt activation (Fig. 15). Experiments to quantify fusion pore formation showed that PI3K-Akt signaling is critical prior to fusion pore formation and/or pore expansion, but not for syncytia maintenance (Fig. 16). These findings suggest that PI3K-Akt signaling is not mediating global transcriptional changes during muscle development, but instead, plays a critical role in the molecular mechanisms underlying cell fusion.

4.3. p14 and the podosome-like-structure fusion model

The involvement of invadopodia/podosomes in cell fusion processes has gained attention in recent years (Brukman et al., 2019; Chuang et al., 2019, 2019; Dufrançais et al., 2021; Kim et al., 2015; Shilagardi et al., 2013a). Podosomes and invadopodia, collectively referred to as invadosomes, are dynamin and branched actin-rich structures on the cell's ventral surface, characterized by an Arp2/3-nucleated F-actin core and a surrounding ring of various proteins. Adhesion proteins in this ring, such as integrins (αvβ3, αvβ5) and talin, facilitate extracellular matrix interaction. Scaffolding proteins like vinculin, paxillin, and Hic-5 anchor the actin core to the membrane, providing structural stability. The dynamics and life cycle of these structures are regulated by signaling proteins, including Src kinase, Cdc42, and Rho-GTPases. Nucleation promoting factors like N-WASP and cortactin catalyze actin polymerization in the core. Tyrosine kinase substrate 5 (TKS5), a key component of invadopodia, connects the actin cytoskeleton to membrane-bound metalloproteases, enabling ECM degradation. (Linder et al., 2023; Murphy & Courtneidge, 2011). The spatial organization of fusogenic invadosomes differs from traditional invadosomes. While classic invadosomes are formed on the ventral cell surface and penetrate vertically into the extracellular matrix, fusogenic invadosomes project perpendicularly from the cell edge and protrude into neighbouring cells.

In osteoclast fusion, the catalytic subunit isoform p110α but not p110β of PI3K is essential for inducing the formation of these fusogenic invadopodia, while scaffold protein TKS5, which binds PIP(3,4) produced from PIP(3,4,5) by phosphatase SHIP2, plays a crucial role in invadopodia formation and function, directly interacting with dynamin-2 and regulating actin filament assembly within the fusogenic podosome (Kodama & Kaito, 2020; Oikawa et al., 2012; Pereira et al., 2018). The specific contribution of Akt to the formation of fusogenic invadopodia in osteoclasts is unclear, as it is negatively regulated by SHIP2 depletion of PIP(3,4,5), however, a separate study demonstrated that mTORC2-Akt signaling is necessary for osteoclast fusion, while mTORC1 is dispensable (Tiedemann et al., 2017a). This finding parallels the isoform

specific kinase requirements for p14-mediated fusion, emphasizing the similarity of PI3K-Akt signalling in both osteoclast fusion and p14-mediated fusion.

Broadly speaking, the plasma membrane of metazoan cells is intricately linked to an elaborate and dynamic underlying cortical cytoskeleton composed of filamentous actin (F-actin) (Chugh & Paluch, 2018). The cortical actin networks comprise both branched and unbranched filaments that are generally lying parallel to the overlaying lipid bilayer. In most metazoan cells, including those capable of cellular fusion, the cortex is a critical determinant of morphology and surface tension. Elizabeth Chen and others have made the case for the presence of significant mechanical tension between apposing cells involving rapid modulation of the cortical network as an essential prerequisite for cell-to-cell fusion. (Chen, 2011; Hammers et al., 2021). Under this model, there exists an underlying asymmetry observed at the fusogenic synapse wherein actin propelled protrusions termed F-actin-enriched podosome-like structure (PLS) from one cell indents and thus elicits a myosin II (MyoII)-mediated mechanosensory induction of actin polymerization in the tightly apposed "recipient" cell that resists the invasive projections (Kim et al., 2015). The ensuing high mechanical tension is proposed to promote both fusogen engagement and, ultimately, fusion of the cell membranes themselves.

The role of membrane tension in the fusion of membranes has been the study of many recent investigations as new tools are developed to measure force in the microenvironment. However, the exact role of mechanical force remains controversial and poorly understood. In one report, Drosophila S2R+ cell lines, which normally do not fuse, were induced to do so by transfecting cells either with the *C. elegans* fusogenic protein Eff-1 alone or in combination with the fusion-competent myoblast (FCM)-specific cell adhesion molecule Sns (Sticks-and-Stones) and co-incubating the two populations (Shilagardi et al., 2013). Actin-propelled podosome-like structures (PLS) were observed protruding from the Sns-Eff-1-expressing "attacking" cells into the Eff-1-expressing "receiving" cells. The receiving cell resists invasion by promoting the accumulation of contractile cortical actin, facilitated by myosin. The cells in this system

appear to impose a mechanical force on the receiving fusion partner with inward membrane curvatures observed in the latter.

In a subsequent study using atomic force microscopy (AFM), a pushing force was applied to the cell cortex using a cantilever (100 nm width) thus approximating the mechanical force observed by PLS invasion in cell-cell fusion, resulting in a similar degree of cortical deformation and cell-cell fusion (Kim et al., 2015). These results highlight the need for membrane tension to allow fusion to occur. Subsequent research has revealed the presence of membrane projections in various cell fusion contexts, including osteoclast and murine myoblast fusion, as well as during *Burkholderia thailandensis* infection (Kostow & Welch, 2022). In addition, increased tension in MCF-7 cells within 3D culture has been shown to induce cell fusion, resulting in multinucleated giant cells (Bühler et al., 2022). Lateral membrane tension has been found to significantly enhance SNARE-mediated fusion of giant unilamellar vesicles with a planar bilipid layer and to be crucial for pore expansion in HIV-1 viral fusion with the plasma membrane (Coomer et al., 2020; Kliesch et al., 2017).

Drawing on recent studies from Dan Fletcher's lab, it appears that FAST proteins, including p14, may drive cell fusion through a membrane projection mechanism. This process is facilitated by the recruitment of cytoskeletal regulatory proteins to stimulate filamentous actin formation at the plasma membrane. Specifically, p14 recruits the growth factor receptor-bound protein 2 (GRB2) by binding to a phosphotyrosine residue at position 116 within its cytoplasmic tail (K. M. C. Chan et al., 2020). Receptor tyrosine kinases (RTKs) frequently function upstream of GRB2, acting as a bridge to transmit signals from activated RTKs to PI3K and other downstream effectors (T. O. Chan et al., 2002; Lowenstein et al., 1992). By binding to the p85 subunit of PI3K, GRB2 facilitates PI3K activation, which in turn impacts various cellular processes (Jiang & Ji, 2019).

The recruitment and activation of GRB2 by p14 appeared to be a promising mechanism for p14's activation of PI3K. However, both the fusion-dead mutant p14G2A and the severe fusion inhibition mutant p14C88, which lacked the polyproline GRB2 binding domain, were able to activate Akt. This suggests that GRB2 is not responsible for

p14's activation of the PI3K-Akt pathway. Moreover, these results indicate that activation of the PI3K-Akt pathway, while necessary, is not sufficient for p14 fusion and occurs prior to fusion. Nevertheless, p14's recruitment of actin polymerizers aligns with the idea that p14-induced fusion, as suggested by Fletcher's work, is one of a growing number of cell fusion paradigms in which cytoskeletal membrane protrusions play a crucial role. The role of membrane projections in mediating cell-cell fusion is an essential area of investigation. These dynamic, actin-rich structures, including filopodia and invadopodia, extend from the cell surface and facilitate cell adhesion, migration, membrane tension, and fusion. Membrane projections are thought to serve as initial contact points between cells, allowing them to come into close proximity and subsequently undergo fusion.

4.4. Unveiling the mechanisms of p14-induced fusion through advanced imaging

To unravel the mysteries of p14-induced fusion and membrane projection-mediated cell fusion, suggested by Fletcher's work, we saw an urgent need for an innovative approach to visualize these processes with unprecedented clarity. p14's activation of the PI3K-Akt pathway through a GRB2-independent mechanism, as indicated by the ability of the fusion-deficient p14G2A and p14C88 mutants to activate Akt, suggested a deeper level of complexity. While PI3K-Akt pathway activation appeared necessary, it was not sufficient for p14 fusion, indicating additional processes or mechanisms at play. One intriguing lead was the involvement of actin polymerizers, hinting at a role for cytoskeletal membrane projections in cell fusion, an emerging paradigm in the field.

Our ambition to visualize and analyze these membrane projections and fusion processes in real-time led us to embrace advanced imaging techniques. New state of the art imaging techniques, including confocal microscopy, total internal reflection fluorescence (TIRF) microscopy, and super-resolution stimulated emission depletion (STED) microscopy, have been employed in live-cell imaging to visualize membrane fusion events in exocytosis of synaptic vesicles and viral envelope-plasma membrane interactions. However, due to the relatively long timescales and stochastic nature of cell

fusion, conducting similar high spatial and temporal resolution microscopy experiments remains challenging. A second challenge is quantifying membrane tension at sites of membrane invasion from one cell into another. A focus of my PHD research has been maximizing the spatial and temporal resolution of the fusion synapse before, during and after fusion which in turn allows for the inference of which direction mechanical force is being applied from one plasma membrane to the other.

Cell-cell fusion studies have historically faced challenges due to the reliance on 2D microscopy techniques to capture fusion events. These methods frequently employ high-magnification objectives that, despite their superior resolution, have a limited depth of field. Consequently, the field of view encompasses a mere 250-300 nanometers on the z-axis, providing only a narrow glimpse of the interface between two opposing cells, which can span up to 3 micrometers before fusion. Alternatively, researchers have used lower magnification objectives with a larger depth of field. While this approach can survey a broader region, it sacrifices lateral resolution, making it ill-suited for accurately capturing the intricate details of the fusion synapse.

In pursuit of a more refined understanding of cellular fusion, we adopted an advanced approach employing live-cell 3D imaging with enhanced temporal resolution. This transition necessitated the mitigation of phototoxicity, a byproduct of reactive oxygen species generation due to laser exposure. Our pioneering experiments served as the springboard for this advancement, revealing that the majority of cell fusion events occurred within 2-3 microns of the coverslip's top. This discovery allowed us to strategically reduce the number of z-slices necessary to capture the fusion site, circumventing the need to image the entire cell height and thereby minimizing laser exposure. This minimization was compounded by our decision to utilize larger gaps between the slices.

Simultaneously, we focused on optimizing the speed of p14 fast protein-induced cell fusion, allowing for a further reduction in laser exposure. We noted that fusion transpired more slowly when cells were seeded on glass coverslips or optical plastic compared to plastic cell culture multi-well plates. This observation led us to hypothesize

that cell adhesion influences fusion kinetics. To test this, we explored various substrates such as fibronectin, Poly-L-lysine, and collagen, aiming to enhance both fusion and cell attachment. Among these, Poly-L-lysine emerged as the most successful in replicating fusion kinetics observed in traditional cell culture.

Our strategy also incorporated the use of Fluorobrite media, a formulation designed specifically to reduce reactive oxygen species production and bolster the signal-to-noise ratio. Used in conjunction with a spinning disk microscope and meticulously optimized capture parameters, we substantially improved the accuracy of our imaging. An integral part of this enhancement came from Noise2Void, an unsupervised machine learning algorithm adept at reducing noise (Krull et al., 2019). By boosting the signal-to-noise ratio, Noise2Void enabled us to depict fusion synapse features more precisely, even while using lower laser intensities.

The culmination of these strategic adjustments resulted in a sophisticated imaging setup. This approach not only allowed for a more nuanced visualization of the fusion synapse but also represented a significant leap from previous methodologies. I first used 3D imaging to investigate the localization of PIP(3,4,5) using the PH(Akt)-GFP biosensor and p14 tagged with the fluorescent protein mRuby, as well as the dynamics of membrane projections at the fusion synapse. This approach allowed tracking spatiotemporal changes in key signaling molecules and observing morphological alterations during fusion. I was able to localize both PIP(3,4,5) and p14 to the fusion synapse prior to fusion (Fig.10A) and accurately determine when fusion occurs by measuring the diffusion of PH(Akt)-GFP to the unlabeled cell (Fig. 10B). Intriguingly, fusion took place near membrane ruffles and upon their closure, as opposed to instances when the largest invasion of one cell into another occurred. Nonetheless, to accurately visualize the plasma membrane remodeling at the fusion synapse, further enhancements in resolution are required, as will be discussed later.

The involvement of PI3K-Akt signaling in the fusion synapse of myoblast fusion and its potential effects on transcriptional or translational activity in osteoclasts should not be ruled out. Numerous studies have indeed implicated PI3K, mTORC2, and Akt as

essential factors for myoblast fusion. Recently, TKS5-positive invadopodia have been observed at the fusion synapse in C2C12 cells, further supporting this hypothesis (Chuang et al., 2019). Additionally, the inhibition of Akt signaling has been shown to decrease DC-STAMP expression, a critical transmembrane protein involved in osteoclast fusion (Tiedemann et al., 2017b). To completely rule out that p14 or the FAST proteins induction of PI3K-Akt signaling is modulating fusion through transcriptional or translational alterations as well as acting at the fusion synapse a more global evaluation of alternations is necessary.

4.5. PI3K-mTORC2-Akt signaling is essential for myoblast fusion via myomerger and myomaker, but not for cell fusion induced by enveloped virus fusogens

The PI3K-Akt pathway is well-established for its roles in cell survival, proliferation, and growth (Martini et al., 2014; Riehle et al., 2013). However, the involvement of this pathway in the fusion activity of small fusogens, such as myomerger and FAST proteins, has not been extensively explored. My collaborative study between Nichole McMullen and Dr. Nandini Margam provides new evidence that the PI3K-Akt pathway is required for cell-cell fusion mediated by small fusogens but is dispensable for enveloped viral fusogens. Furthermore, this study contributes novel information regarding the requirement of mTORC2, but not mTORC1, in myomerger/myomaker-mediated cell fusion.

As previously described, p110α PI3K-Akt signaling is required for both p15 and p14-mediated cell-to-cell fusion. Using the same inhibitor treatments, BYL719, PIK-75, and MK-2206, to inhibit PI3K-Akt signaling in HEK293A cells transduced with myomaker and Tet-On myomerger, we observed a significant decrease in the relative fusion index at 24 hours post-doxycycline induction (Fig. 19B). Induction of myomerger expression increased Akt S473 phosphorylation, which was decreased by the kinase inhibitor treatments (Fig. 19C).

In the context of viral fusogens, previous studies have reported the involvement of different signaling pathways in regulating enveloped virus fusion protein-mediated

cell-cell fusion, such as the Rab family of small GTPases, the endosomal sorting complexes required for transport (ESCRT) machinery, and the actin cytoskeleton (Dittmar et al., 2021; Leroy et al., 2020; Podbilewicz, 2014). However, our findings suggest that the PI3K-Akt pathway may not be universally required by enveloped virus fusogens, as its inhibition by BYL719 and MK-2206 did not affect the fusion activity of SARS-CoV-2 Spike protein (Fig. 17B). This observation implies that the role of the PI3K-Akt pathway in cell-cell fusion processes may be specific to small fusogens and not a general feature of all fusogens.

The selective requirement of the PI3K-Akt pathway for small fusogens may be related to the unique mechanisms underlying their fusion processes. Small fusogens, such as myomerger/myomaker and FAST proteins, may utilize the PI3K-Akt pathway to regulate key aspects of the fusion machinery or coordinate the multiple steps of membrane fusion. Being much smaller than their enveloped virus counterparts, the PI3K-Akt pathway may be required for close membrane opposition that is not needed by their larger counterparts, whose large extracellular domains may easily span the ~20nm aqueous layer between membranes. Alternatively, PI3K-Akt signaling may act in place of the large and energetic conformational changes described in enveloped virus fusogens, which are believed to provide the kinetic energy to drive the energetically unfavorable merging of membranes.

While PI3K and Akt signaling are known to be required for mammalian myoblast differentiation and fusion, the role of mTORC1 and mTORC2 in satellite cell fusion and myotube formation remains debated. It is known that p110α of PI3K signaling through mTORC1-cJun and FOXO3a is necessary and sufficient for the process of quiescence exit to occur in adult muscle satellite cells (G. Wang et al., 2018). Rapamycin, an inhibitor of the mTOR pathway, has been shown to block mTORC1 signaling and inhibit the differentiation of myoblasts into muscle cells (Yoon, 2017). Short-term treatment with rapamycin blocks mTORC1 signaling, while long-term treatment additionally inhibits mTORC2, impairing myotube formation and causing muscle atrophy in animal models(Shu & Houghton, 2009; G. Yang et al., 2021). Recent studies have introduced

ambiguity to the role of mTORC1 and mTORC2 in muscle development. *In vitro* studies have indicated that the mTORC2 protein Rictor is essential for cell fusion in C2C12 cells (Shu & Houghton, 2009). In contrast, *in vivo* studies have demonstrated that muscle-specific deletion of Rictor is dispensable for muscle development in mice, while Raptor, an mTORC1 component, is required (Rion et al., 2019).

In contrast, by studying myomaker and myomerger fusion in non-muscle cells, we were able to directly assess mTOR requirements for fusion, circumventing confounding effects of mTOR inhibition on the differentiation pathway. By utilizing HEK293A cells stably transduced with myomaker and having myomerger under a Tet-inducible promoter, it was possible to acutely treat cells with rapamycin using treatment lengths where rapamycin is known to only inhibit mTORC1. Under such conditions, rapamycin treatment did not significantly inhibit fusion mediated by myomerger and myomaker, indicating that myomerger and myomaker fusion is dependent on mTORC2 function, but not mTORC1. Therefore, while mTOR signaling plays a crucial role in muscle cell growth and development, its specific role in muscle fusogen function requires further investigation. Current knowledge in the field suggests that fusion during muscle differentiation is regulated by multiple signaling pathways, including the RhoA-ROCK and MAPK-ERK pathways (Pavlath, 2010; Schejter, 2016). Our results demonstrate that the PI3K-Akt pathway is required for efficient myomerger/myomaker-mediated cell-cell fusion, providing the first evidence of PI3K(p110α) involvement in myomerger fusion. This finding expands our understanding of the molecular mechanisms governing myomerger/myomaker-mediated fusion and highlights the complexity of the signaling networks underlying this process.

4.6. Macropinocytosis is a central and essential feature of FAST protein mediated cell to cell fusion.

The involvement of MaPi as a central feature in cell-to-cell fusion is a novel discovery. This realization initially stemmed from live imaging of p14 transfected cells transduced with p14-mRuby and PH(Akt)-GFP, which depicted extensive PIP(3,4,5) and p14-

enriched plasma membrane ruffling and the generation of large intracellular vesicles near nascent fusion pores. Notably, both ruffling and large endocytotic vesicles were significantly upregulated in TetOn-p14 HeLa cells induced to express p14. Further investigation reveals that p14 expression in cells not only promotes cell fusion but also increases the macropinocytotic uptake of high molecular weight dextran and the non-specific uptake of latex beads. As with cell fusion, this process is effectively abolished by PI3K inhibition. This marks the first time the PI3K-Akt signaling pathway is implicated in upregulating MaPi to promote cell-cell fusion. Importantly, a panel of inhibitors known to interfere with MaPi also demonstrated an inhibitory effect on cell-cell fusion (Fig. 20B).

Investigations into MaPi in HT1080 cells have uncovered that Arf6 knockdown and Arf6 dominant-negative mutants, or inhibiting Arf6 function with SecinH3, NAV 2729 or nocodazole treatment, do not interfere with the frequency or size of membrane ruffling (Williamson & Donaldson, 2019). Instead, they specifically inhibit macropinosome closure. In contrast, treatment with EIPA, an inhibitor of actin remodeling, directly affects membrane ruffling, emphasizing the distinct impact of these interventions on different aspects of MaPi. All of these inhibitors reduced p14 cell-cell fusion by 53-91%, with NAV 2729 showing the greatest potency (Fig. 21B). While there is always concern with potential off target effects of small molecule inhibitors, the plethora of inhibitors used coupled with functional assays of MaPi (dextran and latex bead uptake) showing p14 upregulates MaPi (Fig. 22&23), imply that MaPi is required for efficient FAST protein-mediated cell-cell fusion.

4.7. What role might MaPi play in cell fusion?

Our understanding of cell-cell fusion has been largely shaped by the observations of actin-mediated membrane projections resulting in membrane invaginations near fusion sites, first identified in Drosophila myogenesis. This led to the development of the actin protrusion-mediated membrane tension model for cell fusion (Kim et al., 2015). Static imaging has detected similar podosome-like structures (PLSs) in fusing osteoclasts,

mammalian myoblasts, and during pathogen-induced cell-cell fusion, thereby further reinforcing the model. Despite these observations, a definitive link between these protrusive forces and increased membrane tension leading to cell fusion has been elusive, primarily due to the challenges associated with performing phototoxic high-resolution live imaging in models where fusion occurs slowly over several days, and the difficulty of measuring plasma membrane tension at subcellular resolutions.

Enter the FAST proteins, with their potent fusogenic activity, characterized by cell fusion events that occur within a span of minutes to hours. This presented a unique opportunity to perform high-resolution live microscopy of cell-cell fusion. While we were unable to perform quantitative measurements of membrane tension at the fusion synapse, our high-resolution imaging managed to capture fusion events within membrane ruffles and observed a relationship between membrane ruffles, macropinosome generation, and the initial site of plasma membrane fusion. By observing the movement and deformation of the plasma membrane in both the invading and invaded cells just before the fusion process, we gleaned a better understanding of how membrane tension might be generated to facilitate fusion. When considering how MaPi might contribute to cell fusion, the critical step is likely the modulation of membrane tension at the fusion synapse. While it is conceivable that MaPi could "indirectly" promote cell-cell fusion, for example by increasing the rate of endocytosis without a corresponding increase in exocytosis which would reduce the surface area of the plasma membrane and increase plasma membrane tension, there are three more specific ways in which MaPi could increase tension between membranes (Fig. 28). The first is membrane invasion, similar to the model described in Drosophila myoblast fusion; the second is a compressive force during the closure of the macropinosome cup; and the third is a retractive force exerted by the pulling of one membrane into the other. Of the 17 cell fusion events captured using either the 63X or 100X objectives with PH(Akt)-GFP or the LCK tagged constructs visualized at the membrane where the site of fusion pore formation was clearly discernible, only one fusion event coincided with the moment of maximal membrane projection from the

invading cell into the recipient cell, when the protrusive force would be at its peak. In contrast, the remaining 16 fusion events were observed to occur during or immediately following the closure or collapse of the membrane ruffle (seen in Fig. 25 D). This pattern of observations suggests that the forces exerted during the closure or collapse of membrane ruffles, which could be considered retractive or compressive forces associated with MaPi, may function in addition to, or possibly instead of, protrusive actin-driven forces to promote the membrane tension needed for cell-to-cell fusion.

MaPi vesicle closure involves the separation of one membrane into two distinct membranes. The closure of MaPi vesicles was classically thought to be a “kissing lip” phenomenon involving fusion of the distal/uppermost margins of ruffles (Canton, 2018) or constriction of large membrane folds through a “purse string” mechanism (Donaldson, 2019). Although this can be observed, it is perhaps too neat a model for the chaotic pre-MaPi cellular membrane landscape which is characterized by ruffles of various shapes and sizes emerging and subsiding. More often, constrictions at mid-level or even near the base of the circular ruffles caused by a proposed twisting movement of tent-pole like actin bundles within the ruffles are seen to close, forming somewhat smaller macropinosomes (Philip & Harrison, 2018). Finally, and similar to our observations, wavelike ruffles arise from lamellipodia like projections at the edge of the cell, and crest and collapse of these ruffles against the dorsal plane of the cell (Fig. 25C). These ruffles can fuse with the dorsal membrane trapping extracellular fluid into plasma membrane-derived vesicles (Mylvaganam et al., 2021). In this regard, so called actin waves capable of exerting considerable force have been previously reported (Bretschneider, Anderson, Ecke, et al., 2009; Gerisch et al., 2019b).

In our model (Fig. 28), the crest of the wave, which can be likened to Chen's invasive podosome, encounters the tightly apposed membrane of the adjacent cell. However, a critical distinction lies in the capture of the opposing plasma membrane of the recipient cell within the lumen of the ruffle. This unique interaction ultimately leads to the merging of membranes from different cells, resulting in cell fusion (Fig. 24B). One difference between the two models is the observed movement of force; rather than

outward-penetrating force directed into the recipient cell described in the Chen model (Shilagardi et al., 2013b), we see an inward pointing force directed back towards the "invading" cell. To explain this, we envision the wave lip curling around and, in the instant just prior to fusion, the greatest apparent force is observed in the final pinching off of a section of the contiguous cell, but rather than the tip of the crest pinching the entrapped section of cell, fusion of the "invading" membrane occurs. Given the variable rather stochastic nature of this process, one might also envision "failed" cell fusion events wherein the wave structure will pinch off a section of the neighbouring cell and successfully form a macropinosome containing the neighbouring cell membrane as well as its some of its cytosolic contents. This is indeed what I have seen in the form of the two coloured macropinosomes depicted in Figure 24D.

As regards the underlying mechanism, it may be the wave like ruffles are formed in regions of the cell not as tightly apposed to the neighbouring cell, but ultimately encounter a region of tighter contiguity and at that stage entrap a portion of the neighbouring cell pulling the membranes taught thereby increasing lateral membrane tension. Our imaging data is not of sufficient resolution to prove or disprove this possibility, although in keeping with this notion the wave structures observed where cells appear overlaid are smaller in size and thus may have less energy and force. In this regard, while class I PI3Ks, most frequently p110α, are occasionally necessary for membrane ruffling, they are nearly always required for macropinosome closure (Buckley & King, 2017; King & Kay, 2019). Furthermore, according to J.A. Swanson et al. (1999), the constriction responsible for sealing ruffles and forming macropinosomes involves a PI3K-dependent contractile activity mediated by non-muscle myosins. This offers a potential alternative explanation for the observed requirement of myosin II in Drosophila myoblast fusion.

Both cell-cell fusion and MaPi are intricate cellular processes that share a dependency on key proteins and lipid dynamics. The Rho family GTPases, particularly Rac1 and Cdc42, are essential regulators in both processes as they modulate actin cytoskeleton remodeling, a central mechanism in these events. Downstream effectors,

including WASP and WAVE, facilitate the formation of actin filaments, driving macropinosome formation in MaPi and contributing to membrane fusion in cell-cell fusion events. Additionally, the lipid milieu, with phosphatidylinositol 4,5-bisphosphate (PIP2) and cholesterol as significant constituents, plays a pivotal role. PIP2 is integral to the initiation of actin polymerization that underlies the formation of membrane ruffles during MaPi (Lambies & Commisso, 2022), while cholesterol imparts fluidity to the membrane, a property that facilitates the mixing of lipid bilayers necessary for fusion. Furthermore, PI3K serves as a bridge between protein and lipid interactions. In MaPi, PI3K generates PIP(3,4,5) attracting and activating downstream proteins essential for macropinocytic cup formation and closure. In cell-cell fusion, PI3K and PIP(3,4,5) can orchestrate the recruitment and activation of fusogens, proteins that directly mediate the fusion of membranes. The interconnectedness between proteins and lipids, as well as their shared molecular components, underscore the mechanistic similarities between MaPi and cell-cell fusion, highlighting the exquisite complexity of these cellular processes. Lastly, the intracellular signaling pathways regulating MaPi can also impact cell fusion. MaPi is controlled by various intracellular signaling molecules, including small GTPases like Rac1 and Cdc42, as well as kinases such as PI3K (Lutton et al., 2022; Mylvaganam et al., 2021; Swanson, 2008). These molecules modulate the actin cytoskeleton and membrane dynamics, which can have a direct impact on cell fusion events. By orchestrating membrane interactions and modulating the overall behavior of the plasma membrane, these signaling pathways can enhance cell fusion through their role in MaPi regulation.

In summary, our research provides compelling evidence that p14 activates PI3K-Akt signaling, which promotes membrane ruffling and MaPi, and plays a critical role in p14-mediated cell-cell fusion. Our live imaging experiments offer insights into the dynamics of plasma membrane fusion, suggesting that fusion can occur within a macropinocytotic cup rather than at the protrusive tip of invasive membrane protrusions. This raises the intriguing concept that retraction forces might provide an alternate means to generate membrane tension and promote membrane fusion.

4.8. Membrane protrusions unlike podosomes mediate FAST protein fusion

The comparatively detailed model of the fusion synapse in Drosophila developmental muscle cell fusion shares some interesting features with the FAST protein fusion synapse I have described in this study, but with some notable exceptions that have important potential implications on the mechanism driving membrane fusion. In this regard, the membrane ruffles and large membrane protrusions that from, fold back, fuse and seal during MaPi share structural similarities with Chen's F-actin-enriched podosome-like structures, but function in a different manner to generate membrane tension. The fusogenic podosome is relatively static and can persist for 30 minutes (Chuang et al., 2019; Sens et al., 2010) while p14 induced membrane ruffles can travel along the edge of the cell and protrude and retract within seconds. MaPi membrane ruffles, like fusogenic podosomes, are rich in dendritically branched actin networks, the result of Rac-dependent, Arp2/3-mediated polymerization, linear F-actin nucleators such as the formin FMNL44 and Spire-family protein Cordon-bleu have also been observed at the leading edge of lamellipodia. Their presence may contribute to the force generation needed for macropinocytotic driven cellular fusion (Mylvaganam et al., 2021). We believe the identical timing and locale of MaPi and cell fusion is not merely coincidental. In our model, the increased level of membrane ruffling alone is insufficient for cell fusion requiring full macropinocytosis. In keeping with this model was our observation of potent fusion inhibition despite unaltered high level membrane ruffling and protrusion formation when p14 induced cell systems were treated with the secinH3, the ARF6 inhibitor known to act at macropinosome closure (Williamson & Donaldson, 2019).

4.9. Expanding the macropinocytosis model: a role for plasma membrane repair pathway?

Elucidating the FAST fusion mechanism necessitates understanding the activation of the PI3K-Akt pathway and p14's role in inducing MaPi. Drawing on insights from the literature, we are currently investigating if p14 triggers the plasma membrane repair (PMR) pathway to drive MaPi and fusion. The p14-induced MaPi and cell fusion share constituent proteins with the PMR pathway. Importantly, FAST protein are viroporins (R. Duncan, 2019), a class of viral proteins known to induce plasma membrane permeability (Nieva et al., 2012), which subsequently stimulates the PMR pathway (Ammendolia et al., 2021; Cooper & McNeil, 2015).

The PMR pathway is a vital cellular defense mechanism activated in response to changes in plasma membrane permeability. This network of proteins rapidly detects and repairs membrane disruptions, preserving cell survival and preventing uncontrolled leakage of intracellular contents(Andrews, 2019; Cooper & McNeil, 2015). Central to this process is lysosome exocytosis, driven by increased intracellular calcium levels and facilitated by the calcium-sensing protein Synaptotagmin-7 (Martinez et al., 2000). This exocytosis event results in the secretion of acid sphingomyelinase (ASM), which converts sphingomyelin into ceramide in the outer leaflet of the plasma membrane, mediating plasma membrane internalization (Andrews, 2019; Nozaki et al., 2022). Annexins, a family of calcium-dependent phospholipid-binding proteins, also play an essential role in membrane fusion events and repair at sites of plasma membrane damage, particularly Annexin A1, A2, A5, and A6 (McNeil et al., 2006; Simonsen et al., 2023). A recent ground-breaking study revealed that MaPi is induced by plasma membrane damage, functioning as a recycling mechanism to restore damaged areas and further emphasizing the interplay between plasma membrane repair and MaPi in maintaining cellular integrity (Sønder et al., 2021).

Several bacterial pathogens exploit the host plasma membrane repair (PMR) pathway, using it to enable their entry into host cells. For example, the epsilon toxin produced by *Clostridium perfringens* forms pores in host cell membranes, prompting endocytosis and cellular entry by hijacking the PMR pathway (Linden et al., 2019). Another example, is the *Clostridium botulinum* C2 toxin, which stimulates the secretion

of ASM and the subsequent generation of ceramide in the plasma membrane, ultimately activating the PMR pathway and facilitating bacterial entry (Nagahama et al., 2017, 2021). Increasing plasma membrane permeability is also a common viral strategy for cellular entry, even though it is not explicitly categorized as PMR induction. For instance, non-enveloped adenoviruses utilize protein VI, which forms a lesion in the plasma membrane, triggering the PMR pathway to facilitate cell entry. Furthermore, research has highlighted the importance of secreted ASM, membrane ceramide enrichment and PMR in the entry of other non-enveloped viruses such as rhinoviruses, Japanese encephalitis virus, measles virus, Ebola virus, and pseudorabies virus (Tani et al., 2010).

In the context of viral proteins that are likely to induce the PMR pathway, viroporins such as FAST proteins, emerge as key players. These proteins, commonly found in viruses, are characterized by their small size and their ability to alter host cell membrane permeability properties. Viroporins have amphipathic helices and transmembrane domains, which enable them to multimerize and alter cellular membranes. Some viroporins modify membrane curvature while others disrupt membrane integrity by forming small pores. Importantly, when trafficked to the plasma membrane they can cause calcium ion influx and increase plasma membrane permeability (Nieva et al., 2012). Although not thoroughly investigated, some researchers hypothesize that these plasma membrane-targeted viroporins have the potential to induce the PMR pathway. Notable viroporins that enhance plasma membrane permeability and contribute to viral replication and pathogenesis include the influenza A virus M2 protein, HIV-1 Vpu protein, hepatitis C virus p7 protein, and SARS-CoV E protein (Cady et al., 2009; Deora & Ratner, 2001; Lee et al., 2020; Liao et al., 2004; Manzoor et al., 2017). It is important to note that FAST proteins are unique among viroporins due to their ability to fuse cells. Consequently, inducing plasma membrane permeability or the PMR pathway alone is not sufficient to promote cell fusion (Ciechonska et al., 2014; Wong et al., 2016).

Ciechonska et al.'s work, linked the PMR pathway with p14-mediated fusion by demonstrating that knockdown of annexin A1 expression and intracellular calcium

chelation inhibited p14-mediated cell fusion. To further investigate the interplay between p14-mediated fusion and calcium signaling, I employed live imaging of TetOn-p14 HeLa cells transduced with the calcium biosensor GCaMP6G (Fig. 27D). Imaging was conducted at a frequency of 35s and revealed that p14 expression increased cytosolic calcium concentration, as evidenced by the enhanced fluorescent intensity of GCaMP6G compared to the baseline fluorescent intensity, starting at 9 hours post-induction. Although the imaging frequency was insufficient to capture all instances of calcium transients, there was a corresponding increase in calcium spikes and an overall increase in fluorescence, as shown by numerous local maxima in the plot of GCaMP6G fluorescence in p14 expressing HeLa cells compared to control HeLa cells. These observations suggest a potential link to increased calcium signaling. However, further studies at higher cellular resolution would be needed to confirm this observation and elucidate the precise relationship between p14-mediated fusion and calcium signaling in the context of the PMR pathway.

Recent preliminary studies led by Nichole McMullen provide compelling evidence for the connection between p14 expression and lysosomal exocytosis. These studies suggest that p14 expression in HeLa TetOn-p14 cells induces lysosomal exocytosis, as measured by extracellular N-acetylglucosaminidase activity (personal communication). Furthermore, *Clostridium botulinum* C2 toxin has been demonstrated to activate PI3K by stimulating the secretion of acid sphingomyelinase (ASMase) (Nagahama et al., 2009). This process generates ceramide in the plasma membrane, which in turn leads to the activation of the PI3K signaling pathway. Ceramide generated by secreted ASMase(sASMase) has also been reported to modulate PI3K/Akt signaling in various cellular contexts, such as during oxidative stress, apoptosis, and cellular migration. However, the exact mechanisms through which ceramide or sASMase modulate PI3K activation have yet to be fully elucidated.

In the context of p14-mediated fusion, preliminary experiments show that the exogenous addition of ASM to HeLa TetOn-p14 cells leads to phosphorylation of AktS473, regardless of p14 expression (Fig. 27 B). On the other hand, inhibition of ASM

activity using vacuolin-1 results in downregulation of AktS473 phosphorylation, which is partially rescued by exogenous ASMase treatment. Treatment of TetOn-p14 HeLa cells with desipramine, known to inhibit lysosomal exocytosis, and vacuolin-1 results in a decrease in the relative fusion index (Fig. 27A), while the addition of ASM moderately increases fusion (Fig. 27B). These findings suggest a functional role for ASM in regulating the PI3K/Akt signaling pathway during p14-mediated fusion events.

A key question in the study of FAST proteins is the mechanisms by which they confer a fitness advantage to orthoreoviruses. One leading hypothesis suggests that cell fusion promotes cell-to-cell transmission, allowing the virus to circumvent extracellular host immune defenses. Supporting this idea, research has demonstrated that the transmission and replication of double-stranded RNA viruses are enhanced by the presence of a FAST protein (Kanai et al., 2019). However, whether fusogenic properties are the sole enhancers of viral fitness remains to be determined. A non-fusogenic p10 has been recently identified in a subclade of Muscovy Duck Reovirus (Y. Yang et al., 2020). Given the significant evolutionary selection of non-enveloped viral genomes, the conservation of a non-fusogenic p10 may imply that FAST proteins have additional uncharacterized pathogenic functions including induction of MaPi and PMR.

4.10. Summary

In conclusion, this thesis investigated the mechanisms of cell-cell fusion mediated by small fusogens, such as the reovirus FAST proteins and myomerger. It was found that these small fusogens co-opt the PI3K(p110α)-Akt kinase pathway to drive syncytiogenesis. The production of PIP(3,4,5), facilitated by PI3K(p110α), was identified as a crucial step in fusion, and its colocalization with the p14 protein at membrane ruffles further supported its role in the process. Additionally, Akt phosphorylation by PDK1 and mTORC2 was shown to be essential for small fusogen-mediated fusion, while mTORC1 was dispensable. The study also revealed the significance of MaPi, which may enhance fusion efficiency by increasing membrane tension through macropinosome formation. Future directions should investigate the specific role of MaPi in myomerger

fusion and explore the interplay between the Plasma Membrane Repair (PMR) pathway and FAST-mediated fusion. Preliminary evidence suggests a potential relationship between PMR and FAST proteins, making it a promising area for further investigation. These future studies will provide insights into the mechanisms of fusion and may uncover novel therapeutic targets for viral infections and muscle disorders.

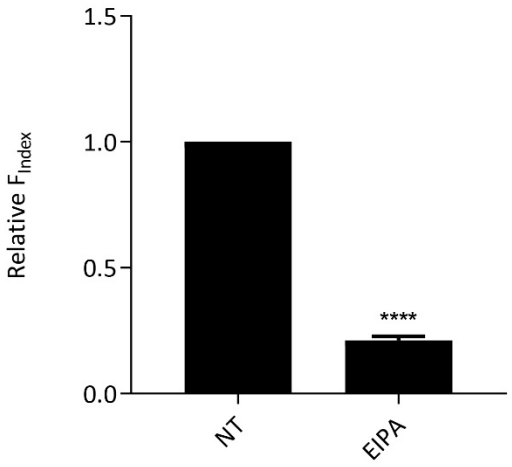

4.11. Figure 26. Macropinocytosis inhibition blocks myomerger fusion.

A graph of the relative fusion index of myomerger-Tet-On 293A cells (expressing Myomaker) treated with doxycycline (5µg/ml) for 24 hours, either alone or in combination with the macropinocytosis inhibitor EIPA (12.5µM) for the final 18 hours.

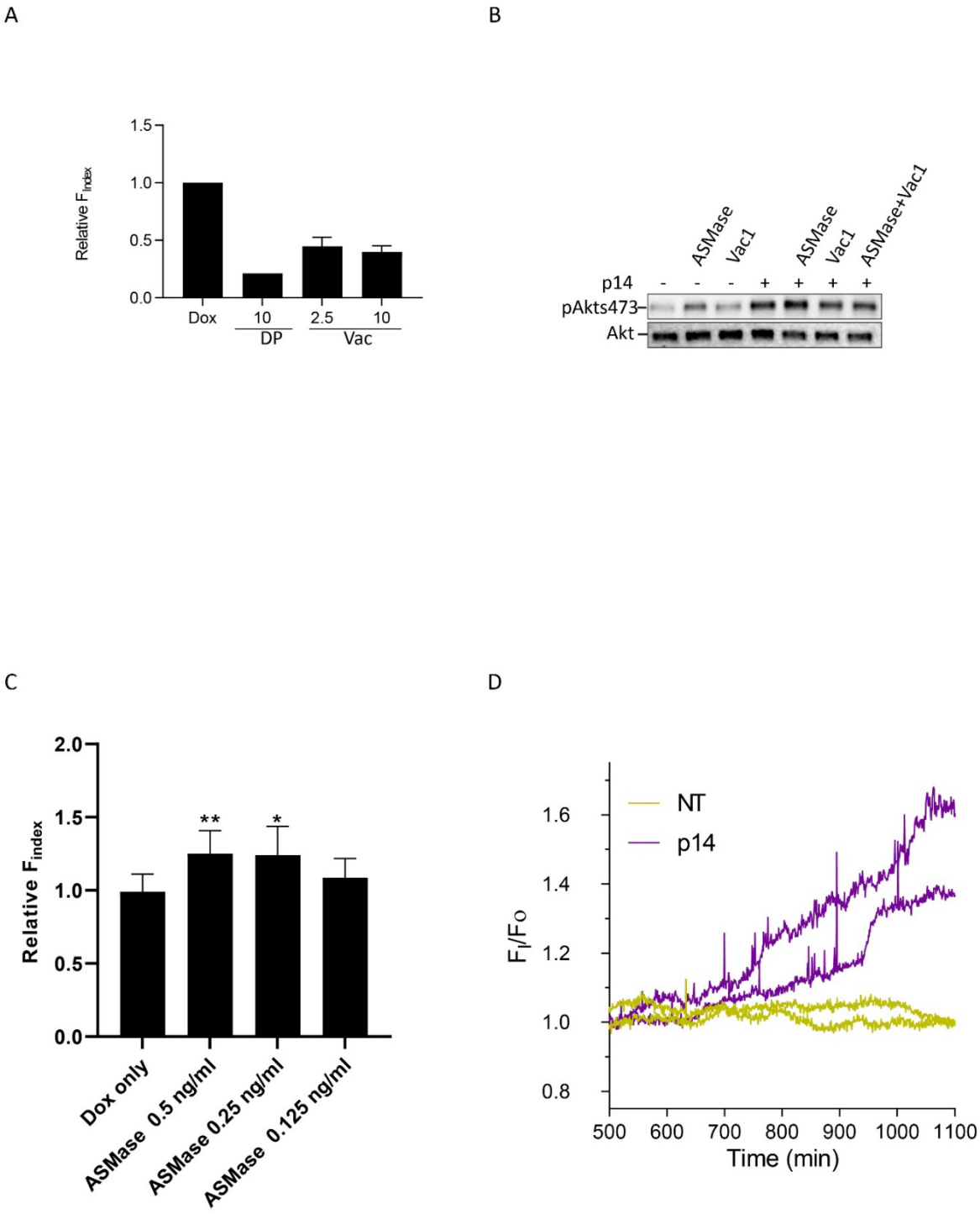

4.12. Figure 27. The activity of acid sphingomyelinase released during lysosomal exocytosis is required for p14 PI3K/Akt and cell fusion.

A. This graph illustrates the relative fusion index of TetOn-p14 HeLa cells following treatment with desipramine (10μM), an inhibitor of lysosomal exocytosis, and vacuolin-1 (10μM) at 5 hours post-doxycycline induction for an 8-hour duration. Both treatments result in a decrease in the relative fusion index. **B.** Displayed are immunoblots of pAktS473 in TetOn-p14 HeLa cells, with or without doxycycline, and treated with Vac-1 (10μM), ASMase (0.5 ng/ml), or both. **C.** Graph of the relative fusion index of TetOn-p14 HeLa cells following a 4 hour treatment with different concentrations of ASMase at 9 hours post-doxycycline induction. **D.** Graph of the relative fluorescence intensity of the calcium biosensor gCaMP6s in a field of view within a population of transduced TetOn-p14 HeLa cells to time 0 min, representing increased cytosolic calcium concentration, and measured every 30 seconds.

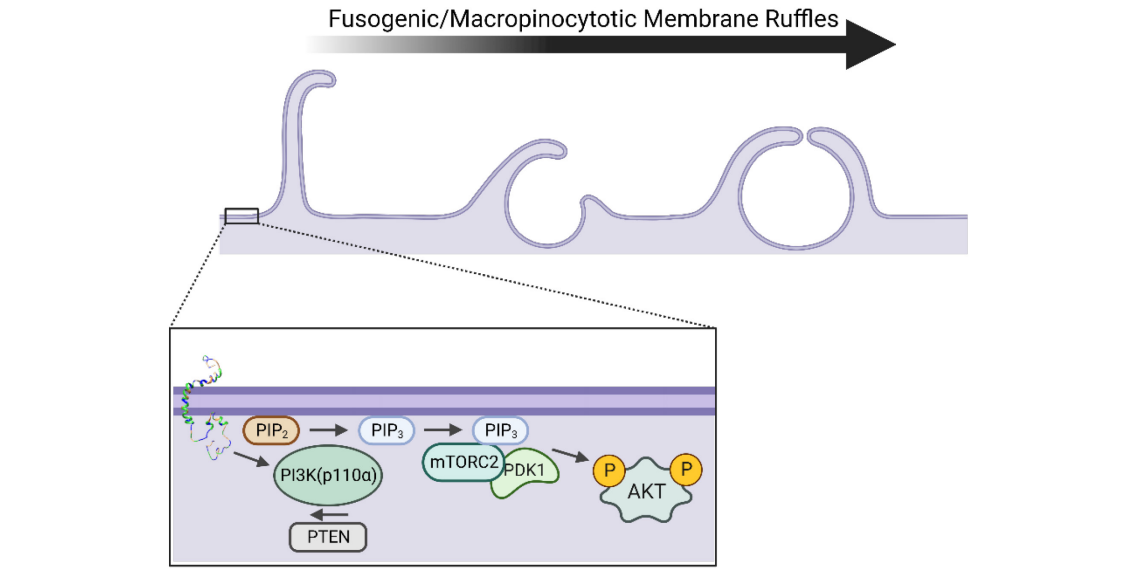
Fusogenic/Macropinocytotic Membrane Ruffles
PIP2
PIP3
PIP3
PI3K(p110α)
mTORC2
PDK1
P
P
AKT
PTEN

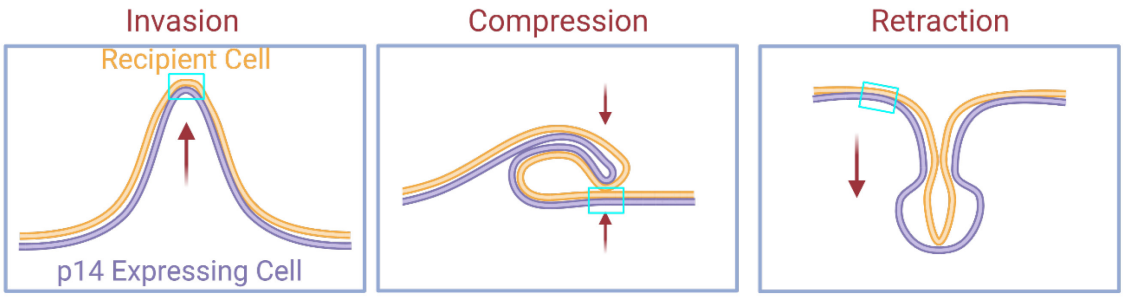
Invasion
Recipient Cell
p14 Expressing Cell
Compression
Retraction

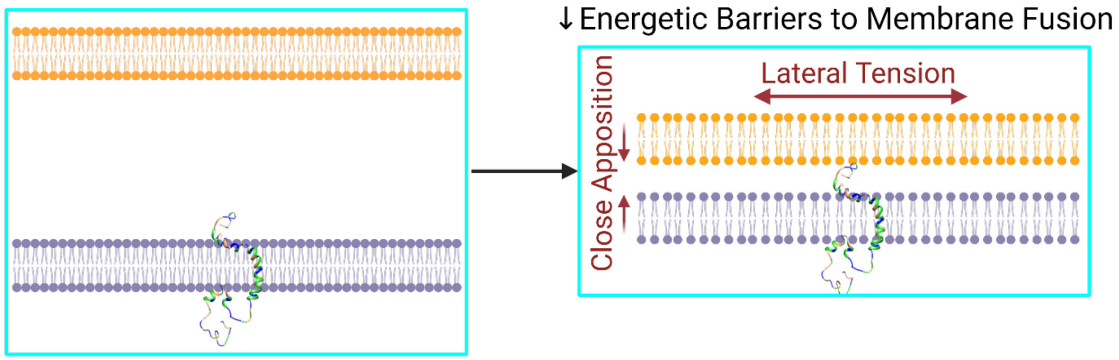
↓Energetic Barriers to Membrane Fusion
Lateral Tension
Close Apposition

4.13. Figure 28 Illustration of the p14-induced cell fusion process through the activation of the PI3K/Akt signaling pathway and macropinocytotic membrane ruffles.

Top panel. Presentation of p14 activation of the PI3K-Akt signaling pathway, which triggers macropinocytotic fusogenic membrane ruffles. **Middle Panel.** Various mechanisms (Invasion, Compression, or Retraction) through which membrane ruffles of the p14 expressing cell can exert force on plasma membrane of the recipient cell catalyzing the cell fusion process. Areas in which these forces may be greatest are highlighted in light blue boxes. **Lower panel.** An expanded view of the light blue boxes from the middle panel. This view showcases how these mechanisms lower the energetic barriers to cell fusion through increased lateral membrane tension and close membrane apposition. While FAST proteins possess innate fusogenic activity, as demonstrated in liposome fusion experiments, they require host machinery, such as macropinocytotic membrane ruffles, to efficiently drive cell fusion by making the process more energetically favorable.

References

A, D., CMU, H., & DM, A. (2006). Inhibition of macropinocytosis blocks antigen presentation of type II collagen in vitro and in vivo in HLA-DR1 transgenic mice. *Arthritis Res Ther*, *8*(4). https://doi.org/10.1186/ar1964

Ahmadzadeh, K., Pereira, M., Vanoppen, M., Bernaerts, E., Ko, J.-H., Mitera, T., Maksoudian, C., Manshian, B. B., Soenen, S., Rose, C. D., Williams, G. R., Bassett, J. H. D., Matthys, P., Wouters, C., & Behmoaras, J. (2023). Multinucleation resets human macrophages for specialized functions at the expense of their identity. *EMBO Reports*, *24*(3), e56310. https://doi.org/10.15252/embr.202256310

Akimov, S. A., Molotkovsky, R. J., Kuzmin, P. I., Galimzyanov, T. R., & Batishchev, O. V. (2020). Continuum Models of Membrane Fusion: Evolution of the Theory. *International Journal of Molecular Sciences*, *21*(11), Article 11. https://doi.org/10.3390/ijms21113875

Alexandrov, I., Mackenzie, M., & Brandina, I. (2019). Abstract 2162: ActivSignal technology for multiplex analysis of signaling protein activation profiles. *Cancer Research*, *79*(13_Supplement), 2162. https://doi.org/10.1158/1538-7445.AM2019-2162

Ammendolia, D. A., Bement, W. M., & Brumell, J. H. (2021). Plasma membrane integrity: Implications for health and disease. *BMC Biology*, *19*(1), 71. https://doi.org/10.1186/s12915-021-00972-y

Andrews, N. W. (2019). Solving the secretory acid sphingomyelinase puzzle: Insights from lysosome-mediated parasite invasion and plasma membrane repair. *Cellular Microbiology*, *21*(11), e13065. https://doi.org/10.1111/cmi.13065

Anshabo, A. T., Milne, R., Wang, S., & Albrecht, H. (2021). CDK9: A Comprehensive Review of Its Biology, and Its Role as a Potential Target for Anti-Cancer Agents. *Frontiers in Oncology*, *11*. https://www.frontiersin.org/articles/10.3389/fonc.2021.678559

Araki, N., Egami, Y., Watanabe, Y., & Hatae, T. (2007). Phosphoinositide metabolism during membrane ruffling and macropinosome formation in EGF-stimulated A431 cells. *Exp Cell Res*, *313*(7). https://doi.org/10.1016/j.yexcr.2007.02.012

Arcucci, S., Ramos-Delgado, F., Cayron, C., Therville, N., Gratacap, M.-P., Basset, C., Thibault, B., & Guillermet-Guibert, J. (2021). Organismal roles for the PI3Kα and β isoforms: Their specificity, redundancy or cooperation is context-dependent. *The Biochemical Journal*, *478*(6), 1199–1225. https://doi.org/10.1042/BCJ20210004

Ballesteros-Álvarez, J., & Andersen, J. K. (2021). mTORC2: The other mTOR in autophagy regulation. *Aging Cell*, *20*(8), e13431. https://doi.org/10.1111/acel.13431

Banerjee, S., Basu, S., & Sarkar, S. (2010). Comparative genomics reveals selective distribution and domain organization of FYVE and PX domain proteins across eukaryotic lineages. *BMC Genomics*, *11*(1), 83. https://doi.org/10.1186/1471-2164-11-83

Barry, C., & Duncan, R. (2009). Multifaceted Sequence-Dependent and -Independent Roles for Reovirus FAST Protein Cytoplasmic Tails in Fusion Pore Formation and Syncytiogenesis. *Journal of Virology*, *83*(23), 12185–12195. https://doi.org/10.1128/JVI.01667-09

Bar-Sagi, D., & Feramisco, J. (1979). Induction of membrane ruffling and fluid-phase pinocytosis in quiescent fibroblasts by ras proteins. *Science*, *1986;233(4768*. https://doi.org/10.1126/science.3090687

Basquin, C., Malardé, V., Mellor, P., Anderson, D. H., Meas-Yedid, V., Olivo-Marin, J.-C., Dautry-Varsat, A., & Sauvonnet, N. (2013). The signalling factor PI3K is a specific regulator of the clathrin-independent dynamin-dependent endocytosis of IL-2 receptors. *Journal of Cell Science*, *126*(5), 1099–1108. https://doi.org/10.1242/jcs.110932

Bastida-Ruiz, D., Van Hoesen, K., & Cohen, M. (2016). The Dark Side of Cell Fusion. *International Journal of Molecular Sciences*, *17*(5), Article 5. https://doi.org/10.3390/ijms17050638

Benabdi, S., Peurois, F., Nawrotek, A., Chikireddy, J., Cañeque, T., Yamori, T., Shiina, I., Ohashi, Y., Dan, S., Rodriguez, R., Cherfils, J., & Zeghouf, M. (2017). Family-wide Analysis of the Inhibition of Arf Guanine Nucleotide Exchange Factors with Small Molecules: Evidence of Unique Inhibitory Profiles. *Biochemistry*, *56*(38), 5125–5133. https://doi.org/10.1021/acs.biochem.7b00706

Bi, P., Ramirez-Martinez, A., Li, H., Cannavino, J., McAnally, J. R., Shelton, J. M., Sánchez-Ortiz, E., Bassel-Duby, R., & Olson, E. N. (2017). Control of muscle formation by the fusogenic micropeptide myomixer. *Science*, *356*(6335), 323–327. https://doi.org/10.1126/science.aam9361

Bilanges, B., Posor, Y., & Vanhaesebroeck, B. (2019). PI3K isoforms in cell signalling and vesicle trafficking. *Nature Reviews Molecular Cell Biology*, *20*(9), 515–534. https://doi.org/10.1038/s41580-019-0129-z

Bjerregaard, B., Holck, S., Christensen, I. J., & Larsson, L.-I. (2006). Syncytin is involved in breast cancer-endothelial cell fusions. *Cellular and Molecular Life Sciences CMLS*, *63*(16), 1906–1911. https://doi.org/10.1007/s00018-006-6201-9

BoseDasgupta, S., & Pieters, J. (2014). Inflammatory Stimuli Reprogram Macrophage Phagocytosis to Macropinocytosis for the Rapid Elimination of Pathogens. *PLoS Pathog*, *10*(1). https://doi.org/10.1371/journal.ppat.1003879

Bothe, I., Deng, S., & Baylies, M. (2014). *PI(4,5)P2 Regulates Myoblast Fusion Through Arp2/3 Regulator Localization at the Fusion Site*. https://doi.org/10.1242/dev.100743

Boye, T. L., Jeppesen, J. C., Maeda, K., Pezeshkian, W., Solovyeva, V., Nylandsted, J., & Simonsen, A. C. (2018). Annexins induce curvature on free-edge membranes displaying distinct morphologies. *Scientific Reports*, *8*(1), Article 1. https://doi.org/10.1038/s41598-018-28481-z

Bretschneider, T., Anderson, K., & Ecke, M. (2009). The three-dimensional dynamics of actin waves, a model of cytoskeletal self-organization. *Biophys J*, *96*(7). https://doi.org/10.1016/j.bpj.2008.12.3942

Bretschneider, T., Anderson, K., Ecke, M., Müller-Taubenberger, A., Schroth-Diez, B., Ishikawa-Ankerhold, H. C., & Gerisch, G. (2009). The Three-Dimensional Dynamics of Actin Waves, a Model of Cytoskeletal Self-Organization. *Biophysical Journal*, *96*(7), 2888–2900. https://doi.org/10.1016/j.bpj.2008.12.3942

Brukman, N. G., Uygur, B., Podbilewicz, B., & Chernomordik, L. V. (2019). How cells fuse. *Journal of Cell Biology*, *218*(5), 1436–1451. https://doi.org/10.1083/jcb.201901017

Buckley, C. M., & King, J. S. (2017). Drinking problems: Mechanisms of macropinosome formation and maturation. *The FEBS Journal*, *284*(22), 3778–3790. https://doi.org/10.1111/febs.14115

Bühler, A., Krüger, R., Monavari, M., Fuentes-Chandía, M., Palmisano, R., Schödel, J., Boccaccini, A. R., Boßerhoff, A. K., Kappelmann-Fenzl, M., Letort, G., & Leal-Egaña, A. (2022). *When Mechanical Stress Matters: Generation of Polyploid Giant Cancer Cells in Tumor-like Microcapsules* (p. 2022.09.22.508846). bioRxiv. https://doi.org/10.1101/2022.09.22.508846

Cady, S. D., Luo, W., Hu, F., & Hong, M. (2009). Structure and Function of the Influenza A M2 Proton Channel. *Biochemistry*, *48*(31), 7356–7364. https://doi.org/10.1021/bi9008837

Canton, J. (n.d.). *Macropinocytosis in Phagocyte Function and Immunity BT - Macropinocytosis: Functions and Mechanisms* (C. Commisso, Ed.; Vol. 2022). Springer International Publishing. https://doi.org/10.1007/978-3-030-94004-1_6

Canton, J. (2018). Macropinocytosis: New Insights Into Its Underappreciated Role in Innate Immune Cell Surveillance. *Frontiers in Immunology*, *9*, 2286. https://doi.org/10.3389/fimmu.2018.02286

Carretero-Ortega, J., Walsh, C. T., Hernández-García, R., Reyes-Cruz, G., Brown, J. H., & Vázquez-Prado, J. (2010). Phosphatidylinositol 3,4,5-triphosphate-dependent Rac exchanger 1 (P-Rex-1), a guanine nucleotide exchange factor for Rac, mediates angiogenic responses to stromal cell-derived factor-1/chemokine stromal cell derived factor-1 (SDF-1/CXCL-12) linked to Rac activation, endothelial cell migration, and in vitro angiogenesis. *Molecular Pharmacology*, *77*(3), 435–442. https://doi.org/10.1124/mol.109.060400

Carter, A. (2008). Cell Fusion Theory: Can It Explain What Triggers Metastasis? *JNCI: Journal of the National Cancer Institute*, *100*(18), 1279–1281. https://doi.org/10.1093/jnci/djn336

Chakraborty, H., Tarafdar, P. K., & Lentz, B. R. (2013). A Novel Assay to Detect Fusion Pore Formation: Implication for Fusion Mechanism. *Biochemistry*, *52*(47), 10.1021/bi401369j. https://doi.org/10.1021/bi401369j

Chan, K. M. C., Arthur, A. L., Morstein, J., Jin, M., Bhat, A., Schlesinger, D., Son, S., Stevens, D. A., Drubin, D. G., & Fletcher, D. A. (2021). Evolutionarily related small viral fusogens hijack distinct but modular actin nucleation pathways to drive cell-cell fusion. *Proceedings of the National Academy of Sciences*, *118*(1), e2007526118. https://doi.org/10.1073/pnas.2007526118

Chan, K. M. C., Son, S., Schmid, E. M., & Fletcher, D. A. (2020). A viral fusogen hijacks the actin cytoskeleton to drive cell-cell fusion. *ELife*, *9*, e51358. https://doi.org/10.7554/eLife.51358

Chan, T. O., Rodeck, U., Chan, A. M., Kimmelman, A. C., Rittenhouse, S. E., Panayotou, G., & Tsichlis, P. N. (2002). Small GTPases and tyrosine kinases coregulate a molecular switch in the phosphoinositide 3-kinase regulatory subunit. *Cancer Cell*, *1*(2), 181–191. https://doi.org/10.1016/S1535-6108(02)00033-8

Chan, T. O., Zhang, J., Rodeck, U., Pascal, J. M., Armen, R. S., Spring, M., Dumitru, C. D., Myers, V., Li, X., Cheung, J. Y., & Feldman, A. M. (2011). Resistance of Akt kinases to dephosphorylation through ATP-dependent conformational plasticity. *Proceedings of the National Academy of Sciences*, *108*(46), E1120–E1127. https://doi.org/10.1073/pnas.1109879108

Chang, J.-C., Chang, H.-H., Lin, C.-T., & Lo, S. J. (2005). The integrin α6β1 modulation of PI3K and Cdc42 activities induces dynamic filopodium formation in human platelets. *Journal of Biomedical Science*, *12*(6), 881–898. https://doi.org/10.1007/s11373-005-9021-2

Charpentier, J. C., Chen, D., & Lapinski, P. E. (2020). Macropinocytosis drives T cell growth by sustaining the activation of mTORC1. *Nat Commun*, *11*(1). https://doi.org/10.1038/s41467-019-13997-3

Chen, E. H. (2011). *Invasive Podosomes and Myoblast Fusion*. https://doi.org/10.1016/b978-0-12-385891-7.00010-6

Chen, E. H., & Olson, E. N. (2005). Unveiling the mechanisms of cell-cell fusion. *Science (New York, N.Y.)*, *308*(5720), 369–373. https://doi.org/10.1126/science.1104799

Chen, P.-W., Gasilina, A., Yadav, M. P., & Randazzo, P. A. (2022). Control of cell signaling by Arf GTPases and their regulators: Focus on links to cancer and other GTPase families. *Biochimica et Biophysica Acta (BBA) - Molecular Cell Research*, *1869*(2), 119171. https://doi.org/10.1016/j.bbamcr.2021.119171

Chernomordik, L. V., & Kozlov, M. M. (2008). Mechanics of membrane fusion. *Nature Structural &Amp; Molecular Biology*, *15*(7). https://doi.org/10.1038/nsmb.1455

Chernomordik, L. V., Melikyan, G. B., & Chizmadzhev, Y. A. (1987). Biomembrane fusion: A new concept derived from model studies using two interacting planar lipid bilayers. *Biochimica et Biophysica Acta (BBA) - Reviews on Biomembranes*, *906*(3), 309–352. https://doi.org/10.1016/0304-4157(87)90016-5

Chitwood, C. A., Dietzsch, C., Jacobs, G., McArdle, T., Freeman, B. T., Banga, A., Noubissi, F. K., & Ogle, B. M. (2018). Breast tumor cell hybrids form spontaneously in vivo and contribute to breast tumor metastases. *APL Bioengineering*, *2*(3), 031907. https://doi.org/10.1063/1.5024744

Chuang, M.-C., Lin, S.-S., Ohniwa, R. L., Lee, G.-H., Su, Y.-A., Chang, Y.-C., Tang, M.-J., & Liu, Y.-W. (2019). Tks5 and Dynamin-2 enhance actin bundle rigidity in invadosomes to promote myoblast fusion. *Journal of Cell Biology*, *218*(5), 1670–1685. https://doi.org/10.1083/jcb.201809161

Ciechonska, M., Key, T., & Duncan, R. (2014). Efficient Reovirus- and Measles Virus-Mediated Pore Expansion during Syncytium Formation Is Dependent on Annexin A1 and Intracellular Calcium. *Journal of Virology*, *88*(11), 6137–6147. https://doi.org/10.1128/JVI.00121-14

Commisso, C. (2019). The pervasiveness of macropinocytosis in oncological malignancies. *Philosophical Transactions of the Royal Society B: Biological Sciences*, *374*(1765). https://doi.org/10.1098/rstb.2018.0153

Commisso, C., Davidson, S. M., & Soydaner-Azeloglu, R. G. (2013). Macropinocytosis of protein is an amino acid supply route in Ras-transformed cells. *Nature*, *497*(7451). https://doi.org/10.1038/nature12138

Coomer, C. A., Carlon-Andres, I., Iliopoulou, M., Dustin, M. L., Compeer, E. B., Compton, A. A., & Padilla-Parra, S. (2020). Single-cell glycolytic activity regulates membrane tension and HIV-1 fusion. *PLoS Pathogens*, *16*(2), e1008359. https://doi.org/10.1371/journal.ppat.1008359

Cooper, S. T., & McNeil, P. L. (2015). Membrane Repair: Mechanisms and Pathophysiology. *Physiological Reviews*, *95*(4), 1205–1240. https://doi.org/10.1152/physrev.00037.2014

Corcoran, J. A., Clancy, E. K., & Duncan, R. (2011). Homomultimerization of the reovirus p14 fusion-associated small transmembrane protein during transit through the ER-Golgi complex secretory pathway. *The Journal of General Virology*, *92*(Pt 1), 162–166. https://doi.org/10.1099/vir.0.026013-0

Corcoran, J. A., & Duncan, R. (2004). Reptilian Reovirus Utilizes a Small Type III Protein with an External Myristylated Amino Terminus To Mediate Cell-Cell Fusion. *Journal of Virology*, *78*(8), 4342–4351. https://doi.org/10.1128/JVI.78.8.4342-4351.2004

Corcoran, J. A., Salsman, J., de Antueno, R., Touhami, A., Jericho, M. H., Clancy, E. K., & Duncan, R. (2006). The p14 Fusion-associated Small Transmembrane (FAST) Protein Effects Membrane Fusion from a Subset of Membrane Microdomains*. *Journal of Biological Chemistry*, *281*(42), 31778–31789. https://doi.org/10.1016/S0021-9258(19)84093-0

Costa, T. J., Potje, S. R., Fraga-Silva, T. F. C., da Silva-Neto, J. A., Barros, P. R., Rodrigues, D., Machado, M. R., Martins, R. B., Santos-Eichler, R. A., Benatti, M. N., de Sá, K. S. G., Almado, C. E. L., Castro, Í. A., Pontelli, M. C., Serra, L. L., Carneiro, F. S., Becari, C., Louzada-Junior, P., Oliveira, R. D. R., … Tostes, R. C. (2022). Mitochondrial DNA and TLR9 activation contribute to SARS-CoV-2-induced endothelial cell damage. *Vascular Pharmacology*, *142*, 106946. https://doi.org/10.1016/j.vph.2021.106946

Coutinho-Budd, J., Ghukasyan, V., Zylka, M. J., & Polleux, F. (2012). The F-BAR domains from srGAP1, srGAP2 and srGAP3 regulate membrane deformation differently. *Journal of Cell Science*, *125*(14), 3390–3401. https://doi.org/10.1242/jcs.098962

Cuesta, C., Arévalo-Alameda, C., & Castellano, E. (2021). The Importance of Being PI3K in the RAS Signaling Network. *Genes*, *12*(7), Article 7. https://doi.org/10.3390/genes12071094

Cullen, A. P., Reid, R., Campion, M., & Lörincz, A. T. (1991). Analysis of the physical state of different human papillomavirus DNAs in intraepithelial and invasive cervical neoplasm. *Journal of Virology*, *65*(2), 606–612. https://doi.org/10.1128/jvi.65.2.606-612.1991

Danila, D. C., Heller, G., Gignac, G. A., Gonzalez-Espinoza, R., Anand, A., Tanaka, E., Lilja, H., Schwartz, L., Larson, S., Fleisher, M., & Scher, H. I. (2007). Circulating Tumor Cell Number and Prognosis in Progressive Castration-Resistant Prostate Cancer. *Clinical Cancer Research*, *13*(23), 7053–7058. https://doi.org/10.1158/1078-0432.CCR-07-1506

Defour, A., Van der Meulen, J. H., Bhat, R., Bigot, A., Bashir, R., Nagaraju, K., & Jaiswal, J. K. (2014). Dysferlin regulates cell membrane repair by facilitating injury-triggered acid sphingomyelinase secretion. *Cell Death & Disease*, *5*(6), Article 6. https://doi.org/10.1038/cddis.2014.272

Delespaul, L., Merle, C., Lesluyes, T., Lagarde, P., Le Guellec, S., Pérot, G., Baud, J., Carlotti, M., Danet, C., Fèvre, M., Rousseau, B., Durrieu, S., Teichmann, M., Coindre, J.-M., Lartigue, L., & Chibon, F. (2019). Fusion-mediated chromosomal instability promotes aneuploidy patterns that resemble human tumors. *Oncogene*, *38*(33), Article 33. https://doi.org/10.1038/s41388-019-0859-6

Deng, P., & Liu, J.-J. G. (2022). Diverse activation mechanisms of PI3Ks. *Nature Structural & Molecular Biology*, *29*(3), 185–187. https://doi.org/10.1038/s41594-022-00744-4

Deora, A., & Ratner, L. (2001). Viral Protein U (Vpu)-Mediated Enhancement of Human Immunodeficiency Virus Type 1 Particle Release Depends on the Rate of Cellular Proliferation. *Journal of Virology*, *75*(14), 6714–6718. https://doi.org/10.1128/jvi.75.14.6714-6718.2001

Dietz, M. S., Sutton, T. L., Walker, B. S., Gast, C. E., Zarour, L., Sengupta, S. K., Swain, J. R., Eng, J., Parappilly, M., Limbach, K., Sattler, A., Burlingame, E., Chin, Y., Gower, A., Mira, J. L. M., Sapre, A., Chiu, Y.-J., Clayburgh, D. R., Pommier, S. J., … Wong, M. H. (2021). Relevance of circulating hybrid cells as a non-invasive biomarker for myriad solid tumors. *Scientific Reports*, *11*(1), Article 1. https://doi.org/10.1038/s41598-021-93053-7

Diller, J. R., Parrington, H. M., Patton, J. T., & Ogden, K. M. (2019). Rotavirus Species B Encodes a Functional Fusion-Associated Small Transmembrane Protein. *Journal of Virology*, *93*(20), e00813-19. https://doi.org/10.1128/JVI.00813-19

Ding, J., Jin, W., Chen, C., Shao, Z., & Wu, J. (2012). Tumor Associated Macrophage × Cancer Cell Hybrids May Acquire Cancer Stem Cell Properties in Breast Cancer. *PLOS ONE*, *7*(7), e41942. https://doi.org/10.1371/journal.pone.0041942

Dittmar, T., Weiler, J., Luo, T., & Hass, R. (2021). Cell-Cell Fusion Mediated by Viruses and HERV-Derived Fusogens in Cancer Initiation and Progression. *Cancers*, *13*(21), Article 21. https://doi.org/10.3390/cancers13215363

Doherty, G. J., & McMahon, H. T. (2009). Mechanisms of endocytosis. *Annu Rev Biochem*, *78*. https://doi.org/10.1146/annurev.biochem.78.081307.110540

Donaldson, J. G. (2019). Macropinosome formation, maturation and membrane recycling: Lessons from clathrin-independent endosomal membrane systems. *Philosophical Transactions of the Royal Society B: Biological Sciences*, *374*(1765), 20180148. https://doi.org/10.1098/rstb.2018.0148

Donaldson, J. G., Porat-Shliom, N., & Cohen, L. A. (2009). Clathrin-independent endocytosis: A unique platform for cell signaling and PM remodeling. *Cell Signal*, *21*(1). https://doi.org/10.1016/j.cellsig.2008.06.020

Dong Woog Lee, Kai Kristiansen, Stephen H. Donaldson, Nicholas Cadirov, Xavier Banquy, & Jacob N. Israelachvili. (2015). Real-Time Intermembrane Force Measurements and Imaging of Lipid Domain Morphology During Hemifusion. *Nature Communications*. https://doi.org/10.1038/ncomms8238

Dufrançais, O., Mascarau, R., Poincloux, R., Maridonneau-Parini, I., Raynaud-Messina, B., & Vérollet, C. (2021). Cellular and molecular actors of myeloid cell fusion: Podosomes and tunneling nanotubes call the tune. *Cellular and Molecular Life Sciences*, *78*(17), 6087–6104. https://doi.org/10.1007/s00018-021-03875-x

Duncan, L., Shay, C., & Teng, Y. (2020). PI3K Isoform-Selective Inhibitors in Cancer. *Advances in Experimental Medicine and Biology*, *1255*, 165–173. https://doi.org/10.1007/978-981-15-4494-1_14

Duncan, R. (2019). Fusogenic Reoviruses and Their Fusion-Associated Small Transmembrane (FAST) Proteins. *Annual Review of Virology*, *6*(1), 341–363. https://doi.org/10.1146/annurev-virology-092818-015523

Ebner, M., Lučić, I., Leonard, T. A., & Yudushkin, I. (2017). PI(3,4,5)P3 Engagement Restricts Akt Activity to Cellular Membranes. *Molecular Cell*, *65*(3), 416-431.e6. https://doi.org/10.1016/j.molcel.2016.12.028

Eledge, M. R., Zita, M. D., & Boehme, K. W. (2019). Reovirus: Friend and Foe. *Current Clinical Microbiology Reports*, *6*(3), 132–138. https://doi.org/10.1007/s40588-019-00121-8

Erbay, E., Park, I.-H., Nuzzi, P. D., Schoenherr, C. J., & Chen, J. (2003). IGF-II transcription in skeletal myogenesis is controlled by mTOR and nutrients. *The Journal of Cell Biology*, *163*(5), 931–936. https://doi.org/10.1083/jcb.200307158

Faust, J. J., Balabiyev, A., Heddleston, J. M., Podolnikova, N. P., Baluch, D. P., Chew, T.-L., & Ugarova, T. P. (2019). An actin-based protrusion originating from a podosome-enriched region initiates macrophage fusion. *Molecular Biology of the Cell*, *30*(17), 2254–2267. https://doi.org/10.1091/mbc.E19-01-0009

Fei, F., Li, C., Wang, X., Du, J., Liu, K., Li, B., Yao, P., Li, Y., & Zhang, S. (2019). Syncytin 1, CD9, and CD47 regulating cell fusion to form PGCCs associated with cAMP/PKA and JNK signaling pathway. *Cancer Medicine*, *8*(6), 3047–3058. https://doi.org/10.1002/cam4.2173

Freeman, S. A., Uderhardt, S., & Saric, A. (1979). Lipid-gated monovalent ion fluxes regulate endocytic traffic and support immune surveillance. *Science*, *2020;367(6475*. https://doi.org/10.1126/science.aaw9544

Fruman, D. A., Chiu, H., Hopkins, B. D., Bagrodia, S., Cantley, L. C., & Abraham, R. T. (2017). The PI3K Pathway in Human Disease. *Cell*, *170*(4), 605–635. https://doi.org/10.1016/j.cell.2017.07.029

Gao, Y., Moten, A., & Lin, H.-K. (2014). Akt: A new activation mechanism. *Cell Research*, *24*(7), Article 7. https://doi.org/10.1038/cr.2014.57

García-Pérez, B. E., Mondragón-Flores, R., & Luna-Herrera, J. (2003). Internalization of Mycobacterium tuberculosis by macropinocytosis in non-phagocytic cells. *Microb Pathog*, *35*(2). https://doi.org/10.1016/S0882-4010(03)00089-5

Gardner, S., Anguiano, M., & Rotwein, P. (2012). Defining Akt actions in muscle differentiation. *American Journal of Physiology-Cell Physiology*, *303*(12), C1292–C1300. https://doi.org/10.1152/ajpcell.00259.2012

Gast, C. E., Silk, A. D., Zarour, L., Riegler, L., Burkhart, J. G., Gustafson, K. T., Parappilly, M. S., Roh-Johnson, M., Goodman, J. R., Olson, B., Schmidt, M., Swain, J. R., Davies, P. S., Shasthri, V., Iizuka, S., Flynn, P., Watson, S., Korkola, J., Courtneidge, S. A., … Wong, M. H. (2018). Cell fusion potentiates tumor heterogeneity and reveals circulating hybrid cells that correlate with stage and survival. *Science Advances*. https://doi.org/10.1126/sciadv.aat7828

Gauck, D., Keil, S., Niggemann, B., Zänker, K. S., & Dittmar, T. (2017). Hybrid clone cells derived from human breast epithelial cells and human breast cancer cells exhibit properties of cancer stem/initiating cells. *BMC Cancer*, *17*(1), 515. https://doi.org/10.1186/s12885-017-3509-9

Gerisch, G., Prassler, J., Butterfield, N., & Ecke, M. (2019a). Actin waves and dynamic patterning of the plasma membrane. *Yale Journal of Biology and Medicine*, *92*(3).

Gerisch, G., Prassler, J., Butterfield, N., & Ecke, M. (2019b). Actin Waves and Dynamic Patterning of the Plasma Membrane. *The Yale Journal of Biology and Medicine*, *92*(3), 397–411.

Giménez-Andrés, M., Čopič, A., & Antonny, B. (2018). The Many Faces of Amphipathic Helices. *Biomolecules*, *8*(3), Article 3. https://doi.org/10.3390/biom8030045

Giménez-Orenga, K., & Oltra, E. (2021). Human Endogenous Retrovirus as Therapeutic Targets in Neurologic Disease. *Pharmaceuticals*, *14*(6), Article 6. https://doi.org/10.3390/ph14060495

Giraudo, C. G., Hu, C., You, D., Slovic, A. M., Mosharov, E. V., Sulzer, D., Melia, T. J., & Rothman, J. E. (2005). SNAREs can promote complete fusion and hemifusion as alternative outcomes. *Journal of Cell Biology*, *170*(2). https://doi.org/10.1083/jcb.200501093

Glass, D. J. (2011). PI3 Kinase Regulation of Skeletal Muscle Hypertrophy and Atrophy. In C. Rommel, B. Vanhaesebroeck, & P. K. Vogt (Eds.), *Phosphoinositide 3-kinase in Health and Disease: Volume 1* (pp. 267–278). Springer. https://doi.org/10.1007/82_2010_78

Gobin, B., Huin, M. B., Lamoureux, F., Ory, B., Charrier, C., Lanel, R., Battaglia, S., Redini, F., Lezot, F., Blanchard, F., & Heymann, D. (2015). BYL719, a new α-specific PI3K inhibitor: Single administration and in combination with conventional chemotherapy for the treatment of osteosarcoma. *International Journal of Cancer*, *136*(4), 784–796. https://doi.org/10.1002/ijc.29040

Goldenberg, N. M., & Steinberg, B. E. (2010). Surface Charge: A Key Determinant of Protein Localization and Function. *Cancer Research*, *70*(4), 1277–1280. https://doi.org/10.1158/0008-5472.CAN-09-2905

Gupta, S., Ramjaun, A. R., & Haiko, P. (2007). Binding of Ras to Phosphoinositide 3-Kinase p110α Is Required for Ras- Driven Tumorigenesis in Mice. *Cell*, *129*(5). https://doi.org/10.1016/j.cell.2007.03.051

Gutierrez-Xicotencatl, L., Pedroza-Saavedra, A., Chihu-Amparan, L., Salazar-Piña, A., Maldonado-Gama, M., & Esquivel-Guadarrama, F. (2021). Cellular Functions of HPV16 E5

Oncoprotein during Oncogenic Transformation. *Molecular Cancer Research*, *19*(2), 167–179. https://doi.org/10.1158/1541-7786.MCR-20-0491

Hafner, M., Schmitz, A., Grüne, I., Srivatsan, S. G., Paul, B., Kolanus, W., Quast, T., Kremmer, E., Bauer, I., & Famulok, M. (2006). Inhibition of cytohesins by SecinH3 leads to hepatic insulin resistance. *Nature*, *444*(7121), 941–944. https://doi.org/10.1038/nature05415

Hamoud, N., Tran, V., Croteau, L.-P., Kania, A., & Côté, J.-F. (2014). G-protein coupled receptor BAI3 promotes myoblast fusion in vertebrates. *Proceedings of the National Academy of Sciences of the United States of America*, *111*(10), 3745–3750. https://doi.org/10.1073/pnas.1313886111

Han, J., Pluhackova, K., & Böckmann, R. A. (2017). The Multifaceted Role of SNARE Proteins in Membrane Fusion. *Frontiers in Physiology*, *8*. https://www.frontiersin.org/articles/10.3389/fphys.2017.00005

Han, X., Sterling, H., Chen, Y., Saginario, C., Brown, E. D., Frazier, W. A., Lindberg, F. P., & Vignery, A. (2000). CD47, a Ligand for the Macrophage Fusion Receptor, Participates in Macrophage Multinucleation. *Journal of Biological Chemistry*, *275*(48). https://doi.org/10.1074/jbc.m002334200

Haque, Md. E., McIntosh, T. J., & Lentz, B. R. (2001). Influence of Lipid Composition on Physical Properties and PEG-Mediated Fusion of Curved and Uncurved Model Membrane Vesicles: "Nature's Own" Fusogenic Lipid Bilayer. *Biochemistry*, *40*(14), 4340–4348. https://doi.org/10.1021/bi002030k

Harrison, S. C. (2015). Viral membrane fusion. *Virology*, *479–480*, 498–507. https://doi.org/10.1016/j.virol.2015.03.043

Heinke, L. (2022). Phosphoinositide signal for lysosomal membrane repair. *Nature Reviews Molecular Cell Biology*, *23*(11), Article 11. https://doi.org/10.1038/s41580-022-00550-2

Helming, L., & Gordon, S. (2009). Molecular mediators of macrophage fusion. *Trends in Cell Biology*, *19*(10), 514–522. https://doi.org/10.1016/j.tcb.2009.07.005

Herbein, G., & Nehme, Z. (2020). Polyploid Giant Cancer Cells, a Hallmark of Oncoviruses and a New Therapeutic Challenge. *Frontiers in Oncology*, *10*. https://www.frontiersin.org/articles/10.3389/fonc.2020.567116

Hernández, J. M., & Podbilewicz, B. (2017). The hallmarks of cell-cell fusion. *Development*, *144*(24), 4481–4495. https://doi.org/10.1242/dev.155523

Hinz, N., & Jücker, M. (2019). Distinct functions of AKT isoforms in breast cancer: A comprehensive review. *Cell Communication and Signaling*, *17*(1), 154. https://doi.org/10.1186/s12964-019-0450-3

Hu, L., Plafker, K., Vorozhko, V., Zuna, R. E., Hanigan, M. H., Gorbsky, G. J., Plafker, S. M., Angeletti, P. C., & Ceresa, B. P. (2009). Human papillomavirus 16 E5 induces bi-nucleated cell formation by cell–cell fusion. *Virology*, *384*(1), 125–134. https://doi.org/10.1016/j.virol.2008.10.011

Huber, R., Römisch, J., & Paques, E. P. (1990). The crystal and molecular structure of human annexin V, an anticoagulant protein that binds to calcium and membranes. *The EMBO Journal*, *9*(12), 3867–3874. https://doi.org/10.1002/j.1460-2075.1990.tb07605.x

Humphrey, S. J., Azimifar, S. B., & Mann, M. (2015). High-throughput phosphoproteomics reveals in vivo insulin signaling dynamics. *Nature Biotechnology*, *33*(9), 990–995. https://doi.org/10.1038/nbt.3327

Humphrey, S. J., Yang, G., Yang, P., Fazakerley, D. J., Stöckli, J., Yang, J. Y., & James, D. E. (2013). Dynamic Adipocyte Phosphoproteome Reveals that Akt Directly Regulates mTORC2. *Cell Metabolism*, *17*(6), 1009–1020. https://doi.org/10.1016/j.cmet.2013.04.010

Ijuin, T., & Takenawa, T. (2012). Regulation of Insulin Signaling and Glucose Transporter 4 (GLUT4) Exocytosis by Phosphatidylinositol 3,4,5-Trisphosphate (PIP3) Phosphatase, Skeletal Muscle, and Kidney Enriched Inositol Polyphosphate Phosphatase (SKIP). *Journal of Biological Chemistry*, *287*(10), 6991–6999. https://doi.org/10.1074/jbc.M111.335539

Itoh, T., Koshiba, S., Kigawa, T., Kikuchi, A., Yokoyama, S., & Takenawa, T. (2001). Role of the ENTH Domain in Phosphatidylinositol-4,5-Bisphosphate Binding and Endocytosis. *Science*, *291*(5506), 1047–1051. https://doi.org/10.1126/science.291.5506.1047

Jackson, S. P., Schoenwaelder, S. M., Goncalves, I., Nesbitt, W. S., Yap, C. L., Wright, C. E., Kenche, V., Anderson, K. E., Dopheide, S. M., Yuan, Y., Sturgeon, S. A., Prabaharan, H., Thompson, P. E., Smith, G. D., Shepherd, P. R., Daniele, N., Kulkarni, S., Abbott, B., Saylik, D., … Salem, H. H. (2005). PI 3-kinase p110beta: A new target for antithrombotic therapy. *Nature Medicine*, *11*(5), 507–514. https://doi.org/10.1038/nm1232

Jasnin, M., Beck, F., & Ecke, M. (2019). The Architecture of Traveling Actin Waves Revealed by Cryo-Electron Tomography. *Structure*, *27*(8). https://doi.org/10.1016/j.str.2019.05.009

Jiang, W., & Ji, M. (2019). Receptor tyrosine kinases in PI3K signaling: The therapeutic targets in cancer. *Seminars in Cancer Biology*, *59*, 3–22. https://doi.org/10.1016/j.semcancer.2019.03.006

Jiménez, C., Portela, R. A., Mellado, M., Rodríguez-Frade, J. M., Collard, J., Serrano, A., Martínez-A, C., Avila, J., & Carrera, A. C. (2000). Role of the Pi3k Regulatory Subunit in the Control of Actin Organization and Cell Migration. *Journal of Cell Biology*, *151*(2), 249–262. https://doi.org/10.1083/jcb.151.2.249

Jin, J., & Woodgett, J. R. (2005). Chronic activation of protein kinase Bbeta/Akt2 leads to multinucleation and cell fusion in human epithelial kidney cells: Events associated with tumorigenesis. *Oncogene*, *24*(35), 5459–5470. https://doi.org/10.1038/sj.onc.1208704

Joseph, G. A., Lu, M., Radu, M., Lee, J. K., Burden, S. J., Chernoff, J., & Krauss, R. S. (2017). Group I Paks Promote Skeletal Myoblast Differentiation In Vivo and In Vitro. *Molecular and Cellular Biology*, *37*(4), e00222-16. https://doi.org/10.1128/MCB.00222-16

Kanai, Y., Kawagishi, T., Sakai, Y., Nouda, R., Shimojima, M., Saijo, M., Matsuura, Y., & Kobayashi, T. (2019). Cell–cell fusion induced by reovirus FAST proteins enhances replication and pathogenicity of non-enveloped dsRNA viruses. *PLOS Pathogens*, *15*(4), e1007675. https://doi.org/10.1371/journal.ppat.1007675

Kano, Y., Hiragami, F., Motoda, H., Akiyama, J., Koike, Y., Gomita, Y., Inoue, S., Kawaura, A., Furuta, T., & Kawamura, K. (2019). C-SH2 point mutation converts p85β regulatory subunit of phosphoinositide 3-kinase to an anti-aging gene. *Scientific Reports*, *9*(1), Article 1. https://doi.org/10.1038/s41598-019-48157-6

Kawamoto, S., & Shinoda, W. (2014). Free energy analysis along the stalk mechanism of membrane fusion. *Soft Matter*, *10*(17). https://doi.org/10.1039/c3sm52344f

Kay, R. R. (2021). Macropinocytosis: Biology and mechanisms. *Cells and Development. Published online*. https://doi.org/10.1016/j.cdev.2021.203713

Kay, R. R., Lutton, J., Coker, H., Paschke, P., King, J. S., & Bretschneider, T. (n.d.). *The Amoebal Model for Macropinocytosis* (C. Commisso, Ed.; Vol. 2022). Functions and Mechanisms. Springer International Publishing. https://doi.org/10.1007/978-3-030-94004-1_3

Kay, R. R., Lutton, J., Coker, H., Paschke, P., King, J. S., & Bretschneider, T. (2022). The Amoebal Model for Macropinocytosis. In C. Commisso (Ed.), *Macropinocytosis: Functions and Mechanisms* (pp. 41–59). Springer International Publishing. https://doi.org/10.1007/978-3-030-94004-1_3

Key, T., & Duncan, R. (2014). A Compact, Multifunctional Fusion Module Directs Cholesterol-Dependent Homomultimerization and Syncytiogenic Efficiency of Reovirus p10 FAST Proteins. *PLOS Pathogens*, *10*(3), e1004023. https://doi.org/10.1371/journal.ppat.1004023

Kim, J. H., Ren, Y., Ng, W. P., Li, S., Son, S., Kee, Y. S., Zhang, S., Zhang, G., Fletcher, D. A., Robinson, D. N., & Chen, E. H. (2015). Mechanical Tension Drives Cell Membrane Fusion. *Developmental Cell*, *32*(5). https://doi.org/10.1016/j.devcel.2015.01.005

King, J. S., & Kay, R. R. (2019). The origins and evolution of macropinocytosis. *Philosophical Transactions of the Royal Society B: Biological Sciences*, *374*(1765), 20180158. https://doi.org/10.1098/rstb.2018.0158

Kliesch, T.-T., Dietz, J., Turco, L., Halder, P., Polo, E., Tarantola, M., Jahn, R., & Janshoff, A. (2017). Membrane tension increases fusion efficiency of model membranes in the presence of SNAREs. *Scientific Reports*, *7*(1), 12070. https://doi.org/10.1038/s41598-017-12348-w

Knight, Z. A., Gonzalez, B., Feldman, M. E., Zunder, E. R., Goldenberg, D. D., Williams, O., Loewith, R., Stokoe, D., Balla, A., Toth, B., Balla, T., Weiss, W. A., Williams, R. L., & Shokat, K. M. (2006). A Pharmacological Map of the PI3-K Family Defines a Role for p110α in Insulin Signaling. *Cell*, *125*(4), 733–747. https://doi.org/10.1016/j.cell.2006.03.035

Kodama, J., & Kaito, T. (2020). Osteoclast Multinucleation: Review of Current Literature. *International Journal of Molecular Sciences*, *21*(16), Article 16. https://doi.org/10.3390/ijms21165685

Koivusalo, M., Welch, C., Hayashi, H., Scott, C. C., Kim, M., Alexander, T., Touret, N., Hahn, K. M., & Grinstein, S. (2010). Amiloride inhibits macropinocytosis by lowering submembranous pH and preventing Rac1 and Cdc42 signaling. *The Journal of Cell Biology*, *188*(4), 547–563. https://doi.org/10.1083/jcb.200908086

Kostow, N., & Welch, M. D. (2022). Plasma membrane protrusions mediate host cell-cell fusion induced by Burkholderia thailandensis. *Molecular Biology of the Cell*, *33*(8), ar70. https://doi.org/10.1091/mbc.E22-02-0056

Kozlov, M. M., & Chernomordik, L. V. (2015). Membrane tension and membrane fusion. *Current Opinion in Structural Biology*, *33*, 61–67. https://doi.org/10.1016/j.sbi.2015.07.010

Kozlov, M. M., & Markin, V. S. (1983). [Possible mechanism of membrane fusion. *Biofizika*, *28*(2), 242–247.

Krey, T., Rey, F. A., Fédry, J., Liu, Y., Pehau-Arnaudet, G., Pei, J., Li, W., Tortorici, M. A., Traincard, F., Meola, A., Bricogne, G., Grishin, N. V., & Snell, W. J. (2017). The Ancient Gamete Fusogen HAP2 Is a Eukaryotic Class II Fusion Protein. *Cell*, *168*(5). https://doi.org/10.1016/j.cell.2017.01.024

Krull, A., Buchholz, T.-O., & Jug, F. (2019). Noise2Void—Learning Denoising From Single Noisy Images. *2019 IEEE/CVF Conference on Computer Vision and Pattern Recognition (CVPR)*, 2124–2132. https://doi.org/10.1109/CVPR.2019.00223

Krygowska, A. A., & Castellano, E. (2018). PI3K: A Crucial Piece in the RAS Signaling Puzzle. *Cold Spring Harbor Perspectives in Medicine*, *8*(6), a031450. https://doi.org/10.1101/cshperspect.a031450

Kuleshov, M. V., Xie, Z., London, A. B. K., Yang, J., Evangelista, J. E., Lachmann, A., Shu, I., Torre, D., & Ma'ayan, A. (2021). KEA3: Improved kinase enrichment analysis via data integration. *Nucleic Acids Research*, *49*(W1), W304–W316. https://doi.org/10.1093/nar/gkab359

Lai, Y., Diao, J., Liu, Y., Ishitsuka, Y., Su, Z., Schulten, K., Ha, T., & Shin, Y.-K. (2013). Fusion pore formation and expansion induced by Ca2+ and synaptotagmin 1. *Proceedings of the National Academy of Sciences*, *110*(4), 1333–1338. https://doi.org/10.1073/pnas.1218818110

Lambies, G., & Commisso, C. (2022). Macropinocytosis and Cancer: From Tumor Stress to Signaling Pathways. In C. Commisso (Ed.), *Macropinocytosis: Functions and Mechanisms* (pp. 15–40). Springer International Publishing. https://doi.org/10.1007/978-3-030-94004-1_2

Lartigue, L., Merle, C., Lagarde, P., Delespaul, L., Lesluyes, T., Le Guellec, S., Pérot, G., Leroy, L., Coindre, J.-M., & Chibon, F. (2020). Genome remodeling upon mesenchymal tumor cell fusion contributes to tumor progression and metastatic spread. *Oncogene*, *39*(21), 4198–4211. https://doi.org/10.1038/s41388-020-1276-6

Lawrence, R. E., & Zoncu, R. (2019). The lysosome as a cellular centre for signalling, metabolism and quality control. *Nat Cell Biol*, *21*(2). https://doi.org/10.1038/s41556-018-0244-7

Lee, H.-R., Lee, G. Y., You, D.-G., Kim, H. K., & Yoo, Y. D. (2020). Hepatitis C Virus p7 Induces Membrane Permeabilization by Interacting with Phosphatidylserine. *International Journal of Molecular Sciences*, *21*(3), 897. https://doi.org/10.3390/ijms21030897

Lehka, L., & Rędowicz, M. J. (2020). Mechanisms regulating myoblast fusion: A multilevel interplay. *Seminars in Cell & Developmental Biology*, *104*, 81–92. https://doi.org/10.1016/j.semcdb.2020.02.004

Leikina, E., Defour, A., Melikov, K., Van der Meulen, J. H., Nagaraju, K., Bhuvanendran, S., Gebert, C., Pfeifer, K., Chernomordik, L. V., & Jaiswal, J. K. (2015). Annexin A1 Deficiency does not Affect Myofiber Repair but Delays Regeneration of Injured Muscles. *Scientific Reports*, *5*(1), Article 1. https://doi.org/10.1038/srep18246

Leikina, E., Melikov, K., Sanyal, S., Verma, S. K., Eun, B., Gebert, C., Pfeifer, K., Lizunov, V. A., Kozlov, M. M., & Chernomordik, L. V. (2013). Extracellular annexins and dynamin are important for sequential steps in myoblast fusion. *The Journal of Cell Biology*, *200*(1), 109–123. https://doi.org/10.1083/jcb.201207012

Lemmon, M. A. (2007). Pleckstrin Homology (PH) domains and phosphoinositides. *Biochemical Society Symposium*, *74*, 81–93. https://doi.org/10.1042/BSS0740081

Lemmon, M. A. (2008). Membrane recognition by phospholipid-binding domains. *Nature Reviews Molecular Cell Biology*, *9*(2), Article 2. https://doi.org/10.1038/nrm2328

Lemmon, M. A., & Schlessinger, J. (2010). Cell signaling by receptor-tyrosine kinases. *Cell*, *141*(7), 1117–1134. https://doi.org/10.1016/j.cell.2010.06.011

Leroy, H., Han, M., Woottum, M., Bracq, L., Bouchet, J., Xie, M., & Benichou, S. (2020). Virus-Mediated Cell-Cell Fusion. *International Journal of Molecular Sciences*, *21*(24), 9644. https://doi.org/10.3390/ijms21249644

Leyden, F., Uthishtran, S., Moorthi, U. K., York, H. M., Patil, A., Gandhi, H., Petrov, E. P., Bornschlögl, T., & Arumugam, S. (2021). Rac1 activation can generate untemplated, lamellar membrane ruffles. *BMC Biology*, *19*, 72. https://doi.org/10.1186/s12915-021-00997-3

Li, H.-S., Shome, K., Rojas, R., Rizzo, M. A., Vasudevan, C., Fluharty, E., Santy, L. C., Casanova, J. E., & Romero, G. (2003). The Guanine Nucleotide Exchange Factor ARNO mediates the activation of ARF and phospholipase D by insulin. *BMC Cell Biology*, *4*, 13. https://doi.org/10.1186/1471-2121-4-13

Li, Y., Zhang, J., He, D., Liang, Q., & Wang, Y. (2012). Characterization of molecular recognition of Phosphoinositide-3-kinase α inhibitor through molecular dynamics simulation. *Journal of Molecular Modeling*, *18*(5), 1907–1916. https://doi.org/10.1007/s00894-011-1211-4

Liang, S., & Blundell, T. L. (2023). Human DNA-dependent protein kinase activation mechanism. *Nature Structural & Molecular Biology*, *30*(2), Article 2. https://doi.org/10.1038/s41594-022-00881-w

Liao, Y., Lescar, J., Tam, J. P., & Liu, D. X. (2004). Expression of SARS-coronavirus envelope protein in Escherichia coli cells alters membrane permeability. *Biochemical and Biophysical Research Communications*, *325*(1), 374–380. https://doi.org/10.1016/j.bbrc.2004.10.050

Liberali, P., Kakkonen, E., Turacchio, G., Valente, C., Spaar, A., Perinetti, G., Böckmann, R. A., Corda, D., Colanzi, A., Marjomaki, V., & Luini, A. (2008). The closure of Pak1-dependent macropinosomes requires the phosphorylation of CtBP1/BARS. *The EMBO Journal*, *27*(7), 970–981. https://doi.org/10.1038/emboj.2008.59

Lim, J. P., Teasdale, R. D., & Gleeson, P. A. (2012). SNX5 is essential for efficient macropinocytosis and antigen processing in primary macrophages. *Biol Open*, *1*(9). https://doi.org/10.1242/bio.20122204

Linden, J. R., Flores, C., Schmidt, E. F., Uzal, F. A., Michel, A. O., Valenzuela, M., Dobrow, S., & Vartanian, T. (2019). Clostridium perfringens epsilon toxin induces blood brain barrier permeability via caveolae-dependent transcytosis and requires expression of MAL. *PLoS Pathogens*, *15*(11), e1008014. https://doi.org/10.1371/journal.ppat.1008014

Linder, S., Cervero, P., Eddy, R., & Condeelis, J. (2023). Mechanisms and roles of podosomes and invadopodia. *Nature Reviews Molecular Cell Biology*, *24*(2), Article 2. https://doi.org/10.1038/s41580-022-00530-6

Liu, X., Wei, L., Xu, F., Zhao, F., Huang, Y., Fan, Z., Mei, S., Hu, Y., Zhai, L., Guo, J., Zheng, A., Cen, S., Liang, C., & Guo, F. (2022). SARS-CoV-2 spike protein–induced cell fusion activates the cGAS-STING pathway and the interferon response. *Science Signaling*, *15*(729), eabg8744. https://doi.org/10.1126/scisignal.abg8744

Liu, Y., Liu, N., Yu, Y., & Wang, D. (2021). Nr4a1 promotes cell adhesion and fusion by regulating Zeb1 transcript levels in myoblasts. *Biochemical and Biophysical Research Communications*, *556*, 127–133. https://doi.org/10.1016/j.bbrc.2021.03.153

Lowenstein, E. J., Daly, R. J., Batzer, A. G., Li, W., Margolis, B., Lammers, R., Ullrich, A., Skolnik, E. Y., Bar-Sagi, D., & Schlessinger, J. (1992). The SH2 and SH3 domain-containing protein GRB2 links receptor tyrosine kinases to ras signaling. *Cell*, *70*(3), 431–442. https://doi.org/10.1016/0092-8674(92)90167-b

Lu, X., Zhang, F., McNew, J. A., & Shin, Y.-K. (2005). Membrane Fusion Induced by Neuronal SNAREs Transits through Hemifusion. *Journal of Biological Chemistry*, *280*(34). https://doi.org/10.1074/jbc.m506862200

Luo, W., Ai, L., Wang, B., & Zhou, Y. (2019). High glucose inhibits myogenesis and induces insulin resistance by down-regulating AKT signaling. *Biomedicine & Pharmacotherapy*, *120*, 109498. https://doi.org/10.1016/j.biopha.2019.109498

Luo, Y., Shoemaker, A. R., Liu, X., Woods, K. W., Thomas, S. A., de Jong, R., Han, E. K., Li, T., Stoll, V. S., Powlas, J. A., Oleksijew, A., Mitten, M. J., Shi, Y., Guan, R., McGonigal, T. P., Klinghofer, V., Johnson, E. F., Leverson, J. D., Bouska, J. J., … Giranda, V. L. (2005). Potent and selective inhibitors of Akt kinases slow the progress of tumors in vivo. *Molecular Cancer Therapeutics*, *4*(6), 977–986. https://doi.org/10.1158/1535-7163.MCT-05-0005

Lutton, E. J., Coker, H. L. E., Paschke, P., Munn, C. J., King, J. S., Bretschneider, T., & Kay, R. R. (2022). *The formation and closure of macropinocytic cups in a model system* (p. 2022.10.07.511330). bioRxiv. https://doi.org/10.1101/2022.10.07.511330

Mahankali, M., Peng, H.-J., Henkels, K. M., Dinauer, M. C., & Gomez-Cambronero, J. (2011). Phospholipase D2 (PLD2) is a guanine nucleotide exchange factor (GEF) for the GTPase Rac2. *Proceedings of the National Academy of Sciences of the United States of America*, *108*(49), 19617–19622. https://doi.org/10.1073/pnas.1114692108

Mañes, S., Real, G., & Martínez-A, C. (2003). Pathogens: Raft hijackers. *Nat Rev Immunol*, *3*(7). https://doi.org/10.1038/nri1129

Manna, P., & Jain, S. K. (2015). Phosphatidylinositol-3,4,5-Triphosphate and Cellular Signaling: Implications for Obesity and Diabetes. *Cellular Physiology and Biochemistry*, *35*(4), 1253–1275. https://doi.org/10.1159/000373949

Manning, B. D., & Toker, A. (2017). AKT/PKB Signaling: Navigating the Network. *Cell*, *169*(3), 381–405. https://doi.org/10.1016/j.cell.2017.04.001

Manzoor, R., Igarashi, M., & Takada, A. (2017). Influenza A Virus M2 Protein: Roles from Ingress to Egress. *International Journal of Molecular Sciences*, *18*(12), 2649. https://doi.org/10.3390/ijms18122649

Martens, S., & McMahon, H. T. (2008). Mechanisms of membrane fusion: Disparate players and common principles. *Nature Reviews Molecular Cell Biology*, *9*(7), Article 7. https://doi.org/10.1038/nrm2417

Martinez, I., Chakrabarti, S., Hellevik, T., Morehead, J., Fowler, K., & Andrews, N. W. (2000). Synaptotagmin VII Regulates Ca2+-Dependent Exocytosis of Lysosomes in Fibroblasts. *The Journal of Cell Biology*, *148*(6), 1141–1150.

Martini, M., De Santis, M. C., Braccini, L., Gulluni, F., & Hirsch, E. (2014). PI3K/AKT signaling pathway and cancer: An updated review. *Annals of Medicine*, *46*(6), 372–383. https://doi.org/10.3109/07853890.2014.912836

Matheny, R. W., Lynch, C. M., & Leandry, L. A. (2012). Enhanced Akt phosphorylation and myogenic differentiation in PI3K p110β-deficient myoblasts is mediated by PI3K p110α and mTORC2. *Growth Factors (Chur, Switzerland)*, *30*(6), 367–384. https://doi.org/10.3109/08977194.2012.734507

Matheny, R. W., Riddle-Kottke, M. A., Leandry, L. A., Lynch, C. M., Abdalla, M. N., Geddis, A. V., Piper, D. R., & Zhao, J. J. (2015). Role of Phosphoinositide 3-OH Kinase p110β in Skeletal Myogenesis. *Molecular and Cellular Biology*, *35*(7), 1182–1196. https://doi.org/10.1128/MCB.00550-14

Mattila, J.-P., Shnyrova, A. V., Sundborger, A. C., Hortelano, E. R., Fuhrmans, M., Neumann, S., Müller, M., Hinshaw, J. E., Schmid, S. L., & Frolov, V. A. (2015). A hemi-fission intermediate links two mechanistically distinct stages of membrane fission. *Nature*, *524*(7563), Article 7563. https://doi.org/10.1038/nature14509

Mbalaviele, G., Chen, H., Boyce, B. F., Mundy, G. R., & Yoneda, T. (1995). The role of cadherin in the generation of multinucleated osteoclasts from mononuclear precursors in murine marrow. *The Journal of Clinical Investigation*, *95*(6), 2757–2765. https://doi.org/10.1172/JCI117979

McNeil, A. K., Rescher, U., Gerke, V., & McNeil, P. L. (2006). Requirement for Annexin A1 in Plasma Membrane Repair *. *Journal of Biological Chemistry*, *281*(46), 35202–35207. https://doi.org/10.1074/jbc.M606406200

Meher, G., & Chakraborty, H. (2019). Membrane Composition Modulates Fusion by Altering Membrane Properties and Fusion Peptide Structure. *The Journal of Membrane Biology*, *252*(4), 261–272. https://doi.org/10.1007/s00232-019-00064-7

Mi, S., Lee, X., Li, X., Veldman, G. M., Finnerty, H., Racie, L., LaVallie, E., Tang, X.-Y., Edouard, P., Howes, S., Keith, J. C., & McCoy, J. M. (2000). Syncytin is a captive retroviral envelope protein involved in human placental morphogenesis. *Nature*, *403*(6771), Article 6771. https://doi.org/10.1038/35001608

Millay, D. P., O'Rourke, J. R., Sutherland, L. B., Bezprozvannaya, S., Shelton, J. M., Bassel-Duby, R., & Olson, E. N. (2013). Myomaker: A membrane activator of myoblast fusion and muscle formation. *Nature*, *499*(7458), 301–305. https://doi.org/10.1038/nature12343

Mohler, W. A., Shemer, G., Campo, J. J. del, Valansi, C., Opoku-Serebuoh, E., Scranton, V., Assaf, N., White, J. G., & Podbilewicz, B. (2002). The Type I Membrane Protein EFF-1 Is Essential for Developmental Cell Fusion. *Developmental Cell*, *2*(3), 355–362. https://doi.org/10.1016/S1534-5807(02)00129-6

Montagnoli, A., Valsasina, B., Croci, V., Menichincheri, M., Rainoldi, S., Marchesi, V., Tibolla, M., Tenca, P., Brotherton, D., Albanese, C., Patton, V., Alzani, R., Ciavolella, A., Sola, F., Molinari, A., Volpi, D., Avanzi, N., Fiorentini, F., Cattoni, M., … Santocanale, C. (2008). A Cdc7 kinase inhibitor restricts initiation of DNA replication and has antitumor activity. *Nature Chemical Biology*, *4*(6), 357–365. https://doi.org/10.1038/nchembio.90

Murphy, D. A., & Courtneidge, S. A. (2011). The "ins" and "outs" of podosomes and invadopodia: Characteristics, formation and function. *Nature Reviews Molecular Cell Biology*, *12*(7), Article 7. https://doi.org/10.1038/nrm3141

Mylvaganam, S., Freeman, S. A., & Grinstein, S. (2021). The cytoskeleton in phagocytosis and macropinocytosis. *Current Biology*, *31*(10), R619–R632. https://doi.org/10.1016/j.cub.2021.01.036

Nagahama, M., Hagiyama, T., Kojima, T., Aoyanagi, K., Takahashi, C., Oda, M., Sakaguchi, Y., Oguma, K., & Sakurai, J. (2009). Binding and Internalization of Clostridium botulinum C2 Toxin. *Infection and Immunity*, *77*(11), 5139–5148. https://doi.org/10.1128/iai.00638-09

Nagahama, M., Kobayashi, K., Ochi, S., & Takehara, M. (2021). Internalization of Clostridium botulinum C2 Toxin Is Regulated by Cathepsin B Released from Lysosomes. *Toxins*, *13*(4), 272. https://doi.org/10.3390/toxins13040272

Nagahama, M., Takehara, M., Takagishi, T., Seike, S., Miyamoto, K., & Kobayashi, K. (2017). Cellular Uptake of Clostridium botulinum C2 Toxin Requires Acid Sphingomyelinase Activity. *Infection and Immunity*, *85*(4), e00966-16. https://doi.org/10.1128/IAI.00966-16

Najafi, M., Farhood, B., & Mortezaee, K. (2019). Cancer stem cells (CSCs) in cancer progression and therapy. *Journal of Cellular Physiology*, *234*(6), 8381–8395. https://doi.org/10.1002/jcp.27740

Nakase, I., Kobayashi, N. B., Takatani-Nakase, T., & Yoshida, T. (2015). Active macropinocytosis induction by stimulation of epidermal growth factor receptor and oncogenic Ras expression potentiates cellular uptake efficacy of exosomes. *Sci Rep*, *5*. https://doi.org/10.1038/srep10300

Nibert, M. L., & Duncan, R. (2013). Bioinformatics of Recent Aqua- and Orthoreovirus Isolates from Fish: Evolutionary Gain or Loss of FAST and Fiber Proteins and Taxonomic Implications. *PLOS ONE*, *8*(7), e68607. https://doi.org/10.1371/journal.pone.0068607

Nichols, C. B., Fraser, J. A., & Heitman, J. (2004). PAK Kinases Ste20 and Pak1 Govern Cell Polarity at Different Stages of Mating in Cryptococcus neoformans. *Molecular Biology of the Cell*, *15*(10), 4476–4489. https://doi.org/10.1091/mbc.e04-05-0370

Nieva, J. L., Madan, V., & Carrasco, L. (2012). Viroporins: Structure and biological functions. *Nature Reviews Microbiology*, *10*(8), 563–574. https://doi.org/10.1038/nrmicro2820

Novack, D. V., & Teitelbaum, S. L. (2008). The Osteoclast: Friend or Foe? *Annual Review of Pathology: Mechanisms of Disease*, *3*(1), 457–484. https://doi.org/10.1146/annurev.pathmechdis.3.121806.151431

Nozaki, K., Maltez, V. I., Rayamajhi, M., Tubbs, A. L., Mitchell, J. E., Lacey, C. A., Harvest, C. K., Li, L., Nash, W. T., Larson, H. N., McGlaughon, B. D., Moorman, N. J., Brown, M. G., Whitmire, J. K., & Miao, E. A. (2022). Caspase-7 activates ASM to repair gasdermin and perforin pores. *Nature*, *606*(7916), Article 7916. https://doi.org/10.1038/s41586-022-04825-8

Ogle, B. M., Cascalho, M., & Platt, J. L. (2005). Biological implications of cell fusion. *Nature Reviews Molecular Cell Biology*, *6*(7), Article 7. https://doi.org/10.1038/nrm1678

Ogura, K., Tsuchiya, S., Terasawa, H., Yuzawa, S., Hatanaka, H., Mandiyan, V., Schlessinger, J., & Inagaki, F. (1999). Solution structure of the SH2 domain of Grb2 complexed with the Shc-derived phosphotyrosine-containing peptide11Edited by P. E. Wright. *Journal of Molecular Biology*, *289*(3), 439–445. https://doi.org/10.1006/jmbi.1999.2792

Oikawa, T., Oyama, M., Kozuka-Hata, H., Uehara, S., Udagawa, N., Saya, H., & Matsuo, K. (2012). Tks5-dependent formation of circumferential podosomes/invadopodia mediates cell–cell fusion. *Journal of Cell Biology*, *197*(4), 553–568. https://doi.org/10.1083/jcb.201111116

Okada, Y. (1962). Analysis of giant polynuclear cell formation caused by HVJ virus from Ehrlich's ascites tumor cells: I. Microscopic observation of giant polynuclear cell formation.

Experimental Cell Research, *26*(1), 98–107. https://doi.org/10.1016/0014-4827(62)90205-7

Omata, W., Iv, W. E. A., Vandre, D. D., & Robinson, J. M. (2013). Trophoblast Cell Fusion and Differentiation Are Mediated by Both the Protein Kinase C and A Pathways. *PLOS ONE*, *8*(11), e81003. https://doi.org/10.1371/journal.pone.0081003

Palm, W. (2019). Metabolic functions of macropinocytosis. *Philosophical Transactions of the Royal Society B: Biological Sciences*, *374*(1765). https://doi.org/10.1098/rstb.2018.0285

Parmar, H. B., & Duncan, R. (2016). A novel tribasic Golgi export signal directs cargo protein interaction with activated Rab11 and AP-1–dependent Golgi–plasma membrane trafficking. *Molecular Biology of the Cell*, *27*(8), 1320–1331. https://doi.org/10.1091/mbc.E15-12-0845

Pavlath, G. K. (2010). Spatial and functional restriction of regulatory molecules during mammalian myoblast fusion. *Experimental Cell Research*, *316*(18), 3067–3072. https://doi.org/10.1016/j.yexcr.2010.05.025

Pereira, M., Petretto, E., Gordon, S., Bassett, J. H. D., Williams, G. R., & Behmoaras, J. (2018). Common signalling pathways in macrophage and osteoclast multinucleation. *Journal of Cell Science*, *131*(11), jcs216267. https://doi.org/10.1242/jcs.216267

Pérez-Vargas, J., Krey, T., Valansi, C., Avinoam, O., Haouz, A., Jamin, M., Raveh-Barak, H., Podbilewicz, B., & Rey, F. A. (2014). Structural Basis of Eukaryotic Cell-Cell Fusion. *Cell*, *157*(2). https://doi.org/10.1016/j.cell.2014.02.020

Pfeffer, P. L., & Pearton, D. J. (2012). Trophoblast development. *Reproduction*, *143*(3), 231–246. https://doi.org/10.1530/REP-11-0374

Pham, T., Perry, J. L., Dosey, T. L., Delcour, A. H., & Hyser, J. M. (2017). The Rotavirus NSP4 Viroporin Domain is a Calcium-conducting Ion Channel. *Scientific Reports*, *7*(1), Article 1. https://doi.org/10.1038/srep43487

Philip, R. V., & Harrison, R. E. (2018). A tent pole twist on membrane ruffles. *The Journal of Cell Biology*, *217*(11), 3774–3775. https://doi.org/10.1083/jcb.201810022

Podbilewicz, B. (2014). Virus and Cell Fusion Mechanisms. *Annual Review of Cell and Developmental Biology*, *30*(1), 111–139. https://doi.org/10.1146/annurev-cellbio-101512-122422

Pontow, S. E., Heyden, N. V., Wei, S., & Ratner, L. (2004). Actin Cytoskeletal Reorganizations and Coreceptor-Mediated Activation of Rac during Human Immunodeficiency Virus-Induced

Cell Fusion. *Journal of Virology*, *78*(13), 7138–7147. https://doi.org/10.1128/jvi.78.13.7138-7147.2004

Porat-Shliom, N., Kloog, Y., & Donaldson, J. G. (2008). A unique platform for H-ras signaling involving clathrin-independent endocytosis. *Mol Biol Cell*, *19*(3). https://doi.org/10.1091/mbc.E07-08-0841

Posor, Y., Jang, W., & Haucke, V. (2022). Phosphoinositides as membrane organizers. *Nature Reviews Molecular Cell Biology*, *23*(12), Article 12. https://doi.org/10.1038/s41580-022-00490-x

Powis, G., Bonjouklian, R., Berggren, M. M., Gallegos, A., Abraham, R., Ashendel, C., Zalkow, L., Matter, W. F., Dodge, J., & Grindey, G. (1994). Wortmannin, a potent and selective inhibitor of phosphatidylinositol-3-kinase. *Cancer Research*, *54*(9), 2419–2423.

Quinn, M. E., Goh, Q., Kurosaka, M., Gamage, D. G., Petrany, M. J., Prasad, V., & Millay, D. P. (2017). Myomerger induces fusion of non-fusogenic cells and is required for skeletal muscle development. *Nature Communications*, *8*(1), Article 1. https://doi.org/10.1038/ncomms15665

Randrianarison-Huetz, V., Papaefthymiou, A., Herledan, G., Noviello, C., Faradova, U., Collard, L., Pincini, A., Schol, E., Decaux, J. F., Maire, P., Vassilopoulos, S., & Sotiropoulos, A. (2017). *SRF Controls Satellite Cell Fusion Through the Maintenance of Actin Architecture*. https://doi.org/10.1083/jcb.201705130

Read, J., Clancy, E. K., Sarker, M., Antueno, R. de, Langelaan, D. N., Parmar, H. B., Shin, K., Rainey, J. K., & Duncan, R. (2015). Reovirus FAST Proteins Drive Pore Formation and Syncytiogenesis Using a Novel Helix-Loop-Helix Fusion-Inducing Lipid Packing Sensor. *PLOS Pathogens*, *11*(6), e1004962. https://doi.org/10.1371/journal.ppat.1004962

Rehan, M., Beg, M. A., Parveen, S., Damanhouri, G. A., & Zaher, G. F. (2014). Computational Insights into the Inhibitory Mechanism of Human AKT1 by an Orally Active Inhibitor, MK-2206. *PLOS ONE*, *9*(10), e109705. https://doi.org/10.1371/journal.pone.0109705

Renaud, S. J., & Jeyarajah, M. J. (2022). How trophoblasts fuse: An in-depth look into placental syncytiotrophoblast formation. *Cellular and Molecular Life Sciences: CMLS*, *79*(8), 433. https://doi.org/10.1007/s00018-022-04475-z

Rhee, I., Davidson, D., Souza, C. M., Vacher, J., & Veillette, A. (2013). Macrophage Fusion Is Controlled by the Cytoplasmic Protein Tyrosine Phosphatase PTP-PEST/PTPN12.

Molecular and Cellular Biology, *33*(12), 2458–2469. https://doi.org/10.1128/MCB.00197-13

Richard, J.-P., Leikina, E., Langen, R., Henne, W. M., Popova, M., Balla, T., McMahon, H. T., Kozlov, M. M., & Chernomordik, L. V. (2011). Intracellular curvature-generating proteins in cell-to-cell fusion. *Biochemical Journal*, *440*(Pt 2), 185–193. https://doi.org/10.1042/BJ20111243

Riehle, R. D., Cornea, S., & Degterev, A. (2013). Role of Phosphatidylinositol 3,4,5-Trisphosphate in Cell Signaling. In D. G. S. Capelluto (Ed.), *Lipid-mediated Protein Signaling* (pp. 105–139). Springer Netherlands. https://doi.org/10.1007/978-94-007-6331-9_7

Rion, N., Castets, P., Lin, S., Enderle, L., Reinhard, J. R., Eickhorst, C., & Rüegg, M. A. (2019). MTOR controls embryonic and adult myogenesis via mTORC1. *Development*, *146*(7), dev172460. https://doi.org/10.1242/dev.172460

Risselada, H. J., Bubnis, G., & Grubmüller, H. (2014). Expansion of the fusion stalk and its implication for biological membrane fusion. *Proceedings of the National Academy of Sciences*, *111*(30), 11043–11048. https://doi.org/10.1073/pnas.1323221111

Rommel, C., Bodine, S. C., Clarke, B. A., Rossman, R., Nunez, L., Stitt, T. N., Yancopoulos, G. D., & Glass, D. J. (2001). Mediation of IGF-1-induced skeletal myotube hypertrophy by PI(3)K/Akt/mTOR and PI(3)K/Akt/GSK3 pathways. *Nature Cell Biology*, *3*(11), Article 11. https://doi.org/10.1038/ncb1101-1009

Salamon, R. S., & Backer, J. M. (2013). Phosphatidylinositol-3,4,5-trisphosphate: Tool of choice for class I PI 3-kinases. *BioEssays*, *35*(7), 602–611. https://doi.org/10.1002/bies.201200176

Salsman, J., Top, D., Barry, C., & Duncan, R. (2008). A Virus-Encoded Cell–Cell Fusion Machine Dependent on Surrogate Adhesins. *PLoS Pathogens*, *4*(3), e1000016. https://doi.org/10.1371/journal.ppat.1000016

Schejter, E. D. (2016). Myoblast fusion: Experimental systems and cellular mechanisms. *Seminars in Cell & Developmental Biology*, *60*, 112–120. https://doi.org/10.1016/j.semcdb.2016.07.016

Schmid, A. C., Byrne, R. D., Vilar, R., & Woscholski, R. (2004). Bisperoxovanadium compounds are potent PTEN inhibitors. *FEBS Letters*, *566*(1–3), 35–38. https://doi.org/10.1016/j.febslet.2004.03.102

Schmidt, U., Weigert, M., Broaddus, C., & Myers, G. (2018). Cell Detection with Star-Convex Polygons. In A. F. Frangi, J. A. Schnabel, C. Davatzikos, C. Alberola-López, & G. Fichtinger (Eds.), *Medical Image Computing and Computer Assisted Intervention – MICCAI 2018* (pp. 265–273). Springer International Publishing. https://doi.org/10.1007/978-3-030-00934-2_30

Schwenen, L. L. G., Hubrich, R., Milovanovic, D., Geil, B., Yang, J., Kros, A., Jahn, R., & Steinem, C. (2015). Resolving single membrane fusion events on planar pore-spanning membranes. *Scientific Reports*, *5*(1), Article 1. https://doi.org/10.1038/srep12006

Segal, D., Dhanyasi, N., Schejter, E. D., & Shilo, B.-Z. (2016). *Adhesion and Fusion of Muscle Cells Are Promoted by Filopodia*. https://doi.org/10.1016/j.devcel.2016.07.010

Segev, N., Avinoam, O., & Podbilewicz, B. (2018). Fusogens. *Current Biology*, *28*(8), R378–R380. https://doi.org/10.1016/j.cub.2018.01.024

Seguin, L. (n.d.). *KRAS Addiction Promotes Cancer Cell Adaptation in Harsh Microenvironment Through Macropinocytosis BT - Macropinocytosis: Functions and Mechanisms* (C. Commisso, Ed.; Vol. 2022). Springer International Publishing. https://doi.org/10.1007/978-3-030-94004-1_10

Sens, K. L., Zhang, S., Jin, P., Duan, R., Zhang, G., Luo, F., Parachini, L., & Chen, E. H. (2010). An invasive podosome-like structure promotes fusion pore formation during myoblast fusion. *Journal of Cell Biology*, *191*(5), 1013–1027. https://doi.org/10.1083/jcb.201006006

Shilagardi, K., Li, S., Luo, F., Marikar, F., Duan, R., Jin, P., Kim, J. H., Murnen, K., & Chen, E. H. (2013a). Actin-Propelled Invasive Membrane Protrusions Promote Fusogenic Protein Engagement During Cell-Cell Fusion. *Science*, *340*(6130), 359–363. https://doi.org/10.1126/science.1234781

Shilagardi, K., Li, S., Luo, F., Marikar, F., Duan, R., Jin, P., Kim, J. H., Murnen, K., & Chen, E. H. (2013b). Actin-propelled invasive membrane protrusions promote fusogenic protein engagement during cell-cell fusion. *Science (New York, N.Y.)*, *340*(6130), 359–363. https://doi.org/10.1126/science.1234781

Shirasawa, H., Tomita, Y., Sekiya, S., Takamizawa, H., & Simizu, B. (1987). Integration and Transcription of Human Papillomavirus Type 16 and 18 Sequences in Cell Lines Derived from Cervical Carcinomas. *Journal of General Virology*, *68*(2), 583–591. https://doi.org/10.1099/0022-1317-68-2-583

Shmulevitz, M., Epand, R. F., Epand, R. M., & Duncan, R. (2004). Structural and Functional Properties of an Unusual Internal Fusion Peptide in a Nonenveloped Virus Membrane Fusion Protein. *Journal of Virology*, *78*(6), 2808–2818. https://doi.org/10.1128/JVI.78.6.2808-2818.2004

Shu, L., & Houghton, P. J. (2009). The mTORC2 Complex Regulates Terminal Differentiation of C2C12 Myoblasts. *Molecular and Cellular Biology*, *29*(17), 4691–4700. https://doi.org/10.1128/MCB.00764-09

Shuhei Kawamoto, Michael L. Klein, & Wataru Shinoda. (2015). Coarse-Grained Molecular Dynamics Study of Membrane Fusion: Curvature Effects on Free Energy Barriers Along the Stalk Mechanism. *The Journal of Chemical Physics*. https://doi.org/10.1063/1.4933087

Simanshu, D. K., v., N. D., & McCormick, F. (2017). RAS Proteins and Their Regulators in Human Disease. *Cell*, *170*(1). https://doi.org/10.1016/j.cell.2017.06.009

Simonsen, A. C., Mularski, A., Nylandsted, J., & Heitmann, A. S. B. (2023). Probing the mechanism of annexin mediated plasma membrane repair. *Biophysical Journal*, *122*(3), 85a. https://doi.org/10.1016/j.bpj.2022.11.662

Sønder, S. L., Häger, S. C., Heitmann, A. S. B., Frankel, L. B., Dias, C., Simonsen, A. C., & Nylandsted, J. (2021). Restructuring of the plasma membrane upon damage by LC3-associated macropinocytosis. *Science Advances*, *7*(27), eabg1969. https://doi.org/10.1126/sciadv.abg1969

Song, G., Ouyang, G., & Bao, S. (2005). The activation of Akt/PKB signaling pathway and cell survival. *Journal of Cellular and Molecular Medicine*, *9*(1), 59–71. https://doi.org/10.1111/j.1582-4934.2005.tb00337.x

Sun, M., Hillmann, P., Hofmann, B. T., Hart, J. R., & Vogt, P. K. (2010). Cancer-derived mutations in the regulatory subunit p85α of phosphoinositide 3-kinase function through the catalytic subunit p110α. *Proceedings of the National Academy of Sciences*, *107*(35), 15547–15552. https://doi.org/10.1073/pnas.1009652107

Swanson, J. A. (2008). Shaping cups into phagosomes and macropinosomes. *Nature Reviews. Molecular Cell Biology*, *9*(8), 639–649. https://doi.org/10.1038/nrm2447

Tahir, M. A., Guven, Z. P., Arriaga, L. R., Tinao, B., Yang, Y.-S. S., Bekdemir, A., Martin, J. T., Bhanji, A. N., Irvine, D., Stellacci, F., & Alexander-Katz, A. (2020). Calcium-triggered fusion of lipid membranes is enabled by amphiphilic nanoparticles. *Proceedings of the*

National Academy of Sciences, *117*(31), 18470–18476. https://doi.org/10.1073/pnas.1902597117

Takahashi, K., & Suzuki, K. (2011). WAVE2, N-WASP, and mena facilitate cell invasion via phosphatidylinositol 3-kinase-dependent local accumulation of actin filaments. *Journal of Cellular Biochemistry*, *112*(11), 3421–3429. https://doi.org/10.1002/jcb.23276

Tiedemann, K., Le Nihouannen, D., Fong, J. E., Hussein, O., Barralet, J. E., & Komarova, S. V. (2017a). Regulation of Osteoclast Growth and Fusion by mTOR/raptor and mTOR/rictor/Akt. *Frontiers in Cell and Developmental Biology*, *5*. https://www.frontiersin.org/articles/10.3389/fcell.2017.00054

Tiedemann, K., Le Nihouannen, D., Fong, J. E., Hussein, O., Barralet, J. E., & Komarova, S. V. (2017b). Regulation of Osteoclast Growth and Fusion by mTOR/raptor and mTOR/rictor/Akt. *Frontiers in Cell and Developmental Biology*, *5*. https://www.frontiersin.org/articles/10.3389/fcell.2017.00054

Toker, A., & Marmiroli, S. (2014). Signaling Specificity in the Akt Pathway in Biology and Disease. *Advances in Biological Regulation*, *0*, 28–38. https://doi.org/10.1016/j.jbior.2014.04.001

Trenerry, M. K., Gatta, P. A. D., & Cameron-Smith, D. (2011). JAK/STAT signaling and human in vitro myogenesis. *BMC Physiology*, *11*(1), 6. https://doi.org/10.1186/1472-6793-11-6

Tretyakova, M. S., Subbalakshmi, A. R., Menyailo, M. E., Jolly, M. K., & Denisov, E. V. (2022). Tumor Hybrid Cells: Nature and Biological Significance. *Frontiers in Cell and Developmental Biology*, *10*. https://www.frontiersin.org/articles/10.3389/fcell.2022.814714

van Kuppeveld, F. J., Hoenderop, J. G., Smeets, R. L., Willems, P. H., Dijkman, H. B., Galama, J. M., & Melchers, W. J. (1997). Coxsackievirus protein 2B modifies endoplasmic reticulum membrane and plasma membrane permeability and facilitates virus release. *The EMBO Journal*, *16*(12), 3519–3532. https://doi.org/10.1093/emboj/16.12.3519

Vance, T. D. R., & Lee, J. E. (2020). Virus and eukaryote fusogen superfamilies. *Current Biology*, *30*(13), R750–R754. https://doi.org/10.1016/j.cub.2020.05.029

Vanhaesebroeck, B., Stephens, L., & Hawkins, P. (2012). PI3K signalling: The path to discovery and understanding. *Nature Reviews Molecular Cell Biology*, *13*(3), Article 3. https://doi.org/10.1038/nrm3290

Vasyutina, E., Martarelli, B., Brakebusch, C., Wende, H., & Birchmeier, C. (2009). *The Small G-Proteins Rac1 and Cdc42 Are Essential for Myoblast Fusion in the Mouse*. https://doi.org/10.1073/pnas.0902501106

Veltman, D. M., King, J. S., Machesky, L. M., & Insall, R. H. (2012). SCAR knockouts in Dictyostelium: WASP assumes SCAR's position and upstream regulators in pseudopods. *Journal of Cell Biology*, *198*(4). https://doi.org/10.1083/jcb.201205058

Veltman, D. M., Lemieux, M. G., Knecht, D. A., & Insall, R. H. (2014). PIP3-dependent macropinocytosis is incompatible with chemotaxis. *Journal of Cell Biology*, *204*(4). https://doi.org/10.1083/jcb.201309081

Veltman, D. M., Williams, T. D., & Bloomfield, G. (2016). A plasma membrane template for macropinocytic cups. *Elife*, *5*(DECEMBER2016). https://doi.org/10.7554/eLife.20085

Verma, S. K., Leikina, E., Melikov, K., & Chernomordik, L. V. (2014). Late stages of the synchronized macrophage fusion in osteoclast formation depend on dynamin. *The Biochemical Journal*, *464*(3), 293–300. https://doi.org/10.1042/BJ20141233

Wang, G., Zhu, H., Situ, C., Han, L., Yu, Y., Cheung, T. H., Liu, K., & Wu, Z. (2018). P110α of PI3K is necessary and sufficient for quiescence exit in adult muscle satellite cells. *The EMBO Journal*, *37*(8), e98239. https://doi.org/10.15252/embj.201798239

Wang, J., Zhao, W., Guo, H., Fang, Y., Stockman, S. E., Bai, S., Ng, P. K.-S., Li, Y., Yu, Q., Lu, Y., Jeong, K. J., Chen, X., Gao, M., Liang, J., Li, W., Tian, X., Jonasch, E., Mills, G. B., & Ding, Z. (2018). AKT isoform-specific expression and activation across cancer lineages. *BMC Cancer*, *18*(1), 742. https://doi.org/10.1186/s12885-018-4654-5

Waters, A. M., & Der, C. J. (2018). KRAS: The critical driver and therapeutic target for pancreatic cancer. *Cold Spring Harb Perspect Med*, *8*(9). https://doi.org/10.1101/cshperspect.a031435

Weichert, M., Lichius, A., Priegnitz, B.-E., Brandt, U., Gottschalk, J., Nawrath, T., Groenhagen, U., Read, N. D., Schulz, S., & Fleißner, A. (2016). Accumulation of specific sterol precursors targets a MAP kinase cascade mediating cell–cell recognition and fusion. *Proceedings of the National Academy of Sciences*, *113*(42), 11877–11882. https://doi.org/10.1073/pnas.1610527113

Weiss, W. A., Taylor, S. S., & Shokat, K. M. (2007). Recognizing and exploiting differences between RNAi and small-molecule inhibitors. *Nature Chemical Biology*, *3*(12), 739–744. https://doi.org/10.1038/nchembio1207-739

Williams, T. D., Peak-Chew, S. Y., Paschke, P., & Kay, R. R. (2019). Akt and SGK protein kinases are required for efficient feeding by macropinocytosis. *J Cell Sci*, *132*(2). https://doi.org/10.1242/jcs.224998

Williamson, C. D., & Donaldson, J. G. (2019). Arf6, JIP3, and dynein shape and mediate macropinocytosis. *Molecular Biology of the Cell*, *30*(12), 1477–1489. https://doi.org/10.1091/mbc.E19-01-0022

Xue, J., Zhu, Y., Sun, Z., Ji, R., Zhang, X., Xu, W., Yuan, X., Zhang, B., Yan, Y., Yin, L., Xu, H., Zhang, L., Zhu, W., & Qian, H. (2015). Tumorigenic hybrids between mesenchymal stem cells and gastric cancer cells enhanced cancer proliferation, migration and stemness. *BMC Cancer*, *15*(1), 793. https://doi.org/10.1186/s12885-015-1780-1

Yang, G., Francis, D., Krycer, J. R., Larance, M., Zhang, Z., Novotny, C. J., Diaz-Vegas, A., Shokat, K. M., & James, D. E. (2021). Dissecting the biology of mTORC1 beyond rapamycin. *Science Signaling*, *14*(701), eabe0161. https://doi.org/10.1126/scisignal.abe0161

Yang, G., Murashige, D. S., Humphrey, S. J., & James, D. E. (2015). A Positive Feedback Loop between Akt and mTORC2 via SIN1 Phosphorylation. *Cell Reports*, *12*(6), 937–943. https://doi.org/10.1016/j.celrep.2015.07.016

Yang, Y., Gaspard, G., McMullen, N., & Duncan, R. (2020). Polycistronic Genome Segment Evolution and Gain and Loss of FAST Protein Function during Fusogenic Orthoreovirus Speciation. *Viruses*, *12*(7), 702. https://doi.org/10.3390/v12070702

Yang, Y., & Margam, N. N. (2021). Structural Insights into Membrane Fusion Mediated by Convergent Small Fusogens. *Cells*, *10*(1), Article 1. https://doi.org/10.3390/cells10010160

Yoon, M.-S. (2017). MTOR as a Key Regulator in Maintaining Skeletal Muscle Mass. *Frontiers in Physiology*, *8*. https://www.frontiersin.org/articles/10.3389/fphys.2017.00788

Yoshida, S., Gaeta, I., Pacitto, R., Krienke, L., Alge, O., Gregorka, B., & Swanson, J. A. (2015). Differential signaling during macropinocytosis in response to M-CSF and PMA in macrophages. *Frontiers in Physiology*, *6*, 8. https://doi.org/10.3389/fphys.2015.00008

Yoshida, S., Hoppe, A. D., Araki, N., & Swanson, J. A. (2009). Sequential signaling in plasma-membrane domains during macropinosome formation in macrophages. *Journal of Cell Science*, *122*(18), 3250–3261. https://doi.org/10.1242/jcs.053207

Yudushkin, I. (2019). Getting the Akt Together: Guiding Intracellular Akt Activity by PI3K. *Biomolecules*, *9*(2), Article 2. https://doi.org/10.3390/biom9020067

Yudushkin, I. (2020). Control of Akt activity and substrate phosphorylation in cells. *IUBMB Life*, *72*(6), 1115–1125. https://doi.org/10.1002/iub.2264

Zammit, P. S. (2017). Function of the myogenic regulatory factors Myf5, MyoD, Myogenin and MRF4 in skeletal muscle, satellite cells and regenerative myogenesis. *Seminars in Cell & Developmental Biology*, *72*, 19–32. https://doi.org/10.1016/j.semcdb.2017.11.011

Zhang, H., Ma, H., Yang, X., Fan, L., Tian, S., Niu, R., Yan, M., Zheng, M., & Zhang, S. (2021). Cell Fusion-Related Proteins and Signaling Pathways, and Their Roles in the Development and Progression of Cancer. *Frontiers in Cell and Developmental Biology*, *9*, 809668. https://doi.org/10.3389/fcell.2021.809668

Zhang, M., Jang, H., & Nussinov, R. (2019). The mechanism of PI3Kα activation at the atomic level †Electronic supplementary information (ESI) available. See DOI: 10.1039/c8sc04498h. *Chemical Science*, *10*(12), 3671–3680. https://doi.org/10.1039/c8sc04498h

Zhang, M., Jang, H., & Nussinov, R. (2020). PI3K inhibitors: Review and new strategies. *Chemical Science*, *11*(23), 5855–5865. https://doi.org/10.1039/D0SC01676D

Zhang, Q., Vashisht, A. A., O'Rourke, J., Corbel, S. Y., Moran, R., Romero, A., Miraglia, L., Zhang, J., Durrant, E., Schmedt, C., Sampath, S. C., & Sampath, S. C. (2017). The microprotein Minion controls cell fusion and muscle formation. *Nature Communications*, *8*(1), Article 1. https://doi.org/10.1038/ncomms15664

Zheng, Z., Amran, S. I., Thompson, P. E., & Jennings, I. G. (2011). Isoform-selective inhibition of phosphoinositide 3-kinase: Identification of a new region of nonconserved amino acids critical for p110α inhibition. *Molecular Pharmacology*, *80*(4), 657–664. https://doi.org/10.1124/mol.111.072546

Zhou, Y., Feng, Z., Cao, F., Liu, X., Xia, X., & Yu, C. (2020). Abl-mediated PI3K activation regulates macrophage podosome formation. *Journal of Cell Science*, *133*(11), jcs234385. https://doi.org/10.1242/jcs.234385

Appendix A: Contributions

The work presented in this thesis was carried out in collaboration with several contributors whose specific roles are detailed below:

Nicole McMullen was instrumental in replicating the SARS-CoV-2 spike fusion experiments, providing valuable insights into viral fusion mechanisms. Her work included the Western blot analysis from lysates and the precise counting of fusion efficiency, which contributed the experimental data of Fig 19. Furthermore, Nicole also contributed significantly by developing the 293a cell line with myomaker and creating a Tet-On myomixer cell line and produced the experiments of Fig 17. Her meticulous work in conducting all experiments involving these cell lines added depth and specificity to the study.

Nandini Margam played a crucial role in the C2C12 fusion inhibition experiments, enhancing our understanding of fusion regulation. She conducted experiments to inhibit fusion in C2C12 cells and counted the fusion index for these experiments. Nandini's contributions were vital in the data analysis and interpretation of this segment of the research.

Gerard Gaspard was responsible for the innovative PIP(3,4,5) exogenous addition experiment of Fig 9 C. His expertise in phosphoinositide signaling contributed to the design, execution, and analysis of the experiment. Gerard's work helped to elucidate the roles of phosphoinositides in cellular processes, adding a novel dimension to the thesis.

The collaboration and collective efforts of these individuals were central to the success of the research presented in this thesis. Their respective roles complemented each other and allowed for a comprehensive and multifaceted investigation into the fields of viral fusion, cell signaling, and cellular processes. The author extends heartfelt gratitude for their hard work, dedication, and invaluable contributions.

Appendix B: Copyright Release

ELSEVIER LICENSE TERMS AND CONDITIONS

Aug 18, 2023

This Agreement between Dalhousie University -- Duncan Mackenzie ("You") and Elsevier ("Elsevier") consists of your license details and the terms and conditions provided by Elsevier and Copyright Clearance Center.

License Number 5612181075047
License date Aug 18, 2023 Licensed Content Publisher Elsevier
Licensed Content Publication Developmental Cell
Licensed Content Title Viral and Developmental Cell Fusion Mechanisms: Conservation and Divergence
Licensed Content Author Amir Sapir,Ori Avinoam,Benjamin Podbilewicz,Leonid V. Chernomordik

Licensed Content Date Jan 1, 2008
Licensed Content Volume 14
Licensed Content Issue 1
Licensed Content Pages 11
Start Page 11
End Page 21
Type of Use reuse in a thesis/dissertation
Portion figures/tables/illustrations
Number of figures/tables/illustrations 1
Format electronic
Are you the author of this Elsevier article? No
Will you be translating? No
Title Dr. Duncan MacKenzie
Institution name Dalhousie University Expected presentation date Aug 2023
Order reference number 4469
Portions Figure 1
Dalhousie University 150 Forward Avenue
Requestor Location
Ottawa, ON K1Y 1K9 Canada
Attn: Dalhousie University
Publisher Tax IDGB 494 6272 12
Total 0.00 CAD
Terms and Conditions
INTRODUCTION

1. The publisher for this copyrighted material is Elsevier. By clicking "accept" in connection with completing this licensing transaction, you agree that the following terms and conditions

apply to this transaction (along with the Billing and Payment terms and conditions established by Copyright Clearance Center, Inc. ("CCC"), at the time that you opened your RightsLink account and that are available at any time at https://myaccount.copyright.com).

GENERAL TERMS

2. Elsevier hereby grants you permission to reproduce the aforementioned material subject to the terms and conditions indicated.

3. Acknowledgement: If any part of the material to be used (for example, figures) has appeared in our publication with credit or acknowledgement to another source, permission must also be sought from that source. If such permission is not obtained then that material may not be included in your publication/copies. Suitable acknowledgement to the source must be made, either as a footnote or in a reference list at the end of your publication, as follows:

"Reprinted from Publication title, Vol /edition number, Author(s), Title of article / title of chapter, Pages No., Copyright (Year), with permission from Elsevier [OR APPLICABLE SOCIETY COPYRIGHT OWNER]." Also Lancet special credit - "Reprinted from The Lancet, Vol. number, Author(s), Title of article, Pages No., Copyright (Year), with permission from Elsevier."

4. Reproduction of this material is confined to the purpose and/or media for which permission is hereby given. The material may not be reproduced or used in any other way, including use in combination with an artificial intelligence tool (including to train an algorithm, test, process, analyse, generate output and/or develop any form of artificial intelligence tool), or to create any derivative work and/or service (including resulting from the use of artificial intelligence tools).

5. Altering/Modifying Material: Not Permitted. However figures and illustrations may be altered/adapted minimally to serve your work. Any other abbreviations, additions, deletions and/or any other alterations shall be made only with prior written authorization of Elsevier Ltd. (Please contact Elsevier’s permissions helpdesk here). No modifications can be made to any Lancet figures/tables and they must be reproduced in full.

6. If the permission fee for the requested use of our material is waived in this instance, please be advised that your future requests for Elsevier materials may attract a fee.

7. Reservation of Rights: Publisher reserves all rights not specifically granted in the combination of (i) the license details provided by you and accepted in the course of this licensing transaction, (ii) these terms and conditions and (iii) CCC's Billing and Payment terms and conditions.

8. License Contingent Upon Payment: While you may exercise the rights licensed immediately upon issuance of the license at the end of the licensing process for the transaction, provided that you have disclosed complete and accurate details of your proposed use, no license

is finally effective unless and until full payment is received from you (either by publisher or by CCC) as provided in CCC's Billing and Payment terms and conditions. If full payment is not received on a timely basis, then any license preliminarily granted shall be deemed automatically revoked and shall be void as if never granted. Further, in the event that you breach any of these terms and conditions or any of CCC's Billing and Payment

terms and conditions, the license is automatically revoked and shall be void as if never granted. Use of materials as described in a revoked license, as well as any use of the materials beyond the scope of an unrevoked license, may constitute copyright infringement and publisher reserves the right to take any and all action to protect its copyright in the materials.

9. Warranties: Publisher makes no representations or warranties with respect to the licensed material.

10. Indemnity: You hereby indemnify and agree to hold harmless publisher and CCC, and their respective officers, directors, employees and agents, from and against any and all claims arising out of your use of the licensed material other than as specifically authorized pursuant to this license.

11. No Transfer of License: This license is personal to you and may not be sublicensed, assigned, or transferred by you to any other person without publisher's written permission.

12. No Amendment Except in Writing: This license may not be amended except in a writing signed by both parties (or, in the case of publisher, by CCC on publisher's behalf).

13. Objection to Contrary Terms: Publisher hereby objects to any terms contained in any purchase order, acknowledgment, check endorsement or other writing prepared by you, which terms are inconsistent with these terms and conditions or CCC's Billing and Payment terms and conditions. These terms and conditions, together with CCC's Billing and Payment terms and conditions (which are incorporated herein), comprise the entire agreement between you and publisher (and CCC) concerning this licensing transaction. In the event of any conflict between your obligations established by these terms and conditions and those established by CCC's Billing and Payment terms and conditions, these terms and conditions shall control.

14. Revocation: Elsevier or Copyright Clearance Center may deny the permissions described in this License at their sole discretion, for any reason or no reason, with a full refund payable to you. Notice of such denial will be made using the contact information provided by you. Failure to receive such notice will not alter or invalidate the denial. In no event will Elsevier or Copyright Clearance Center be responsible or liable for any costs, expenses or damage incurred by you as a result of a denial of your permission request, other than a refund of the amount(s) paid by you to Elsevier and/or Copyright Clearance Center for denied permissions.